Charles University in Prague
Faculty of Science

Department of Cell Biology

CSL proteins of *Schizosaccharomyces pombe*

PhD Thesis

Martin Převorovský

2008

Supervised by RNDr. František Půta, CSc.

I hereby declare that this submission is my own work and that, to the best of my knowledge and belief, it contains no material previously published or written by another person nor material which to a substantial extent has been accepted for the award of any other degree or diploma of the university or other institute of higher learning, except where due acknowledgment has been made in the text.

Prague, December 2008 Martin Převorovský

ACKNOWLEDGEMENTS

Even though most of the work presented in this thesis was done by myself, important results came also from experiments which I supervised or carried out in collaboration. Since I am trying to present a whole story here, which only makes sense when all these bits of information are put together, I will use the "we" form in the text to acknowledge these contributions of other people.

I would like to thank my supervisors Dr. Petr Folk and Dr. František Půta, and the present and former lab members for guidance and support. Special thanks go to Jan Ryneš, Tomáš Groušl, Jana Staňurová and Martina Ptáčková, who all participated in the CSL project, to Wolfgang Nellen and his lab in Kassel, who generously gave me a hand with establishing the DNA-binding assays, and to Jürg Bähler and Stephen Watt for the microarray analyses.

This work was supported by the Grant Agency of the Charles University grant No. 157/2005/B-BIO/PrF, the Czech Science Foundation grant No. 204/03/H066, and the research projects No. MSM0021620858 and LC07032 of the Czech Ministry of Education, Youth and Sports.

Můj největší dík patří mé rodině a Lence za nezměrnou lásku, podporu a důvěru po všechny ty roky. Bez vás by to nešlo…

TABLE OF CONTENTS

ABBREVIATIONS

2H	two-hybrid
AD	activation domain
ADAM	a disintegrin and a metalloprotease domain
BCIP	bromo-chloro-indolyl phosphate
bHlH	basic Helix-loop-Helix
BTD	beta-trefoil domain
CBF1	C-promoter binding factor 1
CBP	CREB-binding protein
CADASIL	cerebral autosomal dominant arteriopathy with subcortical infarcts and leukoencephalopathy
CESR	core environmental stress response
CIR	CBF1-interacting repressor
CREB	cAMP response element binding
CSL	CBF1/RBP-Jκ/Suppressor of Hairless/LAG-1
C_T	threshold cycle
DAPI	4',6-diamidino-2-phenylindole
DABCO	1,4-diazabicyclo[2.2.2]octane
DBD	DNA-binding domain
DEPC	diethylpyrocarbonate
DMSO	dimethyl sulfoxide
DSL	Delta/Serrate/LAG-2
EBV	Epstein-Barr virus
ECL	enhanced chemiluminescence
ECM	extracellular matrix
EGF	epidermal growth factor
EGFP	enhanced green fluorescent protein
EGTA	ethylene glycol tetraacetic acid
EMSA	electromobility shift assay
EYFP	enhanced yellow fluorescent protein
FACS	fluorescence-assisted cell sorter
HDAC	histone deacetylase complex
HEPES	4-(2-hydroxyethyl)-1-piperazineethanesulfonic acid

HERP	HES-related repressor protein
HES	Hairy/Enhancer of Split
IgG	immunoglobulin G
IPTG	isopropyl-beta-D-thiogalactopyranoside
JGI	The U.S. Department of Energy Joint Genome Institute
KI	knock-in
KO	knock-out
KSHV	Kaposi's sarcoma-associated herpesvirus
LAG-1/2/3	lin-12 and glp-1 signaling
MINT	Msx2-interacting nuclear target protein
NBT	nitroblue tetrazolium
NCBI	National Center for Biotechnology Information
NICD	Notch intracellular domain
NRARP	Notch-related ankyrin-repeat protein
OD	optical density
ORF	open reading frame
PAGE	polyacrylamide gel electrophoresis
PCR	polymerase chain reaction
PIPES	piperazine-1,4-bis(2-ethanesulfonic acid)
PMSF	phenylmethylsulphonyl fluoride
qRT-PCR	quantitative reverse transcription-polymerase chain reaction
RBP-Jκ	recombination signal binding protein Jκ
RBP-L	RBP-Jκ-like
RHR	Rel-homology region
SDS	sodium dodecyl sulphate
SHARP	SMRT/HDAC-1-associated repressor protein
SKIP	Ski-interacting protein
SMRT	silencing mediator of retinoid and thyroid receptors
SR	serine/arginine-rich
Su(H)	Suppressor of Hairless
TACE	tumor necrosis factor-α converting enzyme
TAP	tandem affinity purification

1 *INTRODUCTION*

Schizosaccharomyces pombe, also known as the fission yeast, is a versatile and simple unicellular eukaryotic model organism with a completely sequenced genome of 12,57 Mbp, harboring about 5000 genes (Wood *et al.*, 2002). From the phylogenetic point of view, *Schizosaccharomycetes* belong to Taphrinomycotina, the early branching group of ascomycetes (Hedges, 2002). Thus, *S. pombe* is a distant cousin of the notorious budding yeast *Saccharomyces cerevisiae*, however, numerous molecular characteristics of the former species resemble more closely higher eukaryotes, making the fission yeast a superior model for studying the cell cycle and its regulation, cell growth and polarity, the replication and repair of DNA, chromatin architecture and dynamics, and gene expression (Egel, 2004). Consequently, *S. pombe* is sometimes referred to as a "micro mammal" http://www.nih.gov/science/models/Schizosaccharomyces/index.html). With the recent completion of the two related fission yeasts' genomes (*S. japonicus* and *S. octosporus*), *S. pombe* has become a powerful tool for comparative genomics as well (http://www.broad.mit.edu/annotation/genome/schizosaccharomyces_group/).

At the time of this writing, there were 121 transcription factors identified in the fission yeast genome (http://www.genedb.org/genedb/pombe/index.jsp) (Hertz-Fowler *et al.*, 2004). About one half of them have already been characterized, to a varying degree, and implicated in regulating some of the processes mentioned above. However, there are still about 60 predicted but completely uncharacterized regulators of transcription, likely together with other genes yet awaiting their recognition as transcription factors. The principal aim of this study is to characterize one such family of putative transcription factors.

Using a computational approach, we identified putative novel members of the CSL (CBF1/RBP-Jκ/Suppressor of Hairless/LAG-1) family of transcription factors in several fungal species, including *S. pombe*. The CSL family, considered a hallmark of metazoan organisms, participates in the regulation of key developmental processes via its involvement in the Notch signaling pathway (Artavanis-Tsakonas *et al.*, 1999). The surprising existence of CSL genes in evolutionarily distant and simple organisms prompted us to investigate their function in the Notch-less fungal settings.

2 *LITERATURE REVIEW*

2.1 Notch signaling pathway

The Notch signaling pathway is a critical regulatory circuit implicated in mediating a vast number of developmental events in metazoa (Artavanis-Tsakonas *et al.*, 1999;Bray, 2006). Notch is a large single-pass transmembrane receptor protein exposed on the cell surface. Its name was derived from the Notch gene mutation in *Drosophila melanogaster* that resulted in morphological abnormalities – prominent "notches" in the wing margin. During protein maturation, the receptor is cleaved and the proteolytic fragments form a non-covalent heterodimer consisting of a large extracellular domain attached to a transmembrane part that extends into the cell lumen, forming the Notch intracellular domain (NICD) (Fig. 2.1). NICD consists of 7 ankyrin repeats, two nuclear localization signals, two transactivation domains and a C-terminal PEST/OPA domain regulating the stability of the protein. The extracellular part of the receptor contains 29-36 epidermal growth factor (EGF) repeats, a subset of which is important for ligand binding (Lubman *et al.*, 2004). It recognizes ligands of the Delta/Serrate/LAG-2 type (DSL; named after the mammalian, drosophila, and *Caenorhabditis elegans* orthologs) which also are transmembrane proteins, thus permitting only short distance cell-cell signaling via this pathway (Fig. 2.1). Upon ligand binding, two sequential proteolytic events take place, carried out by the ADAM/TACE and γ-secretase proteases, respectively, liberating the NICD, which can translocate to the cell nucleus to exert its coactivator function at target promoters. Interestingly, no second messengers amplify the signal and, consequently, Notch is sometimes referred to as a membrane-bound transcription factor. In the nucleus, NICD interacts with the third pathway component, a DNA-bound transcription factor of the CSL family, an effector protein which in turn switches from a repressive mode (displacement of corepressors) to an activatory state (recruitment of Mastermind and other coactivators) (Fig. 2.1). The principal aim of the signaling is promotion or inhibition of a particular cell fate (lateral inhibition, cell lineage decisions, boundary specification). This simple scheme has been utilized and literally recycled repeatedly in various settings to achieve a plethora of developmental effects ranging from somitogenesis and immune system differentiation to nervous system and muscle tissue specification, etc.

(Artavanis-Tsakonas *et al.*, 1999;Bray, 2006;de la Pompa *et al.*, 1997;Laky and Fowlkes, 2008;Maillard *et al.*, 2003;Weinmaster and Kintner, 2003). The signaling outcome is highly context-dependent and is a subject to complex regulation by both the ligand and receptor expression levels and turnover, their localization pattern (trafficking), and posttranslational modifications (proteolysis, ubiquitinylation, glycosylation) (Bray, 2006). Significantly, several viruses have found ways to harness the Notch pathway to help their own replication cycle (Hayward, 2004). It should also be noted that CSL-independent Notch functions likely exist (Martinez *et al.*, 2002), however, this is still somewhat controversial (Bray, 2006).

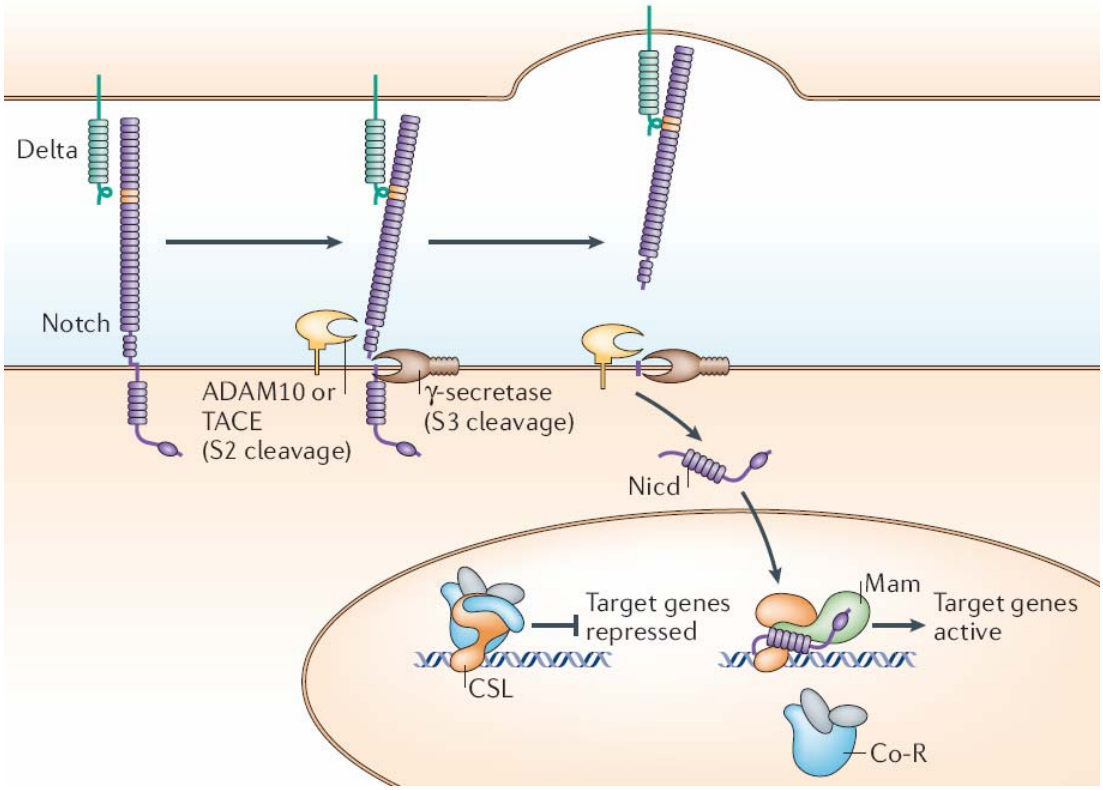

Figure 2.1 – A schematic representation of the Notch signaling pathway, see text for details (adapted from (Bray, 2006)). Co-R – corepressor complex; Mam – Mastermind.

Experimental perturbations of the Notch pathway often lead to pronounced and pleiotropic defects in development, and knocking-out either Notch or CSL results in an embryonic-lethal phenotype (Artavanis-Tsakonas *et al.*, 1999;Oka *et al.*, 1995). It is not surprising then that various mutations and misregulations of the Notch pathway components were found to underlie a number of important (human) diseases such as, among others, the T cell acute lymphoblastic leukemia, prostate

cancer, cervical carcinoma (Weng and Aster, 2004), cognitive deficits, spondylocostal dysostosis (rib fusions and trunk dwarfism), and cerebral autosomal dominant arteriopathy with subcortical infarcts and leukoencephalopathy (CADASIL; dementia, migraines and strokes) (Lai, 2004). The phenotypic complexity outlined above also poses a limitation in the study of the Notch pathway as the interpretation of experimental data is not feasible.

2.2 CSL proteins

As outlined in Chapter 2.1, the CSL (CBF1/RBP-Jκ/Suppressor of Hairless/LAG-1) transcription factors serve as the core effector components in the Notch signaling pathway, which represents their best characterized functional association (Bray and Furriols, 2001;Lai, 2002;Pursglove and Mackay, 2005). Even though it is obvious now that their engagements go beyond the Notch framework (see below), given the wealth of Notch-related experimental data, we will review the CSL family characteristics and features mostly in the "classical" (although likely only recently adopted in evolution) Notch-pathway context.

2.2.1 CSL family phylogeny

Until recently, the presence of CSL genes in the genome was considered to be something typically metazoan, particularly in connection with their elaborate multicellular developmental programs (Weinmaster and Kintner, 2003). Organisms ranging from sea urchins and worms to humans all have a CSL representative displaying a remarkable degree of evolutionary conservation (Fig. 2.2). Moreover, in most vertebrates there are actually two CSL paralogs present. While CBF1/RBP-Jκ participates in the Notch pathway, the precise role of the second paralog named RBP-L (for RBP-Jκ-like), which notably shows less sequence conservancy, is not well understood as yet. Unlike CBF1, which seems to be expressed ubiquitously, RBP-L is confined to only a few organs or tissues, and there are indications of its involvement in the development of pancreas (Beres *et al.*, 2006;Minoguchi *et al.*, 1997;Minoguchi *et al.*, 1999). The latest advancements in the field of the CSL family phylogeny come from this study and will be considered in Chapter 4.

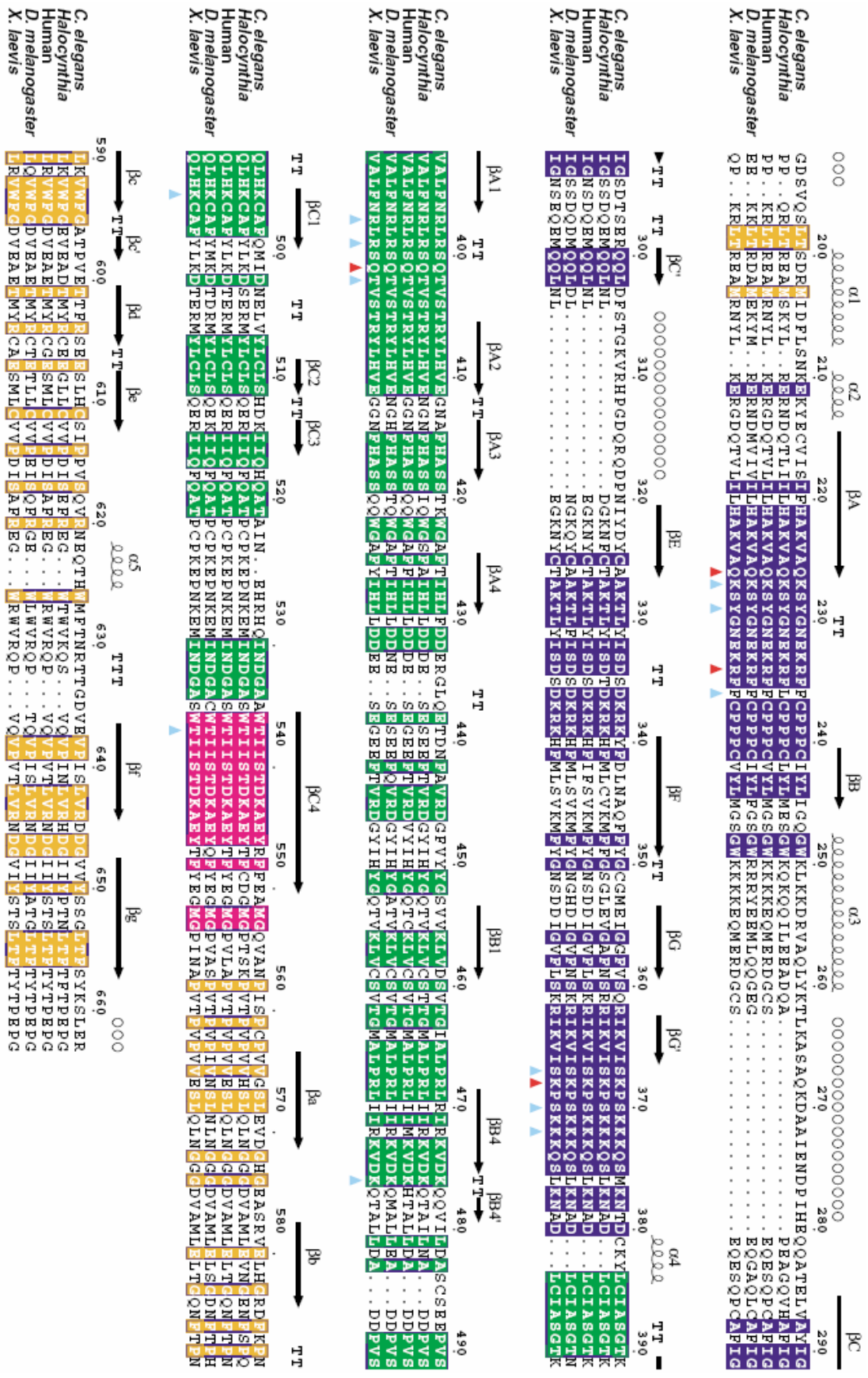

Figure 2.2 – Sequence alignment of CSL core regions from *C. elegans*, *Halocynthia* (tunicates), human, *D. melanogaster*, and *Xenopus laevis*. The domain boundaries are indicated by color (see Fig.

2.3) and secondary structural elements are noted above the sequence. DNA contacts are denoted by colored triagonals below the sequence alignment, red for specific DNA interactions and cyan for DNA backbone contacts (adapted from (Kovall and Hendrickson, 2004)).

2.2.2 CSL protein structure

The crystal structures of the DNA-bound CSL proteins from *C. elegans* and human were recently solved, also as co-crystals with fragments of NICD and the Mastermind coactivator (Kovall and Hendrickson, 2004;Nam *et al.*, 2006;Wilson and Kovall, 2006). The protein (~55-65 kDa depending on species) was found to have a unique fold constituted by three distinct domains, interconnected by a long beta-strand linker (Fig. 2.3). As suspected by earlier sequence comparisons, the N-terminal and C-terminal domains are related to the Rel-protein fold, thus the respective domains were designated RHR-N and RHR-C (for Rel-homology region). Surprisingly, a third domain was inserted in between the Rel-like domains that adopts a beta barrel fold and was designated BTD (beta-trefoil domain).

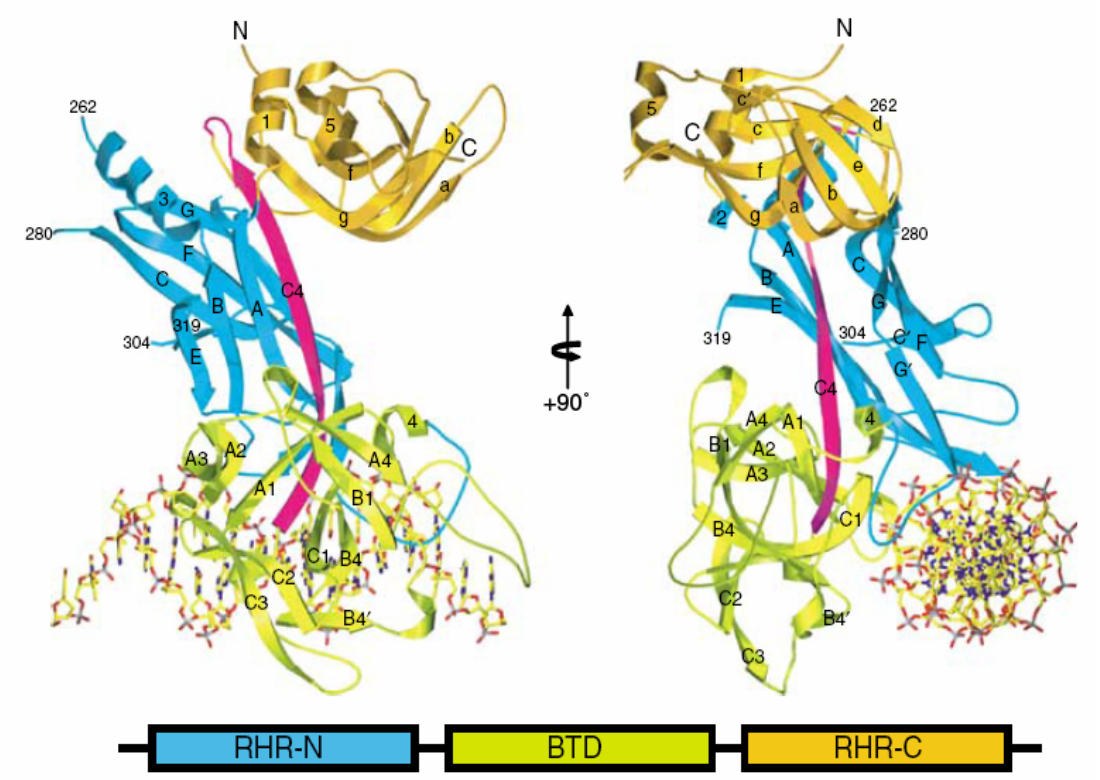

Figure 2.3 – Ribbon representation of the *C. elegans* CSL–DNA complex and domain organization. Orthogonal views are shown. A schematic representation of the domain arrangement is also shown (adapted from (Kovall and Hendrickson, 2004)).

RHR-N and BTD are responsible for binding to DNA, and specific residues mediating the protein-DNA interactions, both sequence-specific and those made with the DNA backbone, were identified (Fig. 2.2). A similar detailed mapping was performed for the known binding sites of various interaction partners (corepressors and coactivators) and most of them cluster to and around a conserved hydrophobic pocket on BTD. However, further interactions of the Mastermind and NICD coactivators with RHR-C were found (Kovall, 2007). Significantly, the regions of the CSL proteins being most conserved throughout evolution are those implicated in DNA binding (Fig. 2.4).

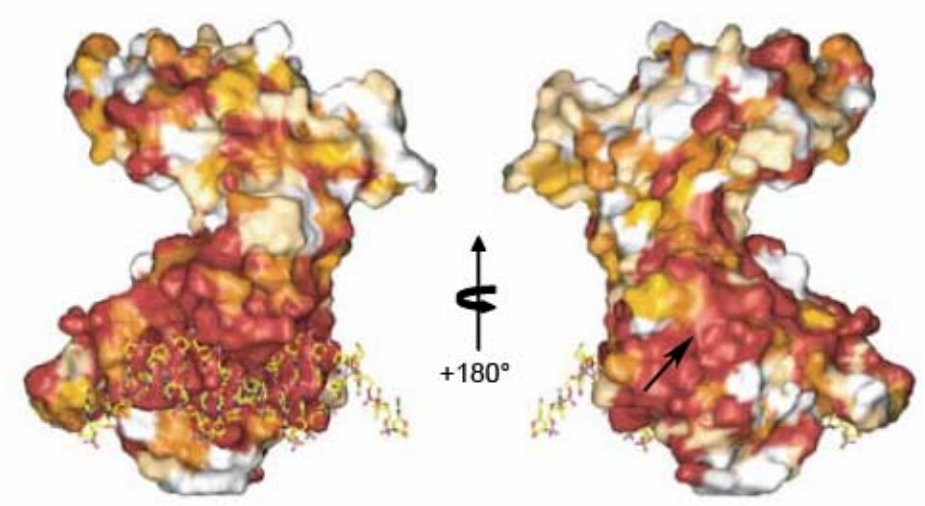

Figure 2.4 – CSL sequence conservation mapped to the molecular surface. Dark red, orange, yellow, and white represent regions of absolute identity, high and moderate similarity, and regions of no conservation, respectively. The protein–DNA interface is entirely conserved. The hydrophobic pocket (arrow) is also highly conserved (adapted from (Kovall and Hendrickson, 2004)).

2.2.3 DNA binding properties and target genes

CSL proteins were originally identified as factors binding to the immunoglobulin Jκ recombination signal sequence (recombination signal binding protein; RBP-Jκ) that consists of a conserved heptamer (CACTGTG) and an A/T-rich nonamer separated by a spacer of 23 bp (Hamaguchi *et al.*, 1989). A putative integrase-related motif was found in the RBP-Jκ amino acid sequence and thus a hypothesis was presented that CSL proteins may participate in the process of immunoglobulin gene recombination (Kawaichi *et al.*, 1992;Matsunami *et al.*, 1989). However, subsequent studies failed to detect any DNA-modifying activity for RBP-Jκ, apart from a reported ligase activity that is rather dubious in the light of more

recent findings (Hamaguchi *et al.*, 1992). Later on, a mutational analysis of Suppressor of Hairless (Su(H)), the drosophila CSL ortholog, ruled out functional significance of the integrase-related motif (Schweisguth *et al.*, 1994). Furthermore, the initially reported CSL binding preferences for the Jκ recombination signal proved to be an artifact caused by the introduction of a *Bam*HI site next to the heptamer sequence, which resulted in the appearance of a suboptimal CSL-binding site (cactGTG+GGAtcc) (Henkel *et al.*, 1994;Honjo, 1996;Matsunami *et al.*, 1989). Additional extensive analyses of the CSL DNA-binding properties yielded the GTG(G/A)GAA canonical response element as we know it today together with a number of more or less variant non-canonical sites such as TGGGAAA, TGGGAAAGAA or CATGGGAA (Barolo *et al.*, 2000;Dou *et al.*, 1994;Lam and Bresnick, 1998;Lee *et al.*, 2000;Morel and Schweisguth, 2000;Oswald *et al.*, 1998;Shirakata *et al.*, 1996;Tun *et al.*, 1994). The mammalian RBP-L paralog seems to have similar target site requirements (Beres *et al.*, 2006). The resolution of the CSL crystal structure brought a molecular-level understanding of the interactions between the CSL proteins and their recognition sequences on DNA (Fig 2.5) (Kovall and Hendrickson, 2004). The murine RBP-Jκ protein was found to bind DNA as a monomer (Chung *et al.*, 1994), however, recent data indicate that cooperative binding with other factors may occur, and the precise architecture of the binding site(s) is also of importance (Miyatsuka *et al.*, 2007). It is also worth noting that the mammalian RBP-Jκ family member was identified in another, independent study as CBF1 – a protein binding to the C promoter in the Epstein-Barr virus genome (Henkel *et al.*, 1994). Therefore, due to the reasons described above, the CBF1 designation should preferentially be used.

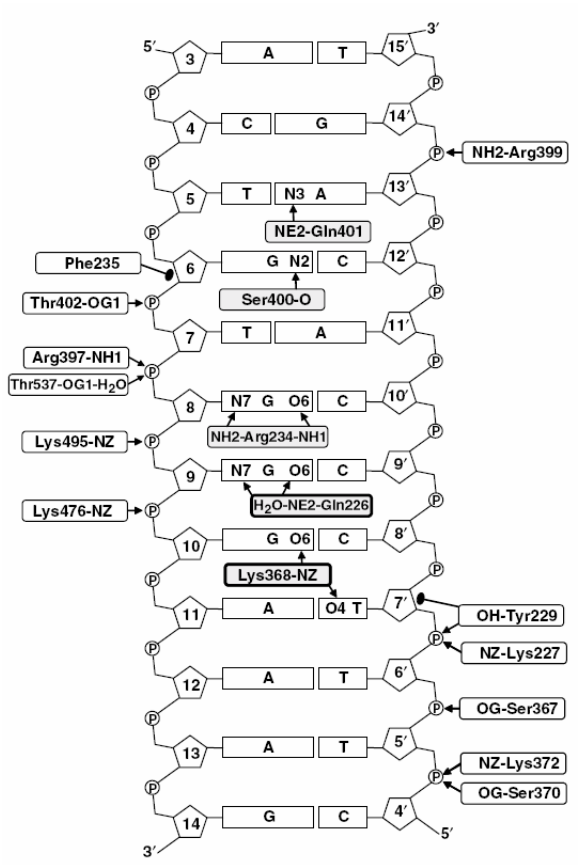

Figure 2.5 – Schematic representation of all protein–DNA interactions in the CSL–DNA complex. Specific interactions with the DNA bases are shaded in gray and nonspecific interactions are clear boxes. Hydrogen-bonding or salt-bridge interactions are denoted as an arrow and Van der Waals interactions are depicted as closed circles (adapted from (Kovall and Hendrickson, 2004)).

Most of the CSL target genes identified up to now seem to be regulated in the context of the Notch signaling pathway. These include the members of the HES (Hairy/Enhancer of Split) and HERP (HES-related repressor protein) families of transcriptional repressors of the basic Helix-loop-Helix (bHlH) type. They function as downstream effectors in the signaling cascade triggered by the Notch receptor activation and regulate negatively the expression of yet another type of developmental, in this case activatory, bHlH genes. Also, elaborate autoregulatory loops can be identified in these processes (Iso *et al.*, 2003;Oswald *et al.*, 1998;Yoo and Greenwald, 2005). Other putative CSL-responsive genes were identified or proposed based on their expression levels being regulated by Notch signaling or by the demonstration of CSL binding to their promoter sequences. Among these additional (putative) targets are MHC class I, CD21, CD23, interleukin 6, β-globin, erbB-2, NF-κB2, cyclin D1, NRARP and even microRNA genes (Chen *et al.*,

1997;Iso *et al.*, 2003;Kannabiran *et al.*, 1997;Lam and Bresnick, 1998;Lamar *et al.*, 2001;Oswald *et al.*, 1998;Plaisance *et al.*, 1997;Ronchini and Capobianco, 2001;Shirakata *et al.*, 1996;Yoo and Greenwald, 2005). Recently, Notch-independent functions were described for CSL proteins as well (Barolo *et al.*, 2000;Beres *et al.*, 2006;Kaspar and Klein, 2006;Koelzer and Klein, 2003). Both CBF1/RBP-Jκ and RBP-L were implicated in a Notch-independent regulation of the pancreas development, and a novel compound binding site was determined in the promoters of several genes encoding digestive enzymes and a homeobox developmental regulator. This novel site is recognized by the PTF1 trimeric transcription factor composed of either CBF1/RBP-Jκ or RBP-L, P48/PTF1a (a pancreas and neural-restricted bHlH protein), and a common class A bHlH protein (Beres *et al.*, 2006;Miyatsuka *et al.*, 2007). The discovery of CSL functions outside the Notch pathway is interesting from the evolutionary point of view as, since the advent of Notch is a rather recent event, these may be closer to the ancestral function of the CSL family.

2.2.4 CSL interaction partners and molecular function

Using biochemical and immunocytochemical techniques, CSL proteins have been shown to be predominantly nuclear in various metazoan organisms and cell lines. There are reports of CSL localization adopting a speckled pattern within the cell nucleus and CSL signal also colocalized with nucleoli in some cell lines (Chen *et al.*, 1997;de la Pompa *et al.*, 1997;Hsieh *et al.*, 1999;Zhou and Hayward, 2001). Some studies report partial cytoplasmic localization of CSL proteins, which seems to be dependent on the availability of specific interaction partners (Gho *et al.*, 1996;Obata *et al.*, 2001;Zhou and Hayward, 2001). Apart from the notorious NICD, a large set of CSL interacting proteins have been identified so far, and they affect the CSL function in various ways. Some of these partners bind directly to CSL proteins and some represent indirect interactions bridged by other constituents of interacting protein complexes. Both inhibitory and activatory CSL complexes contain the SNW/SKIP protein that is involved in the regulation of transcription activation and elongation, and also in pre-mRNA splicing (Folk *et al.*, 2004;Zhou *et al.*, 2000). In the absence of NICD, CSL proteins interact with the SMRT/NCoR corepressors that recruit a repressor complex containing Sin3A, SAP30, HDAC1/2 and CIR (identified as a CBF1-interacting repressor and later classified as an SR protein implicated in

alternative splicing) and turns the target gene expression off (Hsieh *et al.*, 1999;Kao *et al.*, 1998). Several additional factors were shown to exert a negative effect upon CSL functioning. These include the MINT/SHARP and NRARP negative regulators (Kuroda *et al.*, 2003;Lamar *et al.*, 2001;Oswald *et al.*, 2002), and the drosophila-specific Hairless and mammalian KyoT2 proteins that inhibit the CSL binding to DNA (Brou *et al.*, 1994;Taniguchi *et al.*, 1998). There is also evidence showing that CSL proteins may contact directly the basal transcription machinery (subunits of TFIID and TFIIA) and thereby prevent gene expression (Olave *et al.*, 1998). Upon the Notch receptor activation and cleavage, NICD displaces the SMRT/NCoR corepressor from CSL at the target promoter, resulting in its derepression, and recruits the Mastermind/LAG-3 coactivator instead. Mastermind forms a tripartite complex with CSL and NICD and, as a consequence, the target gene is turned on by the further recruitment of the CBP/p300 histone acetyl transferases. Interestingly, Mastermind also downregulates NICD by inducing its phosphorylation and subsequent degradation in the proteasome, thus resetting the regulatory circuit (Fryer *et al.*, 2004;Lai, 2004;Petcherski and Kimble, 2000). The CSL repression/activation switch mechanism is depicted schematically in Fig. 2.6. As mentioned above, several clinically important viruses have taken use of this pathway as well. For example, the Epstein-Barr virus, Kaposi's sarcoma-associated herpesvirus and adenovirus encode protein factors capable of binding to CSL proteins and exploiting them to help the viral replication cycle (Ansieau *et al.*, 2001;Hsieh *et al.*, 1996;Liang *et al.*, 2002;Zhang *et al.*, 2001;Zhao *et al.*, 1996).

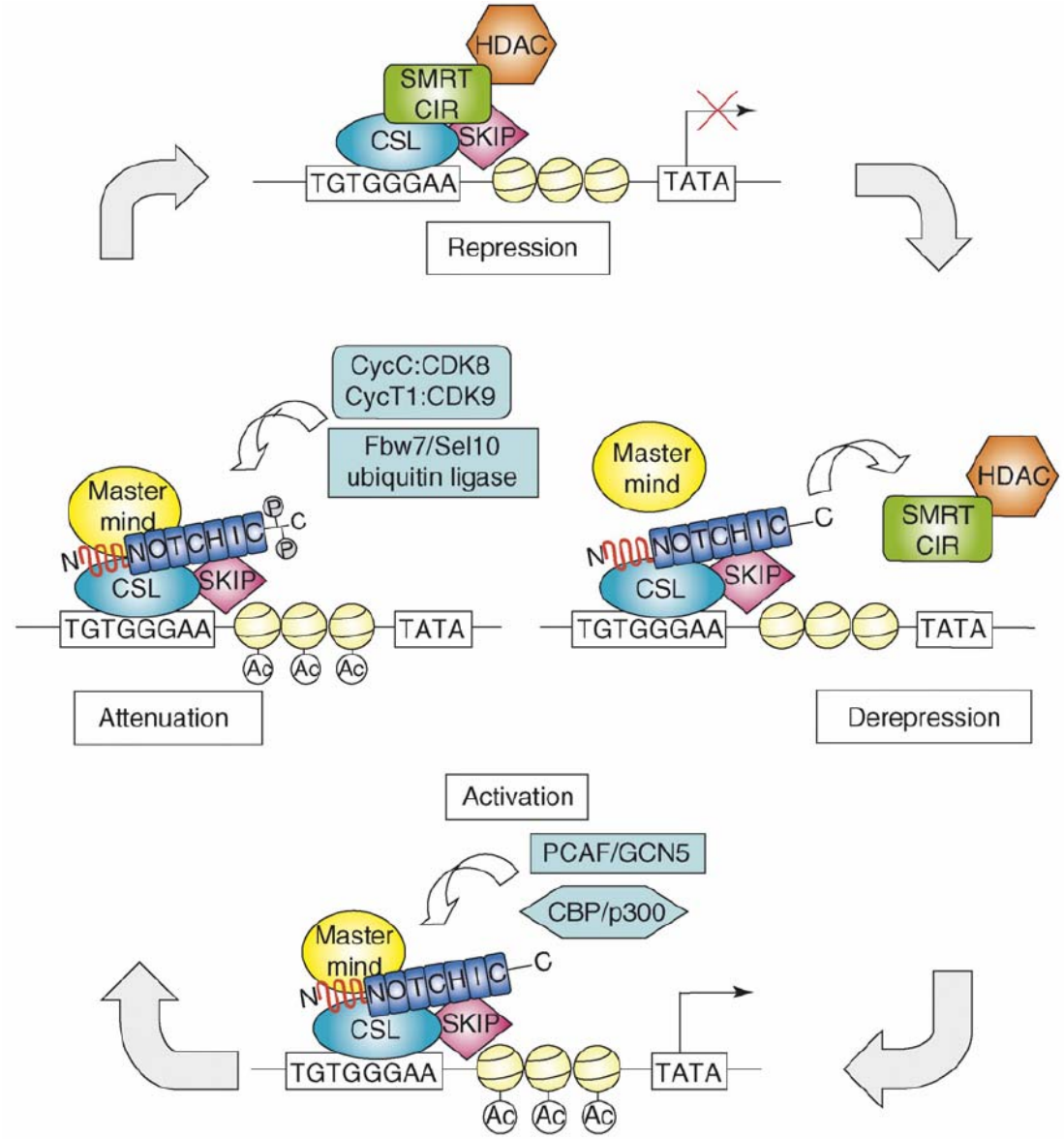

Figure 2.6 – Schematic diagram of CSL-mediated transcriptional regulation. Top: DNA-bound CSL represses transcription of Notch target genes by recruiting corepressors (e.g., SMRT or CIR) and HDACs. Right: NICD (NotchIC) displaces corepressors from CSL upon pathway activation and recruits Mastermind to the complex. Bottom: the CSL–NICD–Mastermind ternary complex activates transcription by recruiting general transcription factors. Left: signaling is turned off by phosphorylation and degradation of NICD (adapted from (Kovall, 2007)).

3 *MATERIALS AND METHODS*

3.1 Microorganisms and cultivations

3.1.1 *Escherichia coli* - cultivation, transformation and protein expression

Bacteria (see Table 3.1) were cultured in the standard LB liquid medium (10 g/l peptone, 5 g/l yeast extract, 5 g/l NaCl) or on Nutrient Agar plates (4% Živný agar č. 2, Imuna, Slovakia) at 37°C. Ampicillin (100 μg/ml) was added to the media where appropriate.

Transformations were carried out by electroporation using the Gene Pulser Apparatus (Bio-Rad) at 25 μF, 2.5 kV and 200 Ω.

Recombinant protein expression was induced with 0.5-1 μM IPTG at 30°C (or at room temperature for His-Cbf12) for 30-60min. Optimal inducer concentrations and induction times were in the lower/shorter range for His-Cbf11 and in the higher/longer range for His-Cbf12, respectively.

Table 3.1 – *E. coli* strains used.

Name	Genotype	Source
DH5α	F^- ϕ80*lac*ZΔM15 Δ(*lac*ZYA-*arg*F)U169 *rec*A1 *end*A1 *hsd*R17(r_K^-, m_K^+) *pho*A *sup*E44 *thi*-1 *gyr*A96 *rel*A1 λ^-	lab stock
BL21(DE3)	F^- *omp*T *gal dcm lon hsd*S_B(r_B^- m_B^-) λ(DE3 [*lac*I *lac*UV5-T7 gene 1 *ind*1 *sam*7 *nin*5])	lab stock

3.1.2 *Saccharomyces* cerevisiae - cultivation, transformation, protein expression and 2H

S. cerevisiae cells (see Table 3.2) were grown in the standard rich YPAD (20 g/l peptone, 10 g/l yeast extract, 2% glucose, 100 μg/l adenine) and minimum SD (6.7 g/l yeast nitrogen base w/o amino acids + appropriate Drop-out Supplement) media at 30°C. Solid media were prepared from the liquid media by adding 2-3% agar.

Transformations were carried out using the lithium acetate method as described (Ito *et al.*, 1983).

For inducible expression from the pYES2 vector SD plates with galactose/raffinose as a carbon source were used.

For the yeast two-hybrid analyses two different systems, both by Clontech, were used according to the manufacturer's instructions – the MATCHMAKER Two-Hybrid System 2 (Gal4-based) and the MATCHMAKER LexA Two-Hybrid System.

Table 3.2 – *S. cerevisiae* strains used.

Name	Genotype	Source
CG-1945	*MATa ura3-52 his3-200 ade2-101 lys2-80 trp1-901 leu2-3,112 gal4-542 gal80-538 cyhr2 LYS2::GAL*$_{UAS}$*-GAL1*$_{TATA}$*-HIS3 URA3::GAL4*17-mers(x3)-*CYC1*$_{TATA}$*-lacZ*	Clontech
EGY48	*MATα ura3 his3 trp1 LexA*(6xop)*-LEU2*	Clontech
AH109	*MATa trp1-901 leu2-3, 112 ura3-52 his3-200 gal4Δ gal80Δ LYS2::GAL1*$_{UAS}$*-GAL1*$_{TATA}$*-HIS3 GAL2*$_{UAS}$*-GAL2*$_{TATA}$*-ADE2 URA3::MEL1*$_{UAS}$*-MEL1*$_{TATA}$*-lacZ MEL1*	Clontech

3.1.3 *Schizosaccharomyces pombe*

3.1.3.1 Cultivation, transformation and protein expression

Fission yeast strains (see Table 3.3) were cultured in the standard rich YES (0.5% yeast extract, 3% glucose, auxotrophic supplements as needed) and minimum MB (Formedium) media. Solid media were prepared from the liquid media by adding 2-3% agar. The G418 (100 μg/ml, Sigma) and/or ClonNAT (90 μg/ml, Werner Bioagents) antibiotics were added to YES for selection purposes where required. The standard cultivation temperature was 30°C.

For long-term storage cells were kept in 30% glycerol at -80°C, working batch of cells was kept at 10°C for up to 6 months. Freshly grown cells were prepared prior to each experiment. In some experiments, 5 μg/ml phloxin B, a red dye staining preferentially dead cells, was added to the media. Fission yeast diploid cultures contain a higher proportion of dead cells and therefore stain darker with phloxin B than haploids (Forsburg, 2003).

Where required, tenfold serial dilutions (10^5-10^1 cells) were prepared of washed cells from exponentially growing liquid cultures and spotted on the desired solid media.

Transformations were carried out using the lithium acetate method modifications as described (Bahler *et al.*, 1998;Morita and Takegawa, 2004;Van Driessche *et al.*, 2005).

For inducible tagged protein expression the thiamine-repressible pREP-based vector series were used (Craven *et al.*, 1998) and the standard cultivation protocol was observed (Basi *et al.*, 1993).

3.1.3.2 Conjugation and sporulation

Diploid strains were prepared by spotting a mixture of h^+ and h^- cells (having different *ade6* mutant alleles) on MES plates (3% malt extract, supplements as needed except lysine, pH adjusted to 5.5 with NaOH). Plates were incubated for 1-3 days at room temperature and cells were then replated on $MB_{-ade+thiamin}$ medium allowing for the growth of diploids (cross-complemented adenine prototrophs) only. Selected emerging diploid clones were kept on YES.

Synchronous induction of sporulation in shaken culture was performed by growing diploid cells in YES at 30°C to OD 0.5, washing them twice with $MB_{-ade-thiamin}$ medium and resuspending them in $MB_{-ade-thiamin}$ followed by further cultivation as required.

The ability to form spores was tested on solid $MB_{-ade+thiamin}$ medium. Diploid monocolonies were grown and allowed time to sporulate (1 week, 30°C). The plates were then treated with iodine vapors, whereby sporulating colonies turn dark brown.

The Δ*cbf11* Δ*cbf12* double mutants were prepared by crossing the respective single mutant strains and performing tetrad analyses of the resulting asci using a micromanipulator. The mating type of the resulting strains was determined by colony PCR using the primers mt1, mm and mp (adapted from (D'Alessio *et al.*, 2003), see Table 3.8).

3.1.3.3 Adhesivity and flocculation assays

Cells were spotted or patched on YES or $MB_{-ura-thiamin}$ plates and grown at 30°C for various times. The adhesivity assay (based on a protocol described in (Guldal and Broach, 2006)) consisted of washing the plates evenly with a stream of water for 1 min. The spot cell mass remaining attached to the plate was then

documented by photography or microphotography using an Olympus CK2 light microscope with an Olympus SP-350 digital camera attached to it.

For flocculation assays, cells were grown in the appropriate YES or MB liquid media, either to the logarithmic or stationary phase, as required. Aggregation was monitored visually and the cell suspension was then transferred to a Petri dish for photography. The sugar-competition assays were performed as described in (Tanaka *et al.*, 1999). Cells from liquid culture were harvested, washed in 10 mM EDTA, and then in deionized water. Flocculation was initiated by the addition of 10 mM $CaCl_2$ in the presence or absence of 100 mM sugars. Cultures were transferred to a Petri dish for imaging.

Table 3.3 – *S. pombe* strains created and used.

Name	**Genotype**	**Source**
PN558	*h^+ leu1-32 ura4-D18 ade6-M210*	A. Decottignies (Decottignies *et al.*, 2003)
PN559	*h^- leu1-32 ura4-D18 ade6-M216*	A. Decottignies (Decottignies *et al.*, 2003)
CBF11 KO	*h^- leu1-32 ura4-D18 ade6-M216 Δcbf11::kan^r*	A. Decottignies (Decottignies *et al.*, 2003)
FY254	*h^- leu1-32 ura4-D18 ade6-M210 can1-1*	S. Forsburg
MP01	*h^+ leu1-32 ura4-D18 ade6-M210 Δcbf12::pCloneNat1*	This study
MP02	*h^+ leu1-32 ura4-D18 ade6-M210 Δcbf12::pCloneNat1*	This study
MP03	*h^- leu1-32 ura4-D18 ade6-M216 Δcbf12::pCloneNat1*	This study
MP04	*h^- leu1-32 ura4-D18 ade6-M216 Δcbf12::pCloneNat1*	This study
MP05	*h^+ leu1-32 ura4-D18 ade6-M216 Δcbf11::kan^r*	This study
MP06	*h^+ leu1-32 ura4-D18 ade6-M210 Δcbf11::kan^r*	This study
MP07	*h^+ leu1-32 ura4-D18 ade6-M210 Δcbf11::kan^r Δcbf12::pCloneNat1*	This study
MP08	*h^+ leu1-32 ura4-D18 ade6-M216 Δcbf11::kan^r Δcbf12::pCloneNat1*	This study
MP09	*h^- leu1-32 ura4-D18 ade6-M210 Δcbf11::kan^r Δcbf12::pCloneNat1$^-$*	This study
MP10	*h^- leu1-32 ura4-D18 ade6-M216 Δcbf11::kan^r Δcbf12::pCloneNat1*	This study
MP12	*h^- leu1-32 ura4-D18 ade6-M216 cbf12$^+$::EGFP-kan^r*	This study
MP13	*h^- leu1-32 ura4-D18 ade6-M216 cbf12$^+$::EGFP-kan^r*	This study
MP14	*h^- leu1-32 ura4-D18 ade6-M216 cbf12$^+$::EGFP-kan^r*	This study

MP15	*h⁻ leu1-32 ura4-D18 ade6-M216 cbf11⁺::CTAP4-natʳ*	This study
MP16	*h⁻ leu1-32 ura4-D18 ade6-M216 cbf11⁺::CTAP4-natʳ*	This study
MP17	*h⁻ leu1-32 ura4-D18 ade6-M216 cbf12⁺::CTAP4-natʳ*	This study
MP18	*h⁻ leu1-32 ura4-D18 ade6-M216 cbf12⁺::CTAP4-natʳ*	This study
MP19	*h⁻ leu1-32 ura4-D18 ade6-M216 cbf12⁺::CTAP4-natʳ*	This study

3.2 Protein techniques

3.2.1 Protein concentration measurement

Concentration of proteins was measured spectrophotometrically using the ROTI-Nanoquant (Carl-Roth) or DC Protein Assay (Bio-Rad) kits according to the manufacturers' instructions.

3.2.2 Affinity purification of His-tagged proteins

His-tagged proteins were isolated from cell lysates with the TALON Superflow Metal Affinity Resin (Clontech). The isolation protocol is a modification of the one recommended by the manufacturer:

S. pombe

1. Grow 50 ml of culture to OD 0.5 ($5x10^8$ cells) and harvest by centrifugation.
2. Wash cells in 5 ml STOP buffer and spin again.
3. Resuspend in 40 µl EQ buffer and disrupt by vortexing with acid-washed beads.
4. Add 2 ml of EQ buffer, transfer the suspension to a new tube and sonicate 3x 20 sec on ice.
5. Incubate 30-60 min on ice.
6. Pellet cell debris, transfer the supernatant to a new tube and centrifuge for 20 minutes at 20,000 g, 4°C.
7. Take the supernatant and add washed TALON resin to the cleared lysates. Incubate for 30 min with agitation, 4°C.
8. Spin 5 min, 700 g, 4°C and wash the resin with 1 ml WASH1 buffer. Incubate 10 min with agitation, 4°C.
9. Repeat the washing with the WASH2 buffer.
10. Pellet the resin at 700 g, 4°C and elute into 200 µl buffer EB1. Incubate 10 min with gentle agitation, 4°C.

11. Repeat the elution with the EB2 buffer.

E. coli

1. Grow 50 ml cells to OD 0.8, induce expression with IPTG and harvest by centrifugation.
2. Resuspend in 2 ml EQ buffer and sonicate 3x 20 sec on ice.

Continue with step 5 as above.

Solutions needed:

Protease inhibitors (1000x)	250 mg/ml Pefabloc SC, 5 mg/ml leupeptin, 5 mg/ml aprotinin, 5 ml/ml pepstatin A, 0.2 M PMSF
STOP	50 mM NaF, 1 mM NaN_3, 25 mM Hepes pH 7.0, 150 mM NaCl
EQ	25 mM HEPES pH 7.6, 400 mM KCl, 1 M urea, 0.5% Triton-X 100, 20% glycerol, 3.5 mM β-mercaptoethanol, protease inhibitors
WASH1	EQ, 20 mM imidazole
WASH2	EQ, 50 mM imidazole
EB1	EQ, 150 mM imidazole
EB2	EQ, 300 mM imidazole

3.2.3 Protein electrophoresis

Proteins were separated by SDS-PAGE using the Mini-Protean 3 apparatus (Bio-Rad) and the standard Tris-glycine buffer system. 7.5-12% non-gradient gels were used as required. Proteins were stained either with Coomassie Brilliant Blue G-250 (Bio-Rad) or the PageSilver Silver Staining Kit (Fermentas) according to the manufacturers' instructions.

3.2.4 Western blotting and immunodetection

Proteins were transferred to a nitrocellulose membrane using the Mini Trans-Blot Module (Bio-Rad) and membranes were blocked with 2-3% milk. Appropriate primary and secondary antibodies (see Tables 3.4 and 3.5) were applied and blots were developed by either the alkaline phosphatase reaction (BCIP and NBT

substrates; Bio-Rad) or with the ECL Western Blotting Detection Reagents (Amersham) according to the instructions of the manufacturers.

Table 3.4 – Primary antibodies used.

Name / Specificity	Dilution	Source (Cat. no.)
anti c-Myc 9E10 ascites fluid (mouse monoclonal)	-	lab stock
HA probe Y-11 (rabbit polyclonal)	1 : 600	Santa Cruz Biotechnology (sc-805)
anti HA.11, purified (mouse monoclonal)	1 : 1000	Covance (MMS-101P)
anti GFP (FL), biotinylated (rabbit polyclonal)	1: 200	Santa Cruz Biotechnology (sc-8334)
anti His hybridoma supernatant (mouse monoclonal)	1 : 5	gift of Prof. W. Nellen, Kassel University, Germany
His•Tag antibody (mouse monoclonal)	1 : 1000	Novagen (70796)
Anti-polyHistidine antibody HIS-1 (mouse monoclonal)	1 : 1000	Sigma (H1029)
anti-TAP antibody (rabbit polyclonal)	1 : 10000	Open Biosystems (CAB1001)

Table 3.5 – Secondary antibodies used.

Name / Specificity	Dilution	Source (Cat. no.)
goat anti-mouse IgG-AP conjugate, IgG (H+L)	1 : 3000	Bio-Rad (170-6520)
goat anti-rabbit IgG-AP conjugate, IgG (H+L)	1 : 3000	Bio-Rad (170-6518)
goat anti-mouse IgG-HRP	1 : 4000	Santa Cruz Biotechnology (sc-2031)
Immun-Star goat anti-rabbit-HRP conjugate	1 : 4000	Bio-Rad (170-5046)

3.3 DNA and RNA techniques

3.3.1 DNA isolation and purification

Small scale plasmid isolations were carried out using the NucleoSpin Plasmid kit (Macherey-Nagel), which was also used for the purification of plasmid DNA prior to sequencing. Large scale plasmid preparations were performed using the standard alkaline extraction method (Birnboim and Doly, 1979) with an additional purification step comprising of precipitating protein impurities with 5 M lithium chloride. Every plasmid isolation was followed by restriction analysis confirming the plasmid's identity.

Double-stranded DNA fragments were purified from agarose gels using the NucleoSpin Extract kit (Macherey-Nagel). The same kit was used for post-reaction clean-up of PCR products and DNA fragments after various other enzymatic reactions.

3.3.2 RNA isolation and purification, microarray analyses

For qRT-PCR analyses, total fission yeast RNA was extracted using the FastPrep instrument (Q-BIOgene) and the RNeasy Mini kit supplemented with the RNase-free DNase set (Qiagen).

RNA for microarray analyses was prepared according to the protocol supplied by Dr. Jürg Bähler, Wellcome Trust Sanger Institute, UK:

1. Harvest cells (usually 25 ml of OD_{600} ~0.2, adjust volume according to OD). Centrifuge 2 min at 2000 RPM and discard supernatant. Snap freeze pellet (liquid nitrogen or dry ice/ethanol). Alternatively, filter cells and snap freeze filter disc. Store cells at -70°C.
2. Thaw cells on ice (~5 min). Add 1 ml of pre-chilled DEPC water, resuspend cells, and transfer to 2 ml eppendorf tubes. Spin 10 sec at 5000 RPM and remove supernatant.
3. To pellet add 750 µl of TES (adjust if total cells are >5 ODs), resuspend cells with pipette, immediately add 750 µl acidic phenol-chloroform (refrigerated, Sigma P-1944), vortex, and incubate in 65°C heat block (use fume hood!). Then do the next sample in the same way.
4. Incubate all samples in 65°C heat block for 1 hr, vortex 10 sec every 10 min.
5. Place samples on ice for 1 min, vortex 20 sec, and centrifuge for 15 min at 14,000 RPM at 4°C.
6. Pre-spin 2 ml yellow phase-lock (heavy) tubes (Eppendorf) for 10 sec. Add 700 µl of acidic phenol-chloroform.
7. Take 700 µl of the water phase from step 5 and add to the phase-lock tubes from step 6, thoroughly mix by inverting (no vortexing), and centrifuge 5 min at 14,000 RPM at 4°C.
8. Pre-spin 2 ml phase-lock tubes as in step 6. Add 700 µl of chloroform:isoamyl alcohol (24:1) (under fume hood, Sigma C-0549).
9. Take 700 µl of the water phase from step 7 and add to the phase-lock tubes

from step 8, thoroughly mix by inverting (no vortexing), and centrifuge 5 min at 14,000 RPM at 4°C.

10. Prepare normal 2 ml eppendorf tubes with 1.5 ml of 100% ethanol (-20°C) and 50 µl of 3 M NaAc pH 5.2.
11. Transfer 500 µl of water phase from step 9 to the tubes from step 10, vortex 10 sec. Samples can be precipitated at -20°C overnight (or at -70°C for 30 min).
12. Centrifuge for 10 min at 14,000 RPM at room temperature. Discard supernatant, add 500 µl 70% ethanol (4°C, made with DEPC water), don't vortex, just add, and spin for 1 min (same tube orientation!). Aspirate most supernatant, spin 5 sec, and remove rest of liquid with pipette. Air dry 5 min at room temperature.
13. Add 100 µl of DEPC water, and incubate 1 min at 65°C (or 10 min at room temperature). Dissolve pellet first by pipetting up and down (~30x) until no particles are left, then gently vortex 10 sec.
14. Measure $OD_{260/280}$: add 5 µl to 995 µl DEPC water (1:200), set reference with water in 500 µl glass cell, then measure RNA (OD should be >0.1). Rinse cell with 0.1 M NaOH, 0.1 M HCl, and thoroughly with ddH_2O.
15. Expect ~400 µg of RNA in total, but it may be less for RNA isolated under some conditions. Use 100 µg of your RNA for Qiagen purification (see step 16). Measure the volume of the remaining RNA, add 3 volumes of 100% ethanol and store at -70°C as a backup.
16. Purify 100 µg of each of your RNAs using RNeasy mini spin columns (Qiagen) as described in the RNeasy Mini Handbook (p. 48-49). Elute twice with 30 µl RNase-free water. Keep on ice!
17. Run 2 µl of purified RNA on a 1% agarose gel (wipe gel apparatus/tray with RNAse-Zap, rinse with water and use new TBE buffer, use RNAse-free loading buffer made with DEPC water). You should see the two ribosomal bands clean, distinct and without smears.
18. Measure $OD_{260/280}$ of purified RNA: add 2 µl to 100 µl DEPC water (1:50), set reference with water in 50 µl glass cell, then measure RNA (OD should be >0.1; ratios 260/280 >1.8). Rinse cell with 0.1 M NaOH, 0.1 M HCl, and thoroughly with ddH_2O.
19. Add DEPC water to every sample such that the end concentration is 20 µg

RNA/13.9 µl.

20. From each sample, use ~50% of your RNA to make up a reference pool by combining equal amounts (e.g., 40 µl) from every timepoint. Mix and make up 12.9 µl aliquots stored at -70°C (ready to use for labeling). Make up 13.9 µl aliquots if not using bacterial control RNA for labeling.
21. With the rest of your RNA, make up 12.9 µl aliquots of each sample and immediately store at -70°C (ready to use for labeling). Make up 13.9 µl aliquots if not using bacterial control RNA for labeling.

TES 10 mM Tris pH 7.5, 10 mM EDTA pH 8, 0.5% SDS
(do not treat Tris stock with DEPC, just use DEPC treated water to make solution; store at room temperature)

The procedure was carried out up to the step 15. The quality of the isolated RNA was checked on a native agarose gel. Aliquots of ~200 µg RNA in 70% ethanol (room temperature) were then sent for analysis to the laboratory of Dr. Jürg Bähler. In-house spotted oligonucleotide arrays were used for the analysis of transcriptome (Lyne *et al.*, 2003). Two biological repetitions were performed for each system (a different media batch used each time, independent RNA isolations, the c-DNA-labeling dyes swapped between the repetitions)

3.3.3 DNA modifying enzymes and procedures

The enzymes (see Table 3.6) were used according to the manufacturers' specifications.

Radioactive terminal labeling of DNA probes was performed using the T4 polynucleotide kinase and γ-^{32}P-ATP (3000 Ci/mmol, 10 µCi/µl). Free radioactive nucleotides were removed by purification on NICK Columns (Amersham).

Most cloning procedures were carried out using the T4 DNA ligase and some PCR products were cloned using the TOPO TA Cloning kit (Invitrogen).

Table 3.6 – DNA modifying enzymes used.

Enzyme	**Source**
restriction endonucleases	Fermentas
T4 polynucleotide kinase	Fermentas

shrimp alkaline phosphatase	USB
T4 DNA ligase	Fermentas
micrococcal nuclease	Fermentas
ribonuclease from bovine pancreas	Reanal
Klenow fragment	Fermentas

3.3.4 PCR and quantitative RT-PCR

3.3.4.1 PCR

The enzymes (see Table 3.7) were used according to the manufacturers' specifications; the primers (see Table 3.8) were used in 0.3-1 μM final concentration. Reactions were run on the Peltier PTC-200 gradient thermal cycler (MJ Research).

Typically, the $MgCl_2$ concentration of 1.5 mM was used. For colony PCR (bacteria, yeast) and amplification from fission yeast chromosomal DNA, 3 mM $MgCl_2$ was present in the reaction. The amplification of the GC-rich nourseothricin resistance cassette was performed with the addition of 5% DMSO and using a special program as described (Janke *et al.*, 2004;Van Driessche *et al.*, 2005).

All PCR-mediated cloning was followed by sequencing verification.

3.3.4.2 Quantitative real-time RT-PCR

2 μg of total RNA were reverse-transcribed with the RevertAid First Strand cDNA Synthesis Kit (Fermentas) and an oligo(dT) primer (total reaction volume 20 μl), 1 μl of cDNA was then used for amplification. Approximately 200 bp of the 3'-regions of *cbf11*$^+$ (mp35, mp45), *cbf12*$^+$ (mp36, mp46) and *act1*$^+$ (mp37, mp38; normalization control) were amplified in separate tubes using the primers indicated (see Table 3.8 for details). The efficiency and linear range of the qRT-PCR was tested as described (Livak and Schmittgen, 2001). The qRT-PCR analysis was performed using the iQ SYBR Green Supermix (Bio-Rad) in the RotorGene 2000 system (Corbett Research) with 0.3 μM each primer and the following program: 95°C for 3 min, 40× (95°C for 30 sec; 53°C for 30 sec; 72°C for 30 sec). Two to four biological repeats were performed, the reactions were run in triplicates and the data were analyzed in the Q-Gene software application (Muller *et al.*, 2002).

Table 3.7 – PCR and qRT-PCR systems used.

System	Source
Taq DNA polymerase	Fermentas
TaKaRa rTaq	TaKaRa
Expand High Fidelity PCR system	Roche
Taq DNA polymerase	gift of Prof. W. Nellen, Kassel University, Germany
RevertAid First Strand cDNA Synthesis Kit	Fermentas
iQ SYBR Green Supermix	Bio-Rad

Table 3.8 – Oligonucleotide primers used.

Primer	Sequence	Purpose
mp20	GTAGGATCCTATGGGGGACTATTTTG	*cbf11*$^+$ cDNA construction (exon 1, fwd, *S. pombe* plasmids)
if03	GTAGGATCCATATGGGGGACTATTTTG	*cbf11*$^+$ cDNA construction (exon 1, fwd, two-hybrid)
mp25	CCATTATTTATGTTGTCCAAGTTCAACTGATTTA AATTTAAGG	*cbf11*$^+$ cDNA construction (exon 1, rev)
mp26	CCTTAAATTTAAATCAGTTGAACTTGGACAACA TAAATAATGG	*cbf11*$^+$ cDNA construction (exon 2, fwd)
if04	GAAGGATCCTCAGTTTCCAAAAGCAC	*cbf11*$^+$ cDNA construction (exon 2, rev)
if05	GTAGAATTCCATATGTCCCCAAACGTTC	*cbf12*$^+$ ORF (fwd)
if06	GCCAGATCTTAGTGACTTTCCAAAGG	*cbf12*$^+$ ORF (rev)
mp27	TATGCTGGACTATAGTGGGC	*cbf11*$^+$ KO verification (ORF, fwd)
mp28	GATACAGCAACTCCTCCCG	*cbf11*$^+$ KO, KI verification (outer genomic, rev)
kan-rev	AATGCTGGTCGCTATACTGC	*cbf11*$^+$ KO and KI, *cbf12*$^+$ KI verification (kanMX6, fwd)
mp31	TGTGCAGATTTGGATGGC	*cbf12*$^+$ KO verification (ORF, fwd)
mp32	AAATCAATCCCCTCCACG	*cbf12*$^+$ KO, KI verification (outer genomic, rev)
mp33	GCGCACGTCAAGACTGTC	*cbf12*$^+$ KO verification (natMX6, fwd)
MP41	CTTTGTTGTTCGTGATTCCAGGTGGGATTGTCAT TATTGGAAAATGCGAGATTTTGCTAACGTCAAG TGCTTTTGGAAACCGGATCCCCGGGTTAATTAA	*cbf11*$^+$ KI (fwd)
MP42	CCTAATTCCATCATTTTGAAAACAAATTGTATTT	*cbf11*$^+$ KI (rev)

	CAATATTTCGCCATATGAAACCACACGTAAAAT TAATCATGATGCAGAATTCGAGCTCGTTTAAAC	
mp43	CAGTGGAATTATCTCCCATTTTATTATTTCAATA CGAGACACTCTTTCATTCTGGATATAAGTGGCC TTTGGAAAGTCACCGGATCCCCGGGTTAATTAA	*cbf12*$^+$ KI (fwd)
mp44	AAAACAAAAAGAGTAAAAATAAATATACTAAT CCCTTGCAAAAACTTTTCAATAATAAAAAAGTA GTAAAGACAAATAATGAATTCGAGCTCGTTTAA AC	*cbf12*$^+$ KI (rev)
mp34	TTTTTTTTTTTTTTTTT	reverse transcription
mp35	ATTTGGCTAGGTGTTCATGG	*cbf11*$^+$, qRT-PCR (fwd)
mp45	TGACGTTAGCAAAATCTCGC	*cbf11*$^+$, qRT-PCR (rev)
mp36	CATTCAAGCCTGATACGACG	*cbf12*$^+$, qRT-PCR (fwd)
mp46	AGTGACTTTCCAAAGGCCAC	*cbf12*$^+$, qRT-PCR (rev)
mp37	GTAAACGATACCAGGTCCGC	*act1*$^+$, qRT-PCR (fwd)
mp38	GGTACCACTATGTATCCCGG	*act1*$^+$, qRT-PCR (rev)
mt1	AGAAGAGAGAGTAGTTGAAG	mating type detection (universal, rev)
mp	GGTAGTCATCGGTCTTCC	mating type detection (h^+, fwd)
mm	TACGTTCAGTAGACGTAGTG	mating type detection (h^-, fwd)

The sequences are given in the 5'-3' orientation. The primers were designed using GeneRunner 3.04 (Hastings Software) and synthesized by BioTez. fwd – forward primer, rev – reverse primer.

3.3.5 Plasmids constructed and used

The following vectors were used for constructions (Figs 3.1-10):

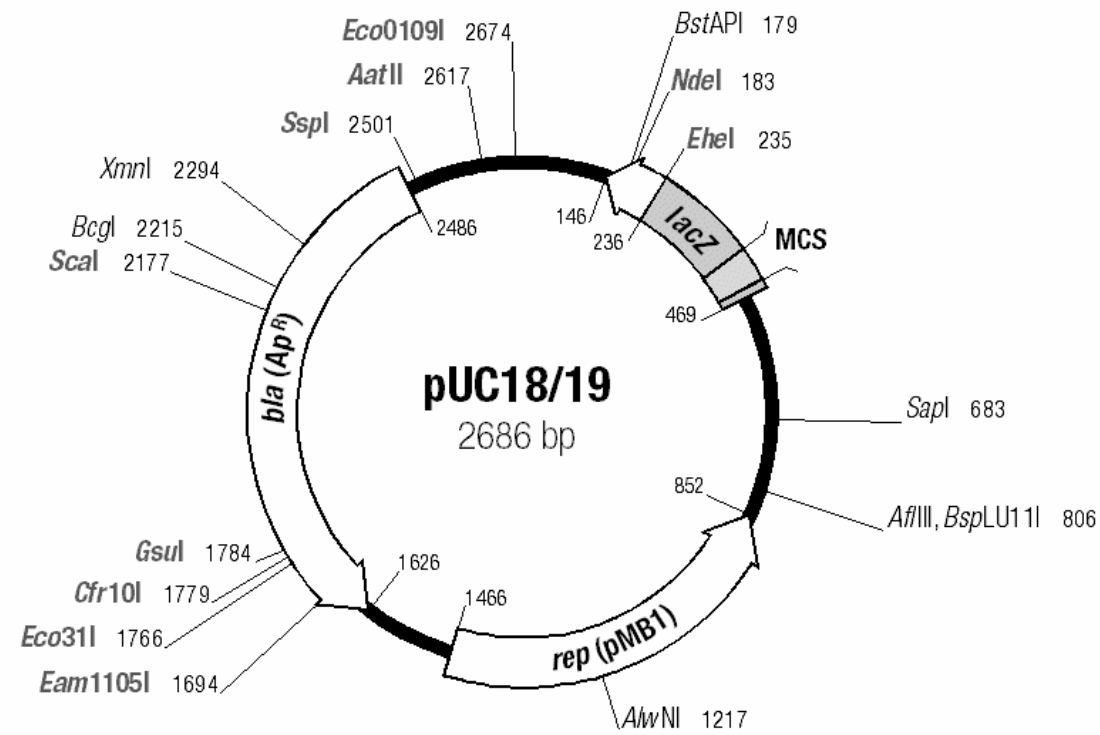

Figure 3.1 – pUC19. A small bacterial cloning vector (adapted from Fermentas).

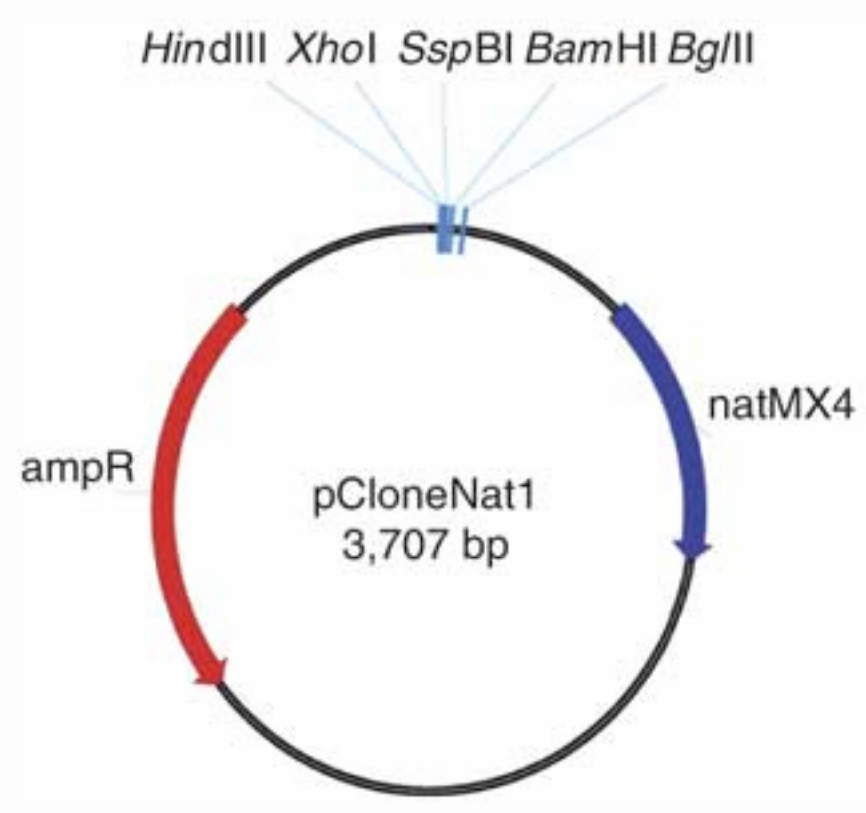

Figure 3.2 – pCloneNAT1. A cloning vector with the nourseothricin resistance gene used for knock-out construction in *S. pombe* (adapted from (Gregan *et al.*, 2006)).

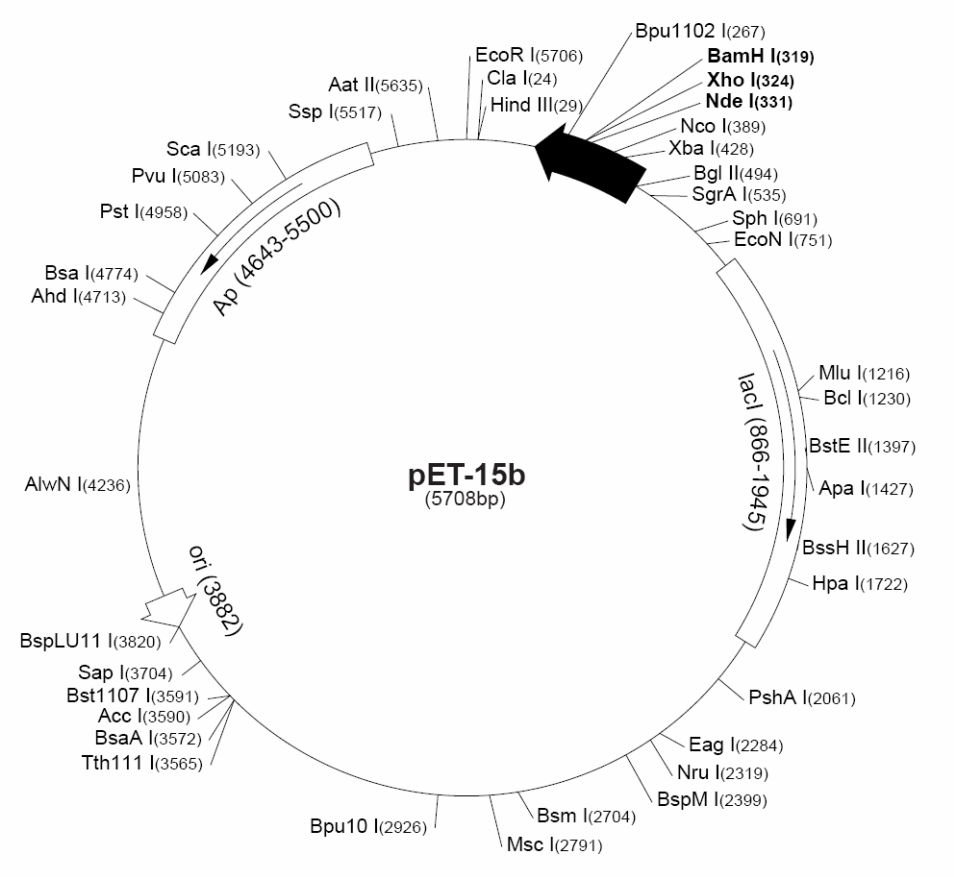

Figure 3.3 – pET-15b. A vector for inducible expression of N-terminally His-tagged proteins in *E. coli* (adapted from Novagen).

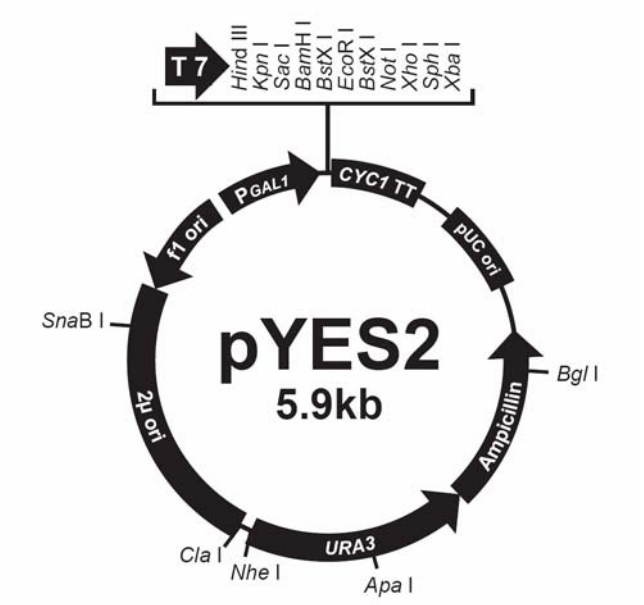

Figure 3.4 – pYES2. A vector for inducible protein expression in *S. cerevisiae* (adapted from Invitrogen).

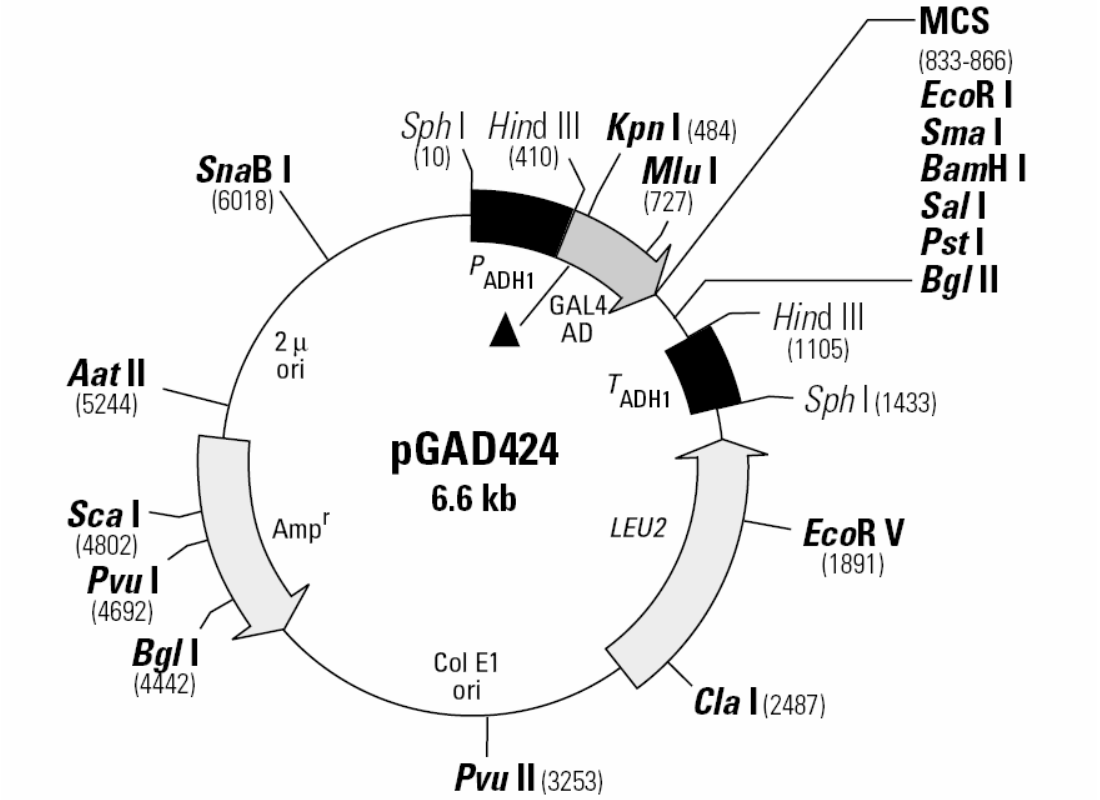

Figure 3.5 – pGAD424. A Gal4 yeast two hybrid system vector; activation domain fusions (adapted from Clontech).

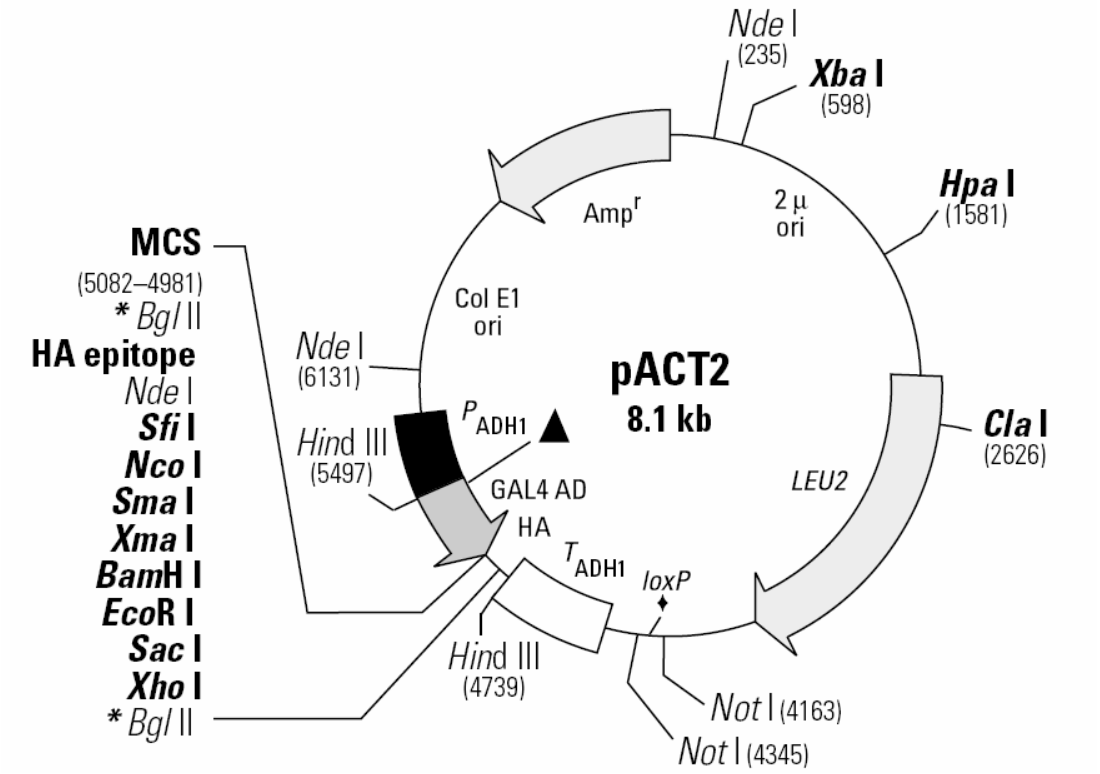

Figure 3.6 – pACT2AD. A Gal4 yeast two hybrid system vector; activation domain fusions (adapted from Clontech).

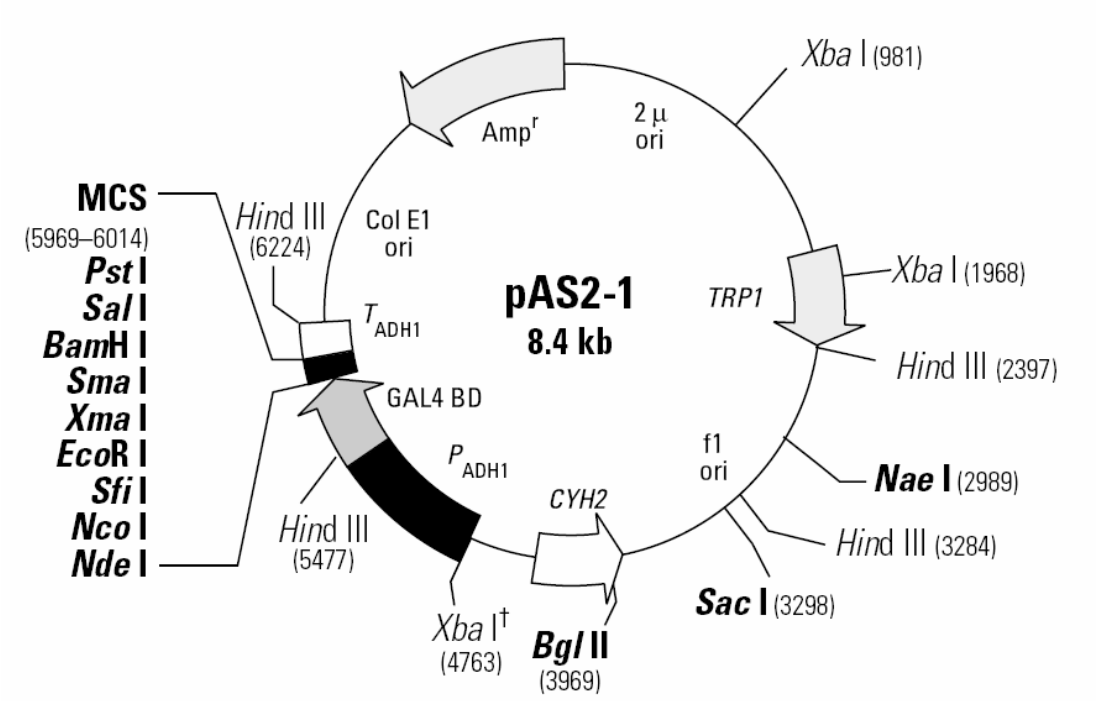

Figure 3.7 – pAS2-1. A Gal4 yeast two hybrid system vector; DNA-binding domain fusions (adapted from Clontech).

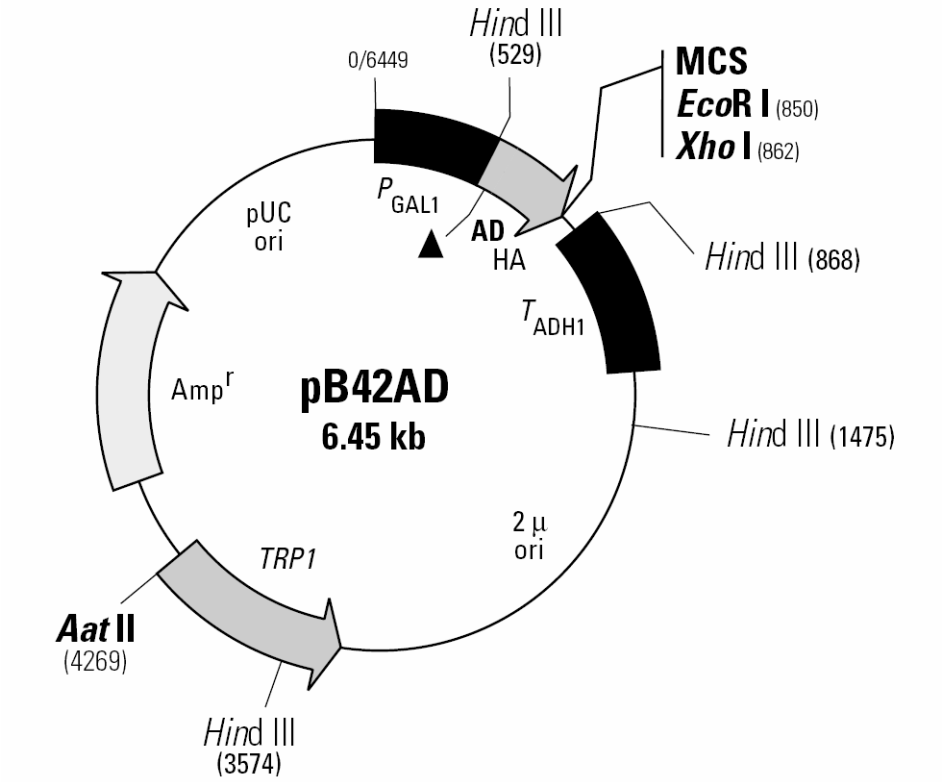

Figure 3.8 – pB42AD. A LexA yeast two hybrid system vector; activation domain fusions (adapted from Clontech).

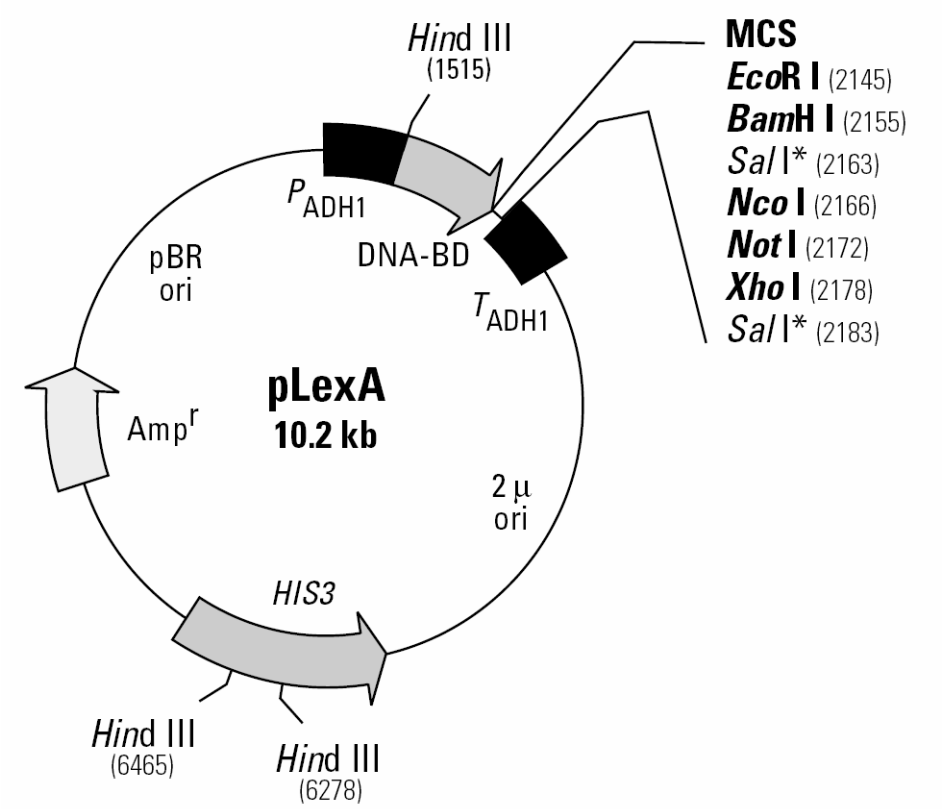

Figure 3.9 – pLexA. A LexA yeast two hybrid system vector; DNA-binding domain fusions (adapted from Clontech).

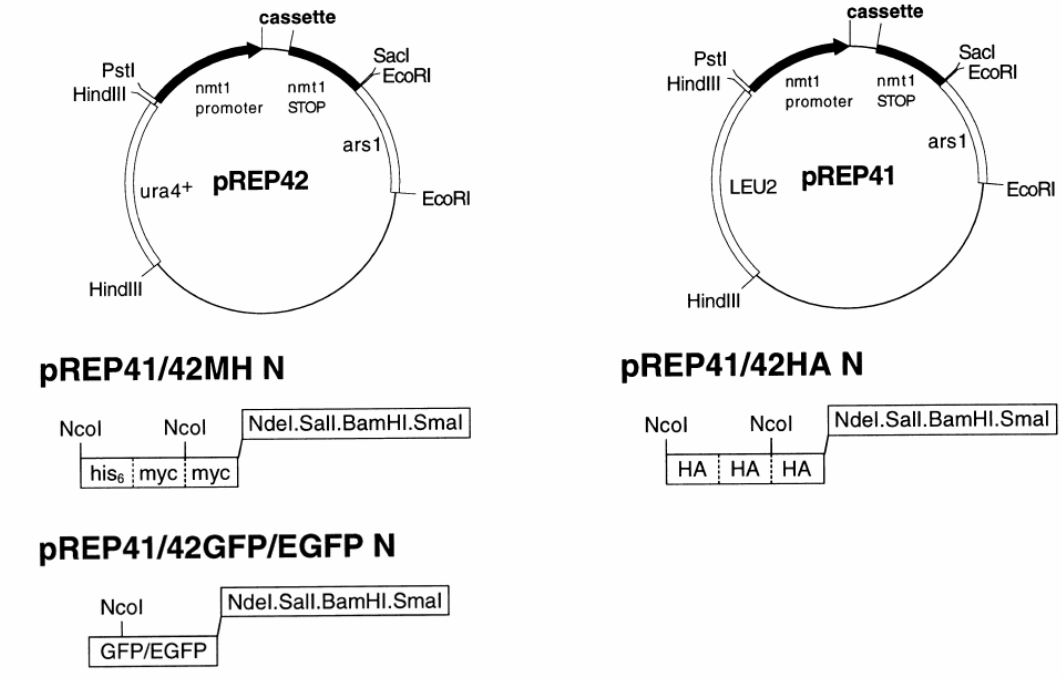

Figure 3.10 – pREP41/42 vector series. Vectors for thiamine controllable expression of N-terminally tagged proteins in *S. pombe* (Craven *et al.*, 1998).

Table 3.9 – Plasmids constructed and/or used in this study.

Name	Backbone	Size in bp (total/insert)	Description	Cloning method
pMP22	pACT2AD	8117 / 1842	AD-Cbf11 Gal4 2H fusion	*Bam*HI
pMP23	pACT2AD	8117 / 1842	AD-Cbf11 Gal4 2H fusion (frameshift at insertion site)	*Bam*HI
pMP24	pACT2AD	8117	empty Gal4 AD vector recreated from pMP22	
pMP25	pYES2	7706 / 1850	Cbf11 expression in *S. cerevisiae*	*Bam*HI
pMP26	pYES2	8464 / 2608	AD-Cbf11 expression in *S. cerevisiae* (*Hind*III fragment from pMP22)	*Hind*III
pMP27	pAS2-1	10242 / 1850	DBD-Cbf11 Gal4 2H fusion	*Bam*HI
pMP28	pGAD424	8358 / 1715	AD-Snw1 Gal4 2H fusion	*Eco*RI / *Sal*I
pMP29	pET-15b	7566 / 1850	His-Cbf11 expression in bacteria	*Bam*HI (Klenow-filled) into *Xho*I (Klenow-filled)
pMP31	pREP41HAN	11751 / 2893	HA-Cbf12 expression in *S. pombe*	*Nde*I / *Bgl*II into *Nde*I / *Bam*HI
pMP32	pREP42MHN	11289 / 2893	MycHis-Cbf12 expression in *S. pombe*	*Nde*I / *Bgl*II into *Nde*I / *Bam*HI
pMP33	pREP41EGFPN	12370 / 2893	EGFP-Cbf12 expression in *S. pombe*	*Nde*I / *Bgl*II into *Nde*I / *Bam*HI
pMP34	pREP42EGFPN	11896 / 2893	EGFP-Cbf12 expression in *S. pombe*	*Nde*I / *Bgl*II into *Nde*I / *Bam*HI
pMP35	pET-15b	8591 / 2893	His-Cbf12 expression in bacteria	*Nde*I / *Bgl*II into *Nde*I / *Bam*HI
pMP36	pLexA	12016 / 1850	DBD-Cbf11 LexA 2H fusion	*Bam*HI
pMP37	pB42AD	8307 / 1854	AD-Cbf11 LexA 2H fusion	*Bam*HI (Klenow-filled) into *Eco*RI (Klenow-filled)
pMP38	pLexA	13056 / 2900	DBD-Cbf12 LexA 2H fusion	*Eco*RI / *Bgl*II into *Eco*RI / *Bam*HI
pMP40	pAS2-1	11258 / 2893	DBD-Cbf12 Gal4 2H fusion	*Nde*I / *Bgl*II into *Nde*I / *Bam*HI
pMP45	pCloneNAT1	4698	*cbf12*$^{+}$ targeting vector (corrected version of the plasmid obtained from (Gregan *et al.*, 2005))	
pJB35	pYES2	~7500 / ~1580	v-src SRA expression in *S. cerevisiae* (Brabek *et al.*, 2002)	*Bam*HI / *Eco*RI
pJR05	pUC19	4516 / 1850	*cbf11*$^{+}$ cDNA	*Nde*I / *Bam*HI

pJR07	pREP41HAN	10708 / 1850	HA-Cbf11 expression in *S. pombe*	*Nde*I / *Bam*HI
pJR08	pREP42MHN	10246 / 1850	MycHis-Cbf11 expression in *S. pombe*	*Nde*I / *Bam*HI
pJR09	pREP41EGFPN	11321 / 1850	EGFP-Cbf11 expression in *S. pombe*	*Nde*I / *Bam*HI
pJR10	pREP42EGFPN	10853 / 1850	EGFP-Cbf11 expression in *S. pombe*	*Nde*I / *Bam*HI
pJR11	pAS2-1	10092 / 1715	DBD-Snw1 Gal4 2H fusion	*Eco*RI / *Sal*I
pFP126	pUC19	5549 / 2900	*cbf12*$^{+}$ ORF	*Eco*RI / *Bgl*II

3.3.6 EMSA

S. pombe lysates for gelshifts were prepared by washing the cells in the STOP buffer (see Chapter 3.2.2) and vortexing with HCl-washed glass beads in the lysis buffer (25 mM Hepes pH 7.6, 0.1 mM EDTA pH 8, 150 mM KCl, 0.1% Triton X-100, 25% glycerol, 2 mM DTT, 1/100 volume of Protease Inhibitor Mix FY (Serva)) at 4°C. The lysates were centrifuged for 20 min at 20,000 g, 4°C and the supernatants were used further. *E. coli* lysates were prepared by sonicating bacteria resuspended in the lysis buffer (up to 10 min, on ice) followed by centrifugation for 20 min at 20,000 g, 4°C. MycHis-tagged Cbf11 and Cbf12 proteins used for the shifts were purified from *S. pombe* by the TALON affinity chromatography (Clontech) according to the manufacturer's instructions (see Chapter 3.2.2). A panel of double stranded DNA oligonucleotide probes containing either the CSL response element or a mutated/scrambled control (see Table 3.10) was synthesized and terminally labeled by incubation with [γ-^{32}P]ATP (see Chapter 3.3.3).

The shift reactions containing the shift buffer (25 mM Hepes pH 7.6, 34 mM KCl, 5 mM $MgCl_2$), 2 ng of radioactively labeled probe, up to 40 ng of unlabeled competitor, 1 μg (for purified proteins) or 20 μg (for cell lysates) of carrier sonicated salmon sperm DNA and either the *S. pombe/E. coli* cell extract (up to 100 μg) or the purified Cbf11/Cbf12 proteins were prepared and incubated on ice for 20 min. The shift reactions were then resolved on a native 5% (with 5% glycerol added) or 8% polyacrylamide gel in 0.5× TBE at room temperature. The gels were visualized with a FUJIFILM BAS Reader Model 1500 imager or using a Kodak BioMAX autoradiography film.

Table 3.10 – Oligonucleotide probes used.

Probe	**Sequence**	**Source**
RBP-fwd	ACAAGGGCCGTGGGAAATTTCCTAAGCCTC	mouse RBP-Jκ promoter (fwd) (Oswald *et al.*, 1998)

RBP-rev	GAGGCTTAGGAAATTTCCCACGGCCCTTGT	mouse RBP-Jκ promoter (rev) (Oswald *et al.*, 2002)
m8-fwd	TCGACGGGGCACTGTGGGAACGGAAAGAGT	drosophila m8 promoter (fwd) (Chung *et al.*, 1994)
m8-rev	ACTCTTTCCGTTCCCACAGTGCCCCGTCGA	drosophila m8 promoter (rev) (Chung *et al.*, 1994)
KSHV-fwd	ATAATCCGGGCGTGAGAAACAGAAACGGCC	KSHV promoter (fwd) (Liang and Ganem, 2004)
KSHV-rev	GGCCGTTTCTGTTTCTCACGCCCGGATTAT	KSHV promoter (rev) (Liang and Ganem, 2004)
mut-fwd	ATAATCCGGGCGTGACAAACAGAAACGGCC	G5C mutant of the KSHV probe (fwd)
mut-rev	GGCCGTTTCTGTTTGTCACGCCCGGATTAT	G5C mutant of the KSHV probe (rev)
del-fwd	ATAATCCGGGCCCAACAAACAGAAACGGCC	scrambled mutant of the KSHV probe (fwd)
del-rev	GGCCGTTTCTGTTTGTTGGGCCCGGATTAT	scrambled mutant of the KSHV probe (rev)
HES-fwd	GATCGTTACTGTGGGAAAGAAAGTTTGGGA	mouse HES-1 promoter (fwd) (Oswald *et al.*, 1998)
HES-rev	TCCCAAACTTTCTTTCCCACAGTAACGATC	mouse HES-1 promoter (rev) (Oswald *et al.*, 2002)

The sequences are given in the 5'-3' orientation. The probes were synthesized by BioTez. fwd – forward strand, rev – reverse strand.

3.3.7 Flow cytometry

Exponentially growing cells were fixed with 70% ethanol, treated with RNase and stained with propidium iodide (4 μg/ml) as described (Sazer and Sherwood, 1990). WT haploid and diploid cells were used as 2C and 4C standards, respectively. DNA content was measured using the Becton Dickinson LSR II instrument; at least 20,000 cells were measured for each sample. Fluorescence intensity histograms were produced in the DiVa software. To asses the ploidy accurately, only cells having single nuclei (as judged by their signal amplitude/width ratio) were included in the final analysis. Thus, the confounding bi-nucleate cells undergoing cytokinesis, as well as spurious doublets and pseudohyphae were removed by gating.

3.4 Microscopy and imaging

3.4.1 Fluorescence and bright field microscopy

Where required, nuclei were stained with DAPI (1 μg/ml). The mounting medium consisted of 23% glycerol, 9% mowiol, 27.3 mM PIPES, 11.3 mM HEPES, 4.5 mM EGTA, 0.45 mM $MgCl_2$, pH 8.3. DABCO was added as antifade (50 mg/ml) prior to mounting.

Confocal fluorescent images were acquired using a Leica TCS SP2 confocal microscope and the accompanying software. Epifluorescence images were taken with either an Olympus IX81 microscope and the cell^R 2.6 software (Olympus) or a Nikon Eclipse TE2000-S microscope and the NIS Elements imaging software (Nikon).

3.4.2 Colony imaging

High-magnification colony images were taken by a Hitachi HV-C20 camera connected to a Navitar Zoom 6000 optical system and the NIS Elements imaging software (Nikon). Agar plates under low magnification were photographed using a Kodak DC290 Zoom or a Panasonic DMC-FZ7 camera.

3.5 Bioinformatics and software

3.5.1 Sequence database searches

Publicly available nucleotide and protein databases were searched for putative CSL family members using the appropriate BLAST algorithm with default settings (see Table 3.11). Initially, the mouse CBF1 protein sequence [GenBank:NP_033061] was used as a query. The searches were subsequently repeated with all newly identified CSL sequences as queries.

3.5.2 Gene models prediction and verification

All newly identified fungal CSL genes were checked for the quality of their ORF prediction. Each database gene model was compared with GenScan and/or WebGene predictions. The models were also compared to a multiple sequence alignment of other CSL proteins. In some cases, the splicing pattern was corrected

manually using Gene Runner 3.04 in order to restore a highly conserved region (see Table 3.11 for more details on the tools used).

3.5.3 Conserved domain search and protein localization prediction

Known domains present in the novel fungal CSL proteins were searched for by the Search Pfam server. Subcellular localization of each CSL protein was predicted by three independent algorithms: SubLoc v1.0, CELLO v.2.5 and PSORT II (see Table 3.11 for more details). The respective sequences received a "+" for each program stating their nuclear localization.

3.5.4 Sequence alignments and phylogenetic analyses

Sequence alignments in this study were produced using the ClustalW and ClustalX (Blosum matrix series) algorithms. Some alignments were then manually edited in BioEdit 7 to correct some obvious alignment errors and to account for information from protein crystal structures.

Prior to phylogenetic tree construction, all positions containing gaps were removed from the respective sequence alignment. An unrooted tree was then generated using the neighbor-joining method in the MEGA 3.1 software package with 2000 bootstrap replicates (more details on the tools used can be found in Table 3.11).

3.5.5 Protein structure modeling

Cbf11 and Cbf12 protein sequences were modeled into the 3D coordinates of the *C. elegans* LAG-1 protein (Kovall and Hendrickson, 2004) using the Swiss-Model server with default settings. The results were visualized in the DeepView PDB viewer (see Table 3.11).

3.5.6 Microarray data analyses and CSL response element searches

Normalized and processed data obtained in the microarray experiments from the laboratory of Dr. Jürg Bähler were analyzed using the Agilent GeneSpring GX suite and Microsoft Excel. A gene was considered to be differentially expressed when showing a 2-fold (or 1.5-fold) difference (as compared with the control) in

both biological replicates. Annotations were obtained from the *S. pombe* GeneDB resource (see Table 3.11).

Table 3.11 – Databases and bioinformatics tools used.

Name	**Description / URL**	**Source**
NCBI databases	Protein and nucleotide sequence database http://www.ncbi.nlm.nih.gov/sites/gquery	
GeneDB	*S. pombe* genome database, annotations and bioinformatics tools http://www.genedb.org/genedb/pombe/	(Aslett and Wood, 2006;Hertz-Fowler *et al.*, 2004;Wood *et al.*, 2002)
UniProt	Protein and nucleotide sequence database http://www.expasy.org/tools/blast/	(UniProt Consortium, 2007)
R. oryzae database	*Rhizopus oryzae s*equencing project http://www.broad.mit.edu/annotation/genome/rhizopus_oryzae	
C. cinereus database	*Coprinus cinereus s*equencing project http://www.broad.mit.edu/annotation/genome/coprinus_cinereus	
P. chrysosporium database	*Phanerochaete chrysosporium* sequencing project http://genome.jgi-psf.org/Phchr1/Phchr1.home.html	
S. japonicus and *S. octosporus* database	*Schizosaccharomyces japonicus* and *Schizosaccharomyces octosporus* sequencing project http://www.broad.mit.edu/annotation/ genome/schizosaccharomyces_japonicus	
P. blakesleeanus database	*Phycomyces blakesleeanus* sequencing project http://genome.jgi-psf.org/Phybl1/Phybl1.home.html	
U. maydis database	*Ustilago maydis* sequencing project http://www.broad.mit.edu/annotation/genome/ustilago_maydis	
C. neoformans database	*Cryptococcus neoformans* sequencing project http://www.tigr.org/tdb/e2k1/cna1/	
P. graminis database	*Puccinia graminis* sequencing project http://www.broad.mit.edu/annotation/genome/puccinia_graminis	
NCBI BLAST	Sequence similarity searches http://www.ncbi.nlm.nih.gov/blast/Blast.cgi	
GenScan	Gene models prediction and verification	(Burge and Karlin, 1997)
WebGene	Gene models prediction and verification	(Milanesi *et al.*, 1999)
GeneRunner 3.04	*In silico* sequence analysis and manipulation suite	Hastings Software
Clone Manager 4	*In silico* sequence analysis and manipulation suite	Scientific &

		Educational Software
Pfam	Protein families and conserved domains database and searches http://www.sanger.ac.uk/Software/Pfam/	(Finn *et al.*, 2006)
SubLoc v1.0	Protein localization prediction http://www.bioinfo.tsinghua.edu.cn/SubLoc/	(Hua and Sun, 2001)
CELLO v.2.5	Protein localization prediction http://cello.life.nctu.edu.tw/	(Yu *et al.*, 2006)
PSORT II	Protein localization prediction http://psort.nibb.ac.jp/form2.html	(Nakai and Horton, 1999)
ClustalW	Sequence alignment http://www.ebi.ac.uk/Tools/clustalw2/index.html	(Chenna *et al.*, 2003)
ClustalX	Sequence alignment http://bips.u-strasbg.fr/en/Documentation/ClustalX/	(Thompson *et al.*, 1997)
BioEdit 7	*In silico* sequence analysis and manipulation suite http://www.mbio.ncsu.edu/BioEdit/bioedit.html	Ibis Biosciences
MEGA 3.1	Phylogenetic analysis suite http://www.megasoftware.net/index.html	(Kumar *et al.*, 1994)
ESPript	PostScript output from aligned sequences http://espript.ibcp.fr/ESPript/ESPript/	(Gouet *et al.*, 1999)
Swiss-Model	Protein structure modeling http://swissmodel.expasy.org/	(Schwede *et al.*, 2003)
DeepView	Protein structure visualization http://swissmodel.expasy.org/spdbv/	(Guex and Peitsch, 1997)
GeneSpring GX	Expression data analysis suite	Agilent
ESPSearch	Sequence pattern searches http://web.chemistry.gatech.edu/~doyle/espsearch/	(Watt and Doyle, 2005)

4 *RESULTS*

4.1 Identification and characterization *in silico* of fungal CSL proteins

4.1.1 Database searches

The CSL transcription factors were, until recently, generally considered to be metazoan-only and confined in their function mostly to the Notch pathway. Only one brief notion existed in the literature that distant CSL homologs may also be found in the genome of the fission yeast *Schizosaccharomyces pombe*, a simple organism that lacks the Notch pathway (Lai, 2002). This notion, however, raises interesting questions regarding the evolutionary origin as well as the ancestral function of the CSL family. We have therefore conducted exhaustive BLAST searches of publicly available sequence data (see Chapter 3.5.1) to asses the presence and conservation of CSL family members in fungi. We have indeed found putative CSL family members in the genomes of representatives of several fungal groups. The phylogenetic distribution of the CSL family is shown in Fig. 4.1.

The results of these searches are summarized in Table 4.1 (the fungal taxonomical nomenclature used was taken from (James *et al.*, 2006)). Nineteen putative CSL genes were found in seven organisms, with *S. pombe* and *S. japonicus* belonging to the Taphrinomycotina basal subphylum of ascomycetes, *Rhizopus oryzae* representing the zygomycetes and *Coprinus cinereus*, *Cryptococcus neoformans*, *Phanerochaete chrysosporium* and *Ustilago maydis* belonging to the basidiomycetes. Protein products of these genes contain motifs typical of the CSL family (see Chapter 4.1.3). In contrast to that, no CSL homologs could be found in either Saccharomycotina (including the budding yeast *Saccharomyces cerevisiae*) or Pezizomycotina, the later branching subphyla of ascomycetes. Our findings and analyses were published (Prevorovsky *et al.*, 2007) (see Appendices).

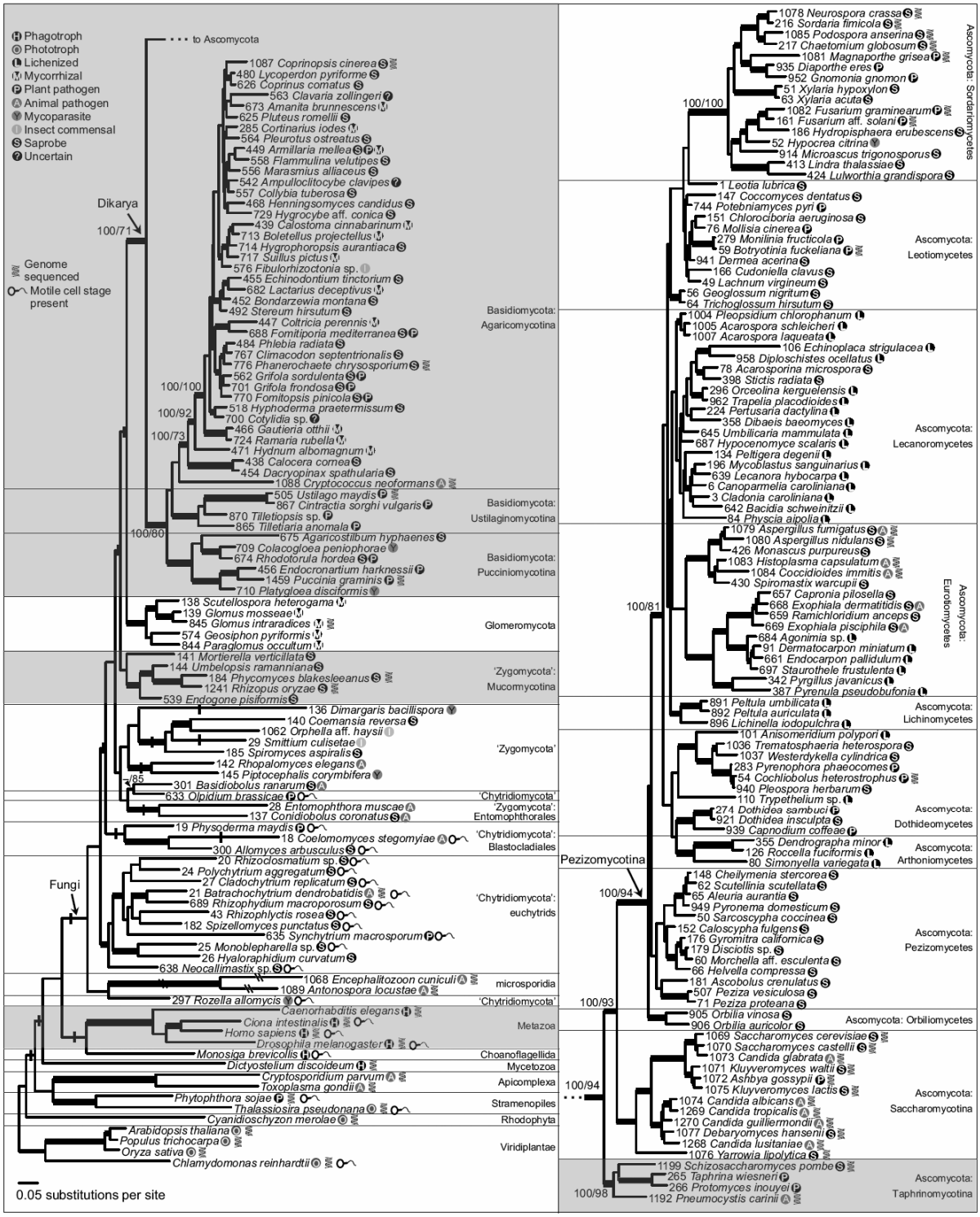

Figure 4.1 – Phylogenetic tree showing the distribution of the CSL family in evolution. The taxonomical groups where CSL genes have been found are shaded in grey (adapted from (James *et al.*, 2006)).

Table 4.1 – Fungal CSL proteins.

Organism	Protein	Accession number / Locus[a]	Length (aa)	Status[b]	Nuclear[c]	Source
Ascomycota: Taphrinomycotina						
Schizosaccharomyces pombe	Cbf12 (SPCC1223.13)	CAA20882	963	Exp[d]	+++	NCBI Protein
	Cbf11 (SPCC736.08)	NP_587779	613	Exp[d]	-	NCBI Protein
Schizosaccharomyces japonicus	SjCSL2	Supercontig 4 (bp 1104530-1107169)	879	Hyp	+++	Broad
	SjCSL1	Supercontig 5 (bp 726033-727712)	559	Hyp	+++	Broad
Zygomycota						
Rhizopus oryzae	RO3G_06481	RO3G_06481.1	694	Hyp	+++	Broad
	RO3G_07636	RO3G_07636.1	662	Hyp	++	Broad
	RO3G_11583	RO3G_11583.1	764	Hyp	+++	Broad
	RO3G_14587	RO3G_14587.1	886	Hyp	+++	Broad
	RO3G_06953	RO3G_06953.1	449	Hyp	+++	Broad
	RO3G_08863	RO3G_08863.1	482	Hyp	+++	Broad
	RO3G_13784	RO3G_13784.1	478	Hyp	+++	Broad
Basidiomycota						
Coprinus cinereus	CC1G_03194	EAU91026	960	Hyp	+++	NCBI Protein
	CC1G_01706	CC1G_01706.1	803	Hyp	+	Broad
Cryptococcus neoformans	CNBD3370	EAL21283	1015	Hyp	+++	NCBI Protein
	CNA01890	AAW40742	776	Exp	+++	NCBI Protein
Phanerochaete chrysosporium	PcCSL2	Scaffold 6 Contig 19 (bp 50978-54385)	1012	Hyp	++	JGI
	Pc6518	protein id "6518"	960	Hyp	++	JGI
Ustilago maydis	UM06280	EAK82808	1482	Hyp	+++	NCBI Protein
	UM05862	EAK86807	1094	Hyp	+++	NCBI Protein

[a]refers to the respective database stated in the "Source" column (see Table 3.11); [b]Exp – expressed protein, Hyp – hypothetical protein; [c]nuclear localization prediction score; [d]this study (adapted from (Prevorovsky *et al.*, 2007)).

Additional searches conducted while this thesis was in preparation identified additional CSL genes in newly sequenced fungal species: *Malassezia globosa*, the dandruff-causing yeast related to *Ustilago* has at least one CSL gene [Genbank:XP_00170963] (class F1, see Chapter 4.1.5). There are at least 3 CSL genes in the basidiomycete *Puccinia graminis*, and, similar to other *Schizosaccharomycetes*, two CSL paralogs can be found in the recently released genome of *S. octosporus* (both species sequenced at the Broad Institute). Finally, *Phycomyces blakesleeanus*, a representative of the basal fungal lineage, harbors about 6 CSL genes (sequenced by JGI, not finalized yet). These additional finding were not included in the analyses described below. It is conceivable that more CSL members will come out as more and more fungal genomes are sequenced.

4.1.2 Novel CSL genes structure verification and protein localization prediction

Most of the candidates are hypothetical proteins with little or no annotation in the databases. Therefore, we have first verified the quality of each ORF prediction (see Chapter 3.5.2). The confidence of exon-intron structure predictions in these less studied organisms is rather limited. Another obstacle is posed by the degree of divergence among the sequences together with the presence of multiple species- and protein-specific insertions. Nevertheless, we were able to construct three completely new gene predictions (designated SjCSL1 and SjCSL2 in *S. japonicus*, and PcCSL2 in *P. chrysosporium*) as well as to identify mispredictions and/or possible sequencing errors in other four genes (see Appendices for a more detailed description). Our corrections comprised of intron inclusion/exclusion, different splice-site selection and exon addition. Some of the intron positions displayed inter-species conservation which supported our predictions (data not shown). We have also identified a less usual intron with a GC-AG boundary in the *R. oryzae* RO3G_07636.1 gene. Such introns were found in other fungi as well (Rep *et al.*, 2006) and are generally a problem for gene prediction algorithms.

Typically, there are two CSL paralogs per genome, differing considerably in length (see Table 4.1) and each belonging to a different class (see Chapter 4.1.5). A notable exception is the genome of *R. oryzae* which harbors seven CSL genes, three of them being class F1 and four of them belonging to class F2.

According to the outputs of three independent localization tools (see Chapter 3.5.3), most candidate CSL proteins are predicted to be nuclear, which supports their possible functioning as transcription factors. Cbf11 of *S. pombe* is the only protein predicted to have exclusively non-nuclear subcellular localization but it was shown experimentally to be nuclear in a large-scale localization study (Matsuyama *et al.*, 2006) and in our experiments (see Chapter 4.4.2).

4.1.3 Sequence conservation of fungal CSL proteins

According to the *C. elegans* LAG-1 protein crystal structure, the CSL fold is related to Rel-domain proteins, but is uniquely composed of three distinct domains (Kovall and Hendrickson, 2004). The amino-terminal RHR-N (Rel-homology region) and central BTD (beta-trefoil domain) domains are involved in DNA-binding. BTD serves also as an interaction platform for Notch/SMRT coregulators. The carboxy-terminal RHR-C domain displays lower conservation in metazoans and its function is not yet clear; one possibility is its participation in Notch-independent regulation of transcription (Tang and Kadesch, 2001).

We have used the Pfam protein domains database (Finn *et al.*, 2006) to search for CSL-specific domains in all our candidate sequences and to identify any other known domains present. The results are schematized in Fig. 4.2.

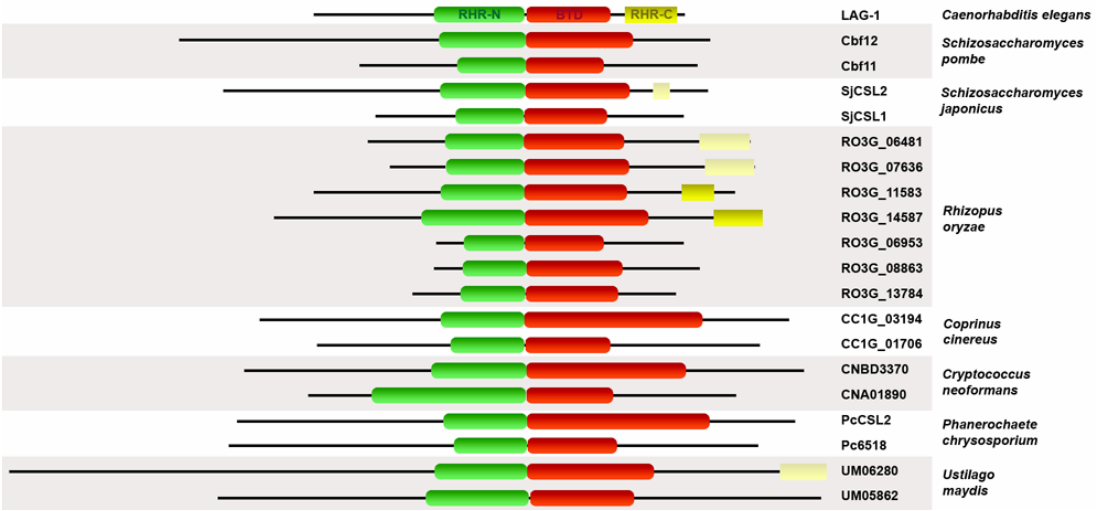

Figure 4.2 – Fungal CSL proteins domain organization. Black lines represent the respective CSL protein sequences (see Table 4.1 for details). The structure of *C. elegans* LAG-1 is shown at the top for comparison (Kovall and Hendrickson, 2004). Recognized Pfam domains are indicated: RHR-N in green, BTD in red and RHR-C in yellow (light yellow for low significance). The proteins are drawn to scale (adapted from (Prevorovsky *et al.*, 2007)).

The RHR-N [Pfam:PF09271] and BTD [Pfam:PF09270] domains were identified in all fungal sequences with high significance, supporting the identity of our candidates as CSL family members. However, the RHR-C [Pfam:PF01833] domain could only be identified in RO3G_11583 and RO3G_14587 from *R. oryzae*. A rather divergent RHR-C domain was also found in *S. japonicus* SjCSL2 and two more *R. oryzae* proteins, RO3G_06481 and RO3G_07636. The lower degree of sequence conservation of RHR-C noted in metazoans is thus even more pronounced in fungi. No other conserved domains could be found, despite the fact that the putative fungal CSL proteins are typically significantly larger than their metazoan counterparts. The overall domain organization of the fungal proteins is the same as in metazoans. The increased size of the fungal candidates was found to be caused by two factors. First, in some proteins, there are pronounced extensions of the amino-terminal part preceding the RHR-N domain. This region is about 200 amino acids long in *C. elegans* and gets much shorter in metazoan evolution. Its crystal structure is not known. Second, there are multiple amino acid insertions of varying length throughout the candidate sequences (see below).

To gain better insight into the specifics of the fungal CSL proteins, we have produced a multiple sequence alignment of all newly identified fungal sequences and selected metazoan family members (see Chapter 3.5.4). There are two sub-types of metazoan CSL proteins; one is represented by the Notch-pathway protein RBP-Jκ (CBF1, SuH, RBPSUH) and the other by the much less known transcription factor RBP-L, the function of which seems to be Notch-independent (Beres *et al.*, 2006;Minoguchi *et al.*, 1997). Both subtypes' representatives were included in the alignment. The most prominent feature of the resulting alignment is the presence of several highly conserved blocks of amino acids separated by species- and protein-specific insertions. These insertions are of considerable length in some cases and are more pronounced in the class F2 proteins. They are rich in amino acids proline, glycine, serine/threonine and lysine/arginine. Overall sequence conservation is highest in the RHR-N and BTD domains, including the immediately following long β-strand (βC4) that was shown to bridge all three CSL domains in the *C. elegans* LAG-1 (Kovall and Hendrickson, 2004). The conservancy of the βC4 linker suggests that the CSL-specific arrangement between RHR-N and BTD is also likely preserved in fungi. The C-termini typically contain only 1-2 well-alignable stretches that can be

identified as fragments of the RHR-C domain. The amino-terminal extensions preceding the RHR-N domain show little if any sequence conservation. As mentioned above, there are several regions located mostly in the RHR-N and BTD domains, that show very high or even absolute sequence conservation (Fig. 4.3). It is notable that, according to the crystallography data, all these conserved blocks are involved in binding of the strictly defined CSL consensus site on DNA (Kovall and Hendrickson, 2004). With the sole exception of the *S. japonicus* SjCSL2 protein (Q567H substitution corresponding to Q401 in *C. elegans* LAG-1, Fig. 4.3), all residues required for sequence specific binding of the GTG(G/A)GAA response element are absolutely conserved in all fungal proteins, which strongly supports their inclusion in the CSL family. The interactions of CSL proteins with their coactivators Notch/EBNA2 and corepressors SMRT/NCoR and CIR have been mapped to and around a hydrophobic pocket on the surface of BTD (Fuchs *et al.*, 2001;Hsieh *et al.*, 1999;Kovall and Hendrickson, 2004;Sakai *et al.*, 1998). Not surprisingly, the residues mediating these interactions are generally not conserved in fungi, although some of them are found in class F2 fungal CSL proteins. However, the potential to form a hydrophobic pocket in BTD seems to be preserved (data not shown).

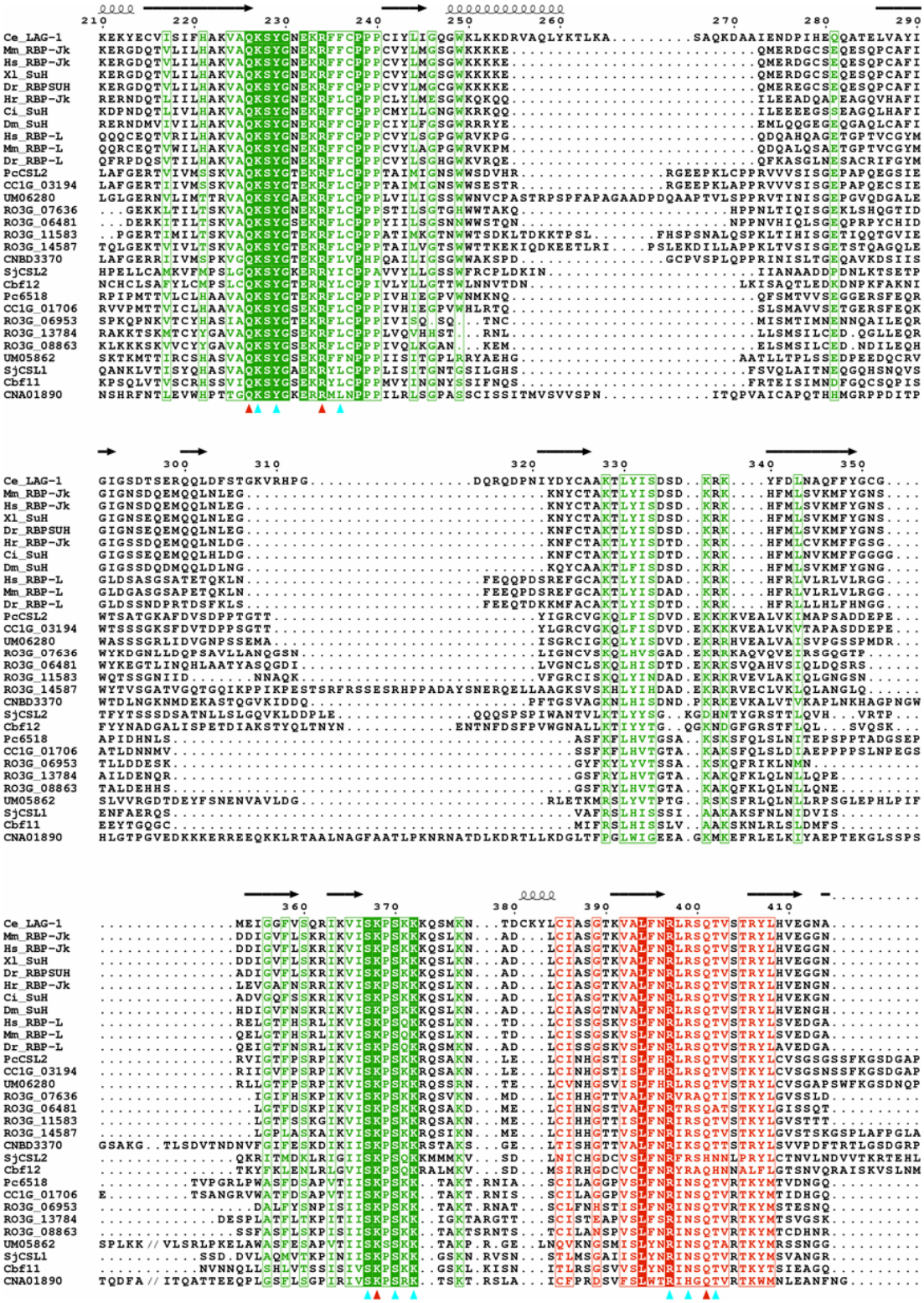

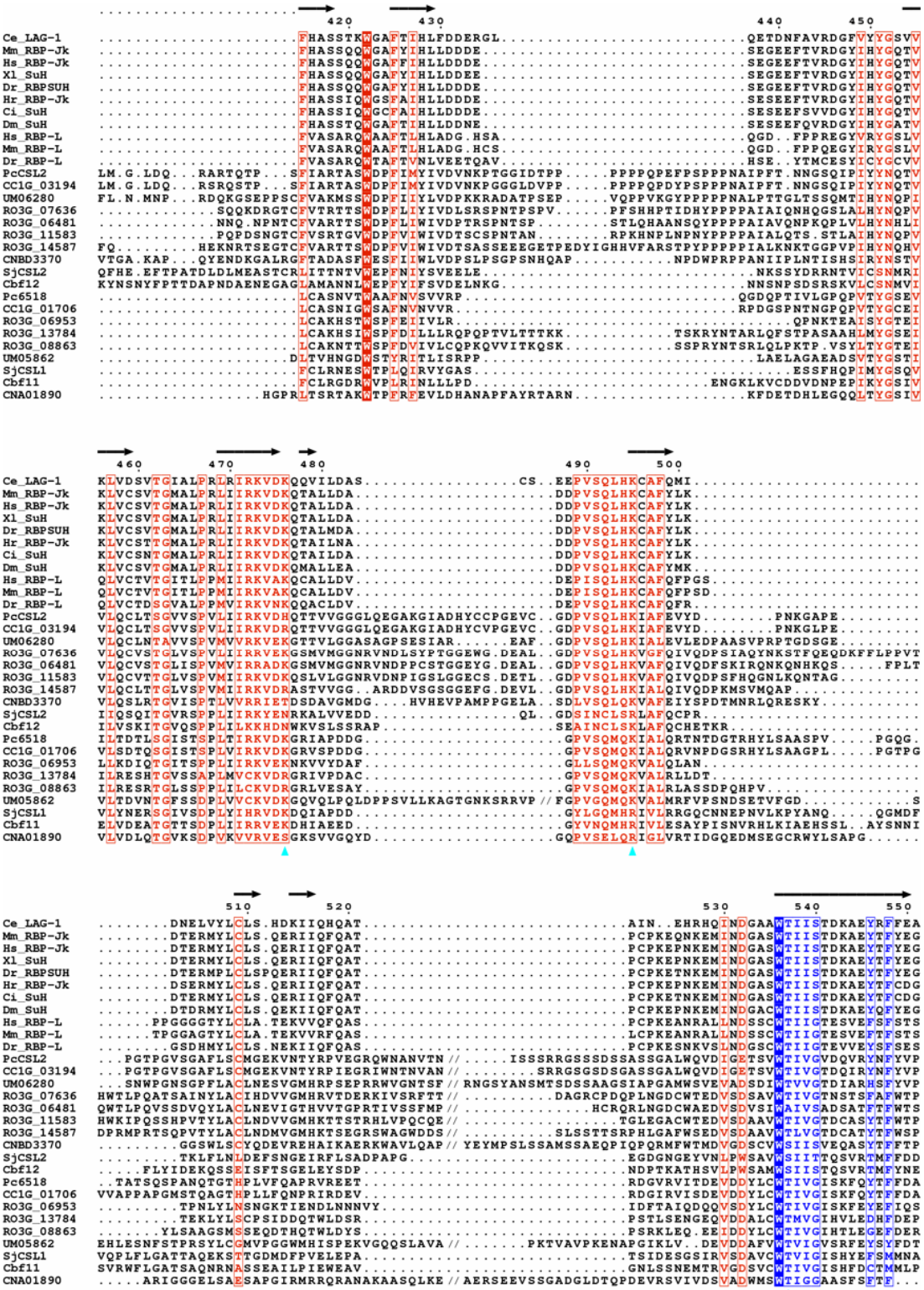

Figure 4.3 – Evolutionary conservation of the DNA-binding regions. The alignment of fungal and selected metazoan CSL protein sequences (see Table 4.1 and Appendices for details) shows high degree of conservation in regions responsible for DNA binding. Absolutely conserved residues are inverse-printed, positions with high residue similarity are boxed. Domain boundaries are indicated by color: green for RHR-N, red for BTD and blue for the βC4 linker connecting all three CSL domains. Red and cyan triangles below the alignment denote residues required for sequence specific and backbone DNA binding, respectively. The position numbering and secondary structures indicated

above the sequences correspond to *C. elegans* LAG-1 (Kovall and Hendrickson, 2004). The picture shows only a selected region of the whole alignment and, in order to save space, some parts of the long inserts are not shown (indicated by "/ /"). The picture was created using ESPript (Gouet *et al.*, 1999) (adapted from (Prevorovsky *et al.*, 2007)).

4.1.4 *S. pombe* CSL proteins 3D structure modeling

To further document the similarity of the novel fungal CSL proteins to the well-established metazoan family members we have attempted to fit the fission yeast Cbf11 and Cbf12 protein sequences (due to our focus on *S. pombe*) into the 3D coordinates of the *C. elegans* LAG-1 crystal structure [NCBI Structure:1ttu, chain A] (Kovall and Hendrickson, 2004) (see Chapter 3.5.5).

The fitting was relatively successful for Cbf11, as residues 179-429 could be well modeled into the LAG-1 coordinates (Fig. 4.4). This is not surprising as these correspond to the well-conserved RHR-N and BTD domains. However, only a short DNA-binding loop within the N-terminal part of RHR-N could be fitted in the case of Cbf12. This is likely due to the presence of longer inserts in class F2 proteins as compared with class F1, which could not be processed correctly by the modeling algorithm. Taken together, this simulation further points out the conservation of the DNA-binding regions of the fungal CSL proteins.

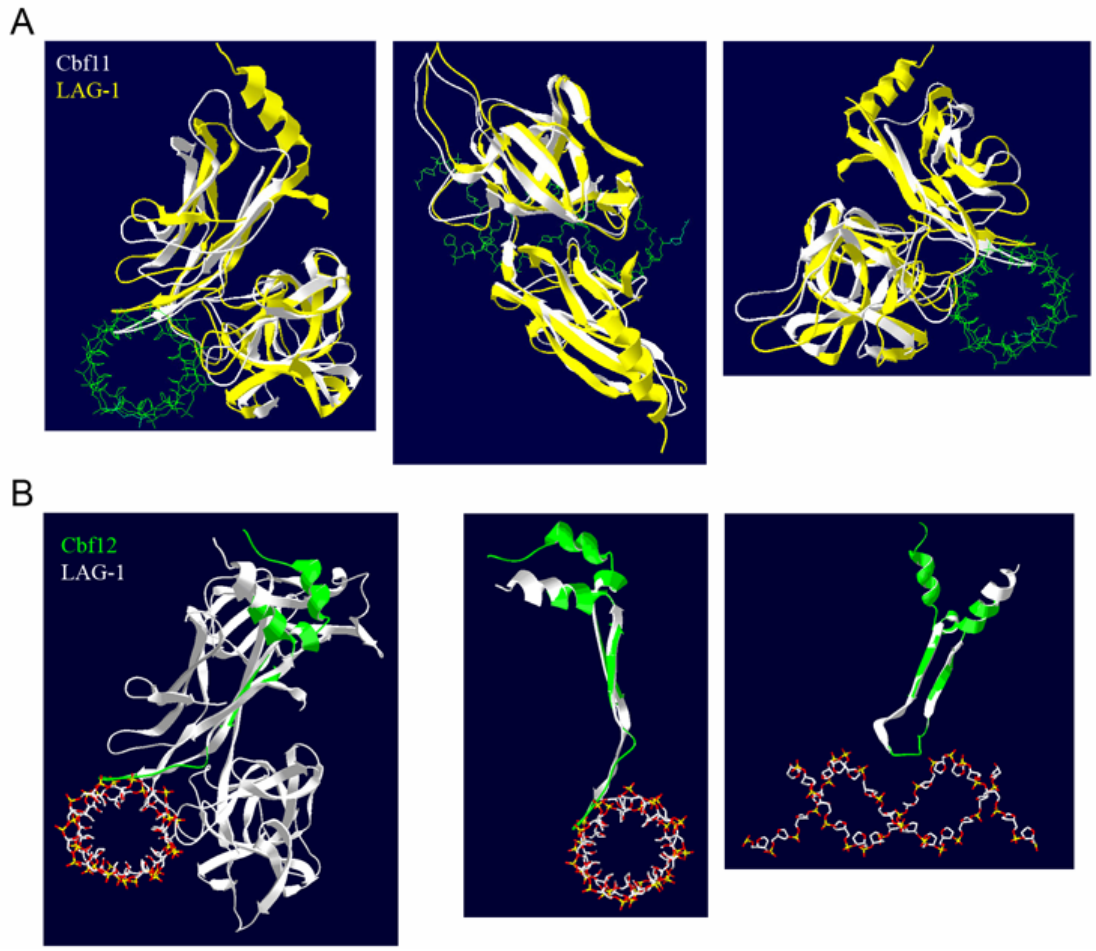

Figure 4.4 – Structure fitting of Cbf11 and Cbf12 into DNA-bound LAG-1. (A) Overlay of Cbf11 (residues 179-429, white) and the corresponding part of LAG-1 (yellow). The structures are shown from various angles, DNA is green. (B) Overlay of Cbf12 (residues 447-510, green) and LAG-1 (white), only a small part of Cbf12 could be fitted.

4.1.5 Phylogenetic analysis of the CSL protein family

As noted earlier, there are usually two fungal CSL paralogs per genome. We wanted to see whether these paralogs cluster to some well-defined groups and what their relationship to the metazoan CSL family members is. For this purpose, we have constructed an unrooted phylogenetic tree for the regions that could be aligned with confidence, that is, the RHR-N and BTD domains (see Chapter 3.5.4 and Fig. 4.5). As expected, the fungal CSL proteins form two distinct classes, designated class F1 and F2, with each class being represented in all fungal taxons included in the analysis. It should be noted at this point that the positions of *S. pombe* Cbf12 and *S. japonicus* SjCSL2 proteins are slightly ambiguous, branching off either immediately before or after the class F2 core (data not shown). The intra-class branch topology roughly follows the taxonomical relations (Kuramae *et al.*, 2006)

with the notable exception of the divergent *C. neoformans* CNA01890 and CNBD3370 proteins. It can be inferred from the branch lengths that the rate of divergence among the fungal protein sequences is much higher than in metazoa. Metazoan CSL proteins (designated class M) form a very coherent group that can be divided to RBP-Jκ and RBP-L subgroups. The RBP-Jκ subgroup displays an especially low extent of divergence, which may be due to their involvement in the developmentally critical Notch pathway. Of the two fungal CSL classes the class F2 proteins show higher similarity to the metazoan class M.

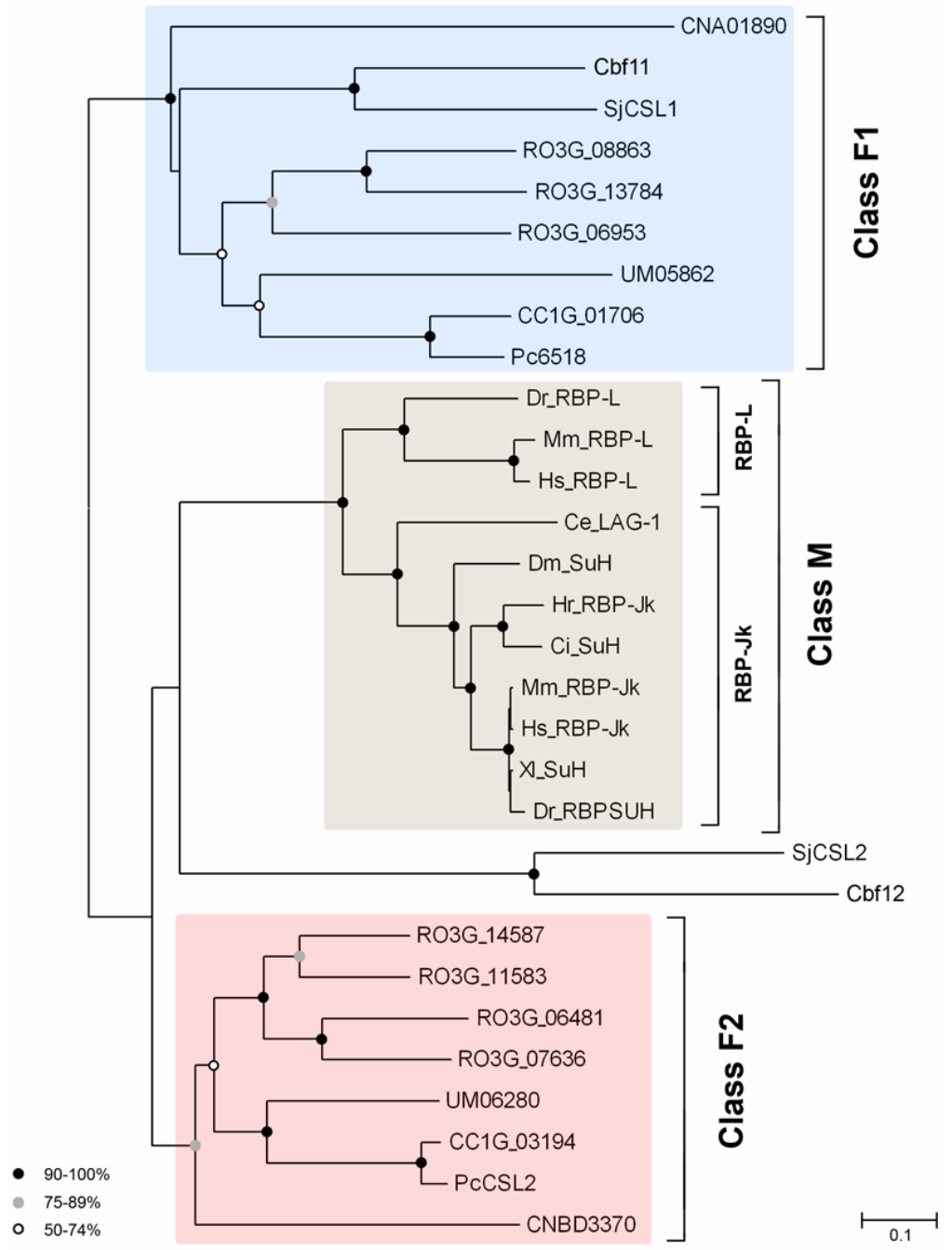

Figure 4.5 – Phylogenetic analysis of the CSL protein family. An unrooted neighbor-joining phylogenetic tree of the region corresponding to RHR-N and BTD domains. For protein descriptions see Table 4.1 and Appendices. For class F2 only the unambiguous core, not including the *S. pombe* Cbf12 and *S. japonicus* SjCSL2, is indicated by shading. Symbols at nodes indicate percentual bootstrap values, no symbol means less than 50% node stability. The scale bar indicates the number of amino acid substitutions per site (adapted from (Prevorovsky *et al.*, 2007)).

4.2 Cloning of fission yeast *cbf11*$^+$ and *cbf12*$^+$

Using our bioinformatics data as a basis, we sought to gain more insight into the nature and function of CSL proteins in fungi. With fission yeast being our organism of choice, we decided to characterize experimentally the two *S. pombe* CSL genes in detail.

We have dubbed the two paralogs *cbf11*$^+$ (SPCC736.08) and *cbf12*$^+$ (SPCC1223.13), respectively – names referring to CBF1 (C-promoter element Binding Factor 1), the prototypical metazoan family member. Both genes are located on chromosome 3. The intron-containing *cbf11*$^+$ codes for a 613 aa class F1 protein with a predicted molecular mass of 67.1 kDa. To allow for the expression of *cbf11*$^+$ in various systems, we first prepared its cDNA by PCR-mediated exon joining ((Higuchi *et al.*, 1988), schematized in Fig. 4.6). The list of all primers used in this study may be found in Table 3.8. Sequencing of the resulting cDNA (plasmid pJR05) revealed a single silent point mutation A294G, as compared with the GeneDB sequence (Hertz-Fowler *et al.*, 2004;Wood *et al.*, 2002). Since the mutation does not result in an amino acid substitution, we decided to use the cDNA further. The cloning procedure is described in more detail in the master's thesis of Jan Ryneš (Ryneš, 2005).

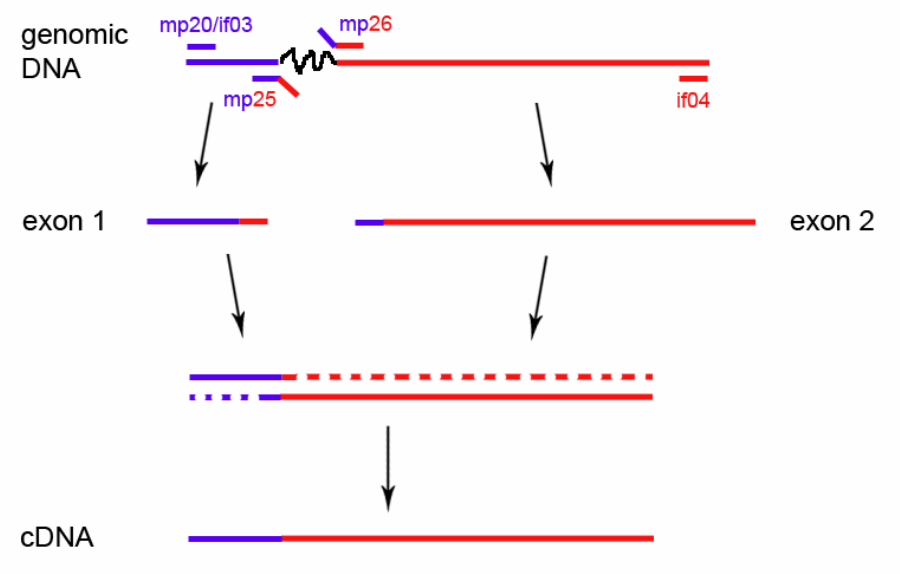

Figure 4.6 – *cbf11*$^+$ cDNA construction procedure. The two exons were amplified separately from chromosomal DNA of the FY254 strain (in two reading frames). The resulting PCR products were annealed and used in a second round of PCR with the outer pair of primers to generate full-length cDNA. A proof-reading DNA polymerase and low number of amplification cycles were used.

The second paralog, *cbf12*$^+$, does not contain any introns and codes for a 963 aa class F2 protein with a predicted molecular mass of 108.3 kDa. Its ORF was obtained from chromosomal DNA (strain FY254) using a conventional one-step PCR procedure, and was verified by sequencing (plasmid pFP126). To facilitate protein purification and/or detection, we then subcloned both *cbf11*$^+$ and *cbf12*$^+$ ORFs into a number of plasmid vectors for the expression of tagged and fusion variants. The thiamin-regulated pREP41/42xxxN series of tagging vectors (Craven *et al.*, 1998) was used to get N-terminally MycHis- and HA-tagged Cbf11 and Cbf12 proteins in *S. pombe* (EGFP fusions produced in these vectors will be described in Chapter 4.4). We have also prepared IPTG-regulated expression plasmids (pET-15b backbone) for the production of His-tagged proteins in *E. coli*. All constructs were verified by western analysis using appropriate antibodies (see Chapter 3.2.4) and representative blots are shown in Fig. 4.7 and Fig. 4.8. Fusion constructs related to 2H analyses will be considered in the respective chapter below (Chapter 4.5). The list of all plasmids constructed and used in this study may be found in Table 3.9.

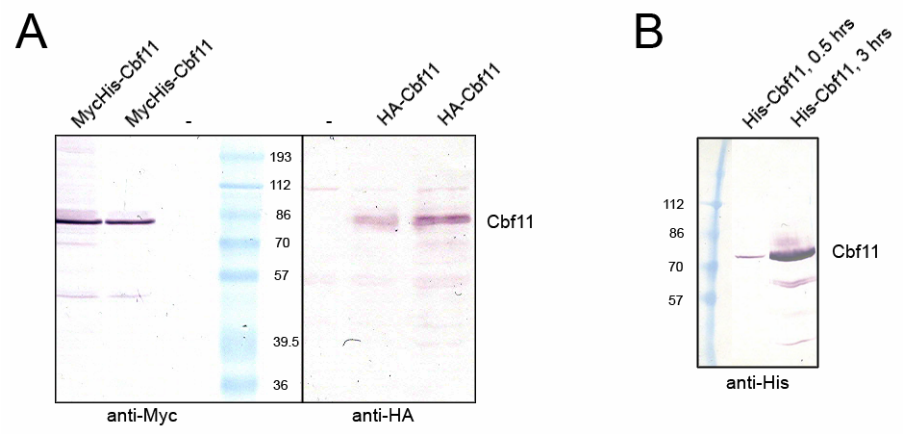

Figure 4.7 – Tagged expression of Cbf11. (A) Western analysis of MycHis- (plasmid pJR08, pREP42MHN backbone) and HA-tagged (plasmid pJR07, pREP41HAN backbone) Cbf11 in FY254 *S. pombe*. Cells were induced by the removal of thiamin from the media. Lysate of the untransformed FY254 fission yeast cells was used as a negative control. (B) Western analysis of His-tagged (plasmid pMP29, pET-15b backbone) Cbf11 in BL21 *E. coli*. Induction was carried out by the addition of IPTG. Samples taken at two different time points are shown for comparison.

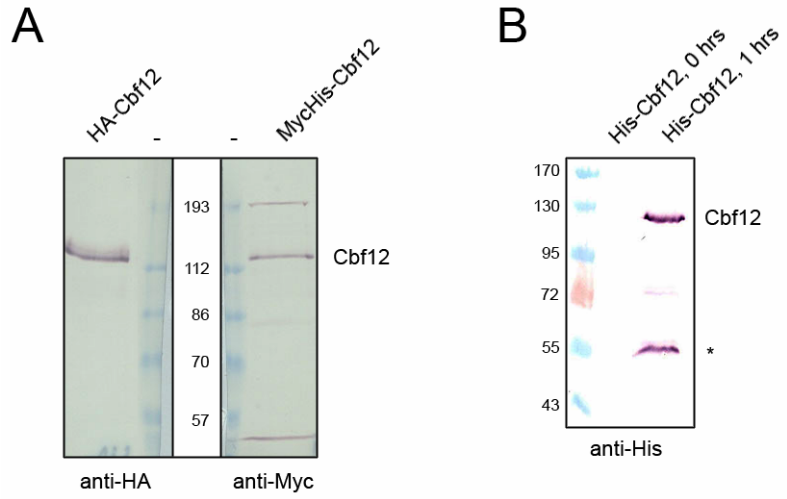

Figure 4.8 – Tagged expression of Cbf12. (A) Western analysis of HA- (plasmid pMP31, pREP41HAN backbone) and MycHis-tagged (plasmid pMP32, pREP42MHN backbone) Cbf12 in FY254 *S. pombe*. Cells were induced by the removal of thiamin from the media. Lysate (mixed with molecular weight markers) of the untransformed FY254 fission yeast cells was used as a negative control. (B) Western analysis of His-tagged (plasmid pMP35, pET-15b backbone) Cbf12 in BL21 *E. coli*. Induction was carried out by the addition of IPTG. A pre-induction sample (0 hrs) was used as a negative control. The asterisk denotes a degradation product of His-Cbf12.

4.3 Expression profiles of *cbf11*$^+$ and *cbf12*$^+$

To investigate the dynamics of the *cbf11*$^+$ and *cbf12*$^+$ genes expression, we decided to use quantitative real-time RT-PCR (qRT-PCR) to map their mRNA levels

at various stages of the fission yeast life cycle. The *act1*$^+$ gene coding for the fission yeast actin was chosen as a normalization control. Several assumptions regarding the qRT-PCR procedure had to be tested prior to the expression analysis itself (see Chapter 3.3.4.2).

4.3.1 qRT-PCR setup verification

Primer pairs were designed to amplify ~200 bp fragments close to the 3' termini of the target mRNAs (cDNAs). The primers were first tested in conventional PCR settings to select the most suitable annealing temperature and to verify their specificity (a single band on an agarose gel, shown as insets in Fig. 4.10B). Once this was accomplished, we proceeded to qRT-PCR calibration. To obtain accurate and reliable data, the PCR amplification efficiency for all genes analyzed must be similar and close to 100% over a range of target cDNA concentrations (Livak and Schmittgen, 2001). To test these premises we prepared twofold serial dilutions of the FY254 strain chromosomal DNA (100-1.5 ng) and subjected them to the qPCR analysis. With the sole exception of the lowest concentration (excluded from all calculations), we obtained good results confirming a roughly 100% efficiency of the amplification reaction. The range of C_Ts measured corresponded to the range expected for the actual analysis of cDNA. As stated above, the differences in amplification efficiencies of all genes analyzed have to be within a certain interval. Described in more detail, the differences in C_Ts of the corresponding samples (*cbf11*$^+$/*12*$^+$ vs. the *act1*$^+$ control) have to be calculated and regression lines constructed for these data. The absolute numeric values of the slopes of these lines should be close to zero (i.e., very small differences in the efficiency). The results of these calculations are plotted in Fig. 4.9.; the *cbf11*$^+$ vs. *act1*$^+$ ratio was found to be within limits, and the *cbf12*$^+$ vs. *act1*$^+$ ratio exceeded the limits, although not critically.

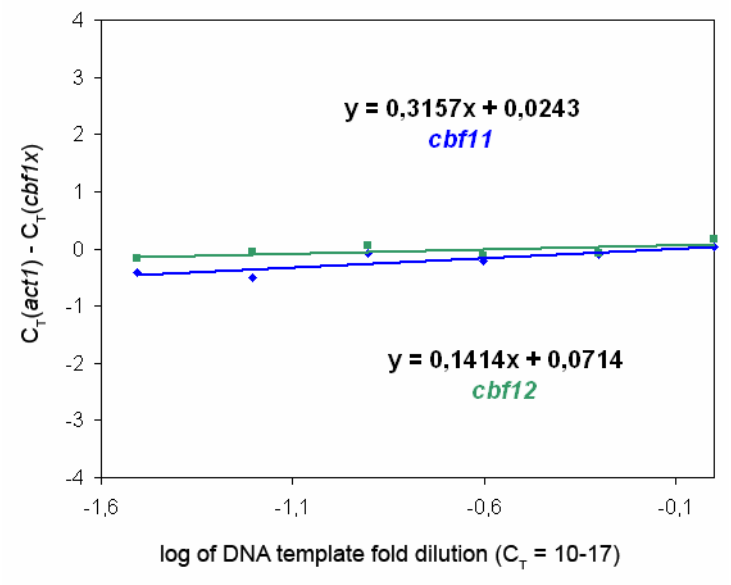

Figure 4.9 – Regression analysis of the differences in amplification efficiencies of the individual genes tested. Differences in C_Ts of the corresponding *cbf11*$^+$/*12*$^+$ and control reactions were plotted against the log(dilution) and regression lines were constructed. The regression line equation (y = kx + q) parameters were calculated and the slope (k) determined.

Next, we prepared cDNA from exponentially growing cells of the PN558 wild type strain and performed another round of qRT-PCR. This time, to get a rough estimate of the relative abundance of each target mRNA, and to asses the efficiency of DNase treatment during RNA isolation (see Chapters 3.3.2 and 3.3.4.2). Melting analysis of all reactions was also run to verify that only one DNA species is amplified. The results are presented in Fig. 4.10. Reverse transcription reactions where no RTase was present (and thus only genomic DNA contaminations were amplified) all gave similar and sufficiently low signals. Also, single fluorescence peaks were detected in all reactions proving that only the one desired PCR product was amplified.

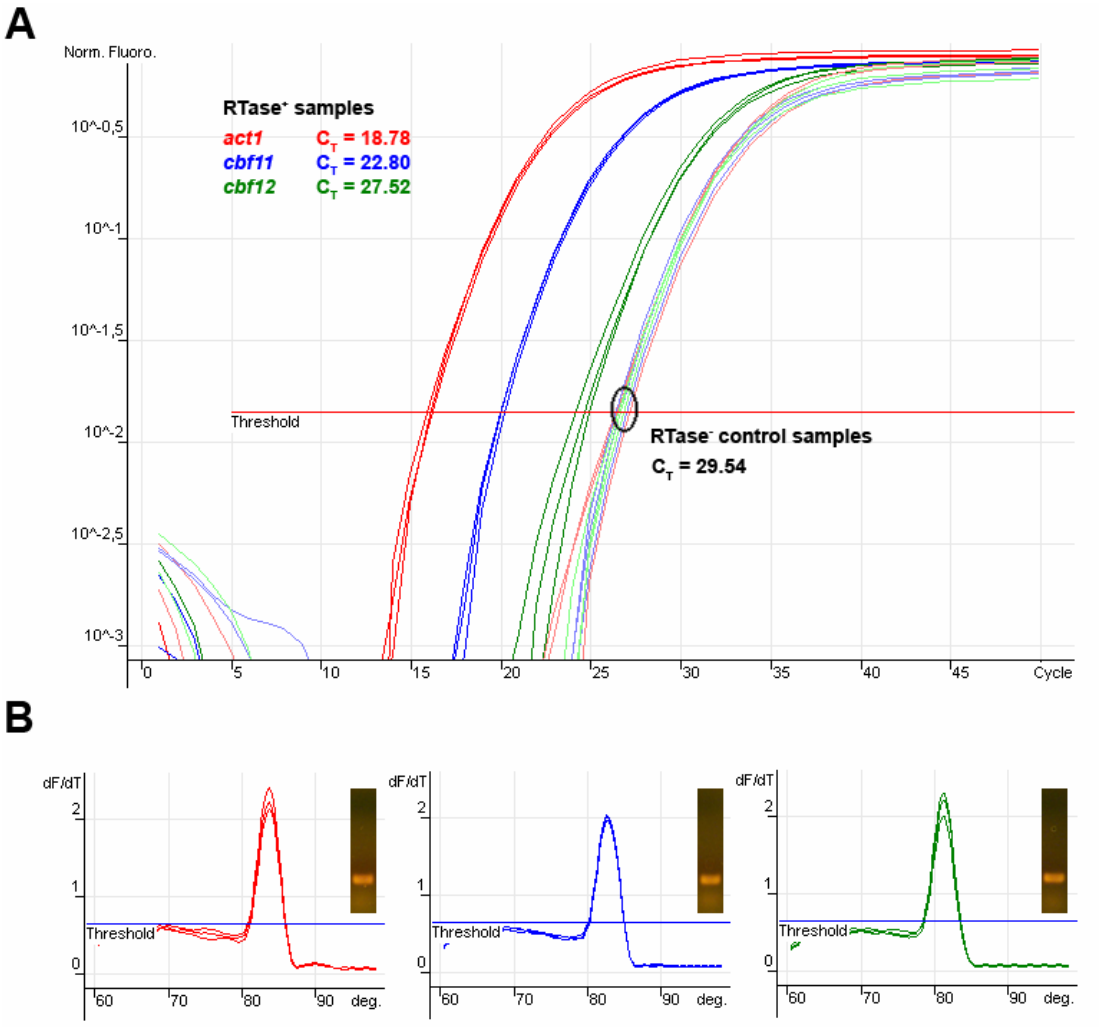

Figure 4.10 – qRT-PCR settings verification. (A) Wild type strain cDNA was analyzed and the relative abundance of *cbf11*$^+$, *cbf12*$^+$ and *act1*$^+$ mRNAs was measured. Mock-reverse transcribed control samples indicate the background (genomic) DNA content in our cDNA preparation. (B) Melting analysis of all samples shows a single peak for each pair of primers (color coding as in A). The insets show the respective PCR products run on a 2% agarose gel.

4.3.2 *cbf11*$^+$ and *cbf12*$^+$ expression analysis

Having passed all these tests successfully, we moved on to the actual cDNA levels analysis. We have analyzed RNA samples from haploid PN559 cells at various points of the growth curve, and from diploid cells (PN559 crossed with PN558) under vegetative growth conditions or after induction of sporulation (see Chapter 3.1.3.2). Both CSL genes are expressed at detectable levels (Fig. 4.11), with the *cbf11*$^+$ mRNA being roughly 50× less abundant, and the *cbf12*$^+$ mRNA being roughly 170× less abundant than the *act1*$^+$ normalization control during the early logarithmic phase of growth. There is an approximately two-fold downregulation of

the *act1*$^+$ normalization control during sporulation (Mata *et al.*, 2002). For this reason, the sporulation samples are not directly comparable with the others, although mutual comparisons between *cbf11*$^+$ and *cbf12*$^+$ mRNA levels under these conditions can still be made.

The expression of *cbf11*$^+$ seems to be fairly constant throughout the growth phases of haploid cells and similar mRNA levels were found in vegetative diploid cells. The less abundant *cbf12*$^+$ mRNA has a more variable profile with a marked increase (up to the levels of *cbf11*$^+$) as the cells enter the stationary phase, with a statistically significant peak at the late stationary phase (two-tailed independent Student's t-test, $p = 0.05$). A similar increase in the *cbf12*$^+$ mRNA levels was found in the sporulating cells, which is in accord with published data from the microarray profiling of the fission yeast meiotic transcriptome (Mata *et al.*, 2002). The *cbf12*$^+$ expression in vegetative diploid cells is similar to early-log phase haploids. The differences in expression patterns between the two CSL paralogs strongly suggest they play distinct roles in fission yeast.

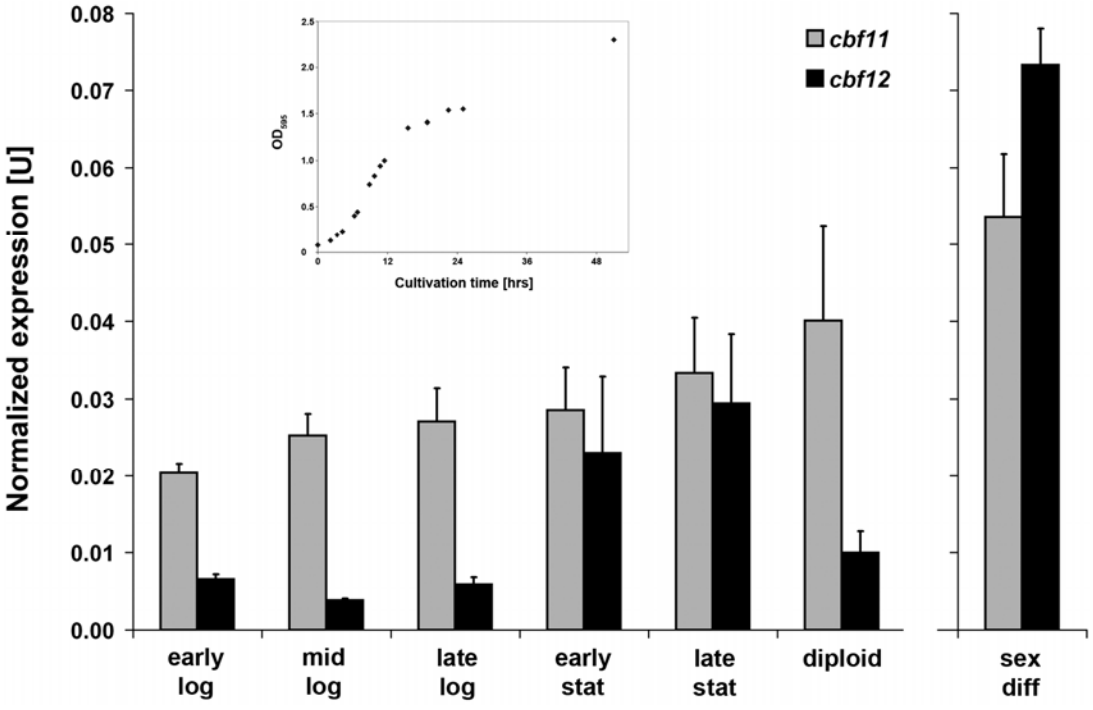

Figure 4.11 – Expression profiles of *cbf11*$^+$ and *cbf12*$^+$. The expression of *cbf11*$^+$ and *cbf12*$^+$ mRNAs was measured under various cultivation conditions using qRT-PCR. Samples were taken at different time points along the growth curve – the early, mid and late logarithmic phase ("log"), early and late stationary phase ("stat"), from diploid cells growing vegetatively ("diploid") and 8 hours after

induction of sporulation ("sex diff"). Mean values for 2-4 independent experiments are shown, the error bars represent the standard error. The inset shows a growth curve of the haploid PN559 cells used for RNA extraction.

4.4 Subcellular localization of Cbf11 and Cbf12

Important clues regarding the function of a protein may be learnt from its localization within the cell. Therefore, we have created EGFP fusion plasmid constructs for both fission yeast CSL genes. Furthermore, we attempted to create chromosomally tagged EGFP knock-in (KI) strains, as these settings provide information of high physiological relevance. All constructs were then used for microscopic localization analyses.

4.4.1 EGFP fusion plasmids and knock-in generation

Episomal vectors from the above-mentioned pREP41/42 series (Craven *et al.*, 1998) were used for the thiamin-regulatable expression of N-terminal EGFP fusions with Cbf11 and Cbf12. Two variants were created, bearing either the *ura4*$^{+}$ or the *LEU2* selection marker, respectively, and expression of the fusion proteins was verified by western blotting (Fig. 4.12 and Fig. 4.13). Interestingly, the *LEU2* constructs gave consistently higher fusion protein expression levels. Since *LEU2* is a gene of *S. cerevisiae*, inefficient inter-species complementation may be responsible for higher copy numbers of the *LEU2* plasmids, and thus for higher protein production.

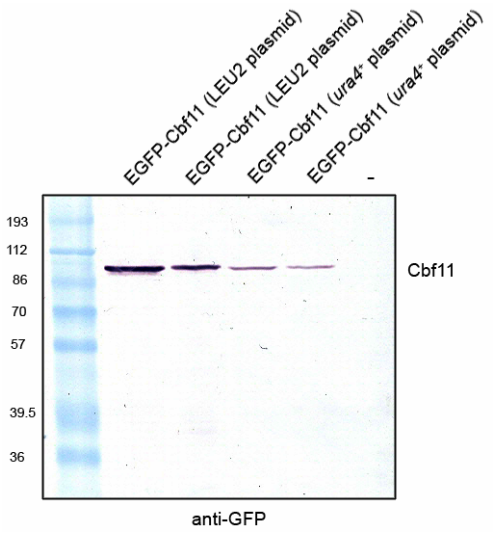

Figure 4.12 – Western verification of EGFP-tagged Cbf11 expression in FY254 *S. pombe* (plasmid pJR09, pREP41EGFPN backbone, *LEU2* marker; plasmid pJR10, pREP42EGFPN backbone, *ura4*$^+$ marker). The lysate of the untransformed FY254 fission yeast cells was used as a negative control.

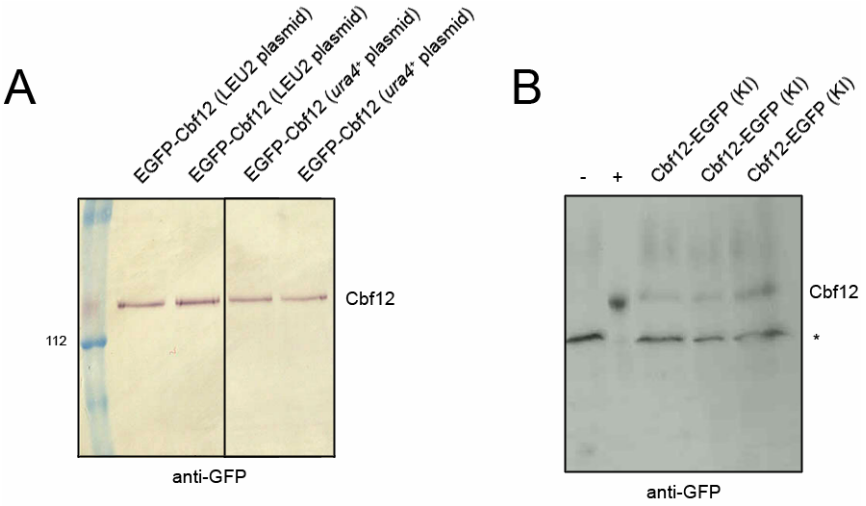

Figure 4.13 – EGFP-tagged expression of Cbf12. (A) Western verification of EGFP-tagged Cbf12 expression in FY254 *S. pombe* (plasmid pMP33, pREP41EGFPN backbone, *LEU2* marker; plasmid pMP34, pREP42EGFPN backbone, *ura4*$^+$ marker). (B) ECL detection of Cbf12-EGFP expressed from a knock-in allele constructed in the PN559 background. The lysate of the untransformed FY254 fission yeast cells was used as a negative control, and the lysate of the FY254 cells carrying the pMP34 plasmid were used as a positive control, respectively. The asterisk indicates a non-specific band.

A number of cassettes are available for one-step PCR-mediated chromosomal gene tagging in *S. pombe* (Bahler *et al.*, 1998;Van Driessche *et al.*, 2005). We have chosen to create C-terminal EGFP chromosomal fusions in the *cbf11*$^+$ and *cbf12*$^+$ loci. The tagging cassette (vector pFA6a-GFP(S65T)-kanMX6; (Bahler *et al.*, 1998)) contains a kanamycin resistance gene for the selection of recombinant clones. The original and recombinant tagged loci of both CSL genes are depicted in Fig. 4.14 and 4.15. While we have succeeded in the case of *cbf12*$^+$ (see PCR verification in the inset of Fig 4.15 and western analysis in Fig. 4.13B), we have repeatedly failed to produce a KI for *cbf11*$^+$ in this manner, in spite of trying several modifications of the tagging protocol (targeting cassette purification methods, transformation and selection protocol details). We only got non-specific integrations elsewhere in the genome or PCR-positive clones that, however, failed to display any GFP signal when analyzed microscopically or by western blotting (data not shown). We have repeated the whole procedure with a different cassette (pFA6-EYFP-natMX6), consisting of

EYFP, a yellow mutant of GFP, and a nourseothricin resistance gene, however, with no success. We suspect that locus-specific constrains do not allow for tagging the *cbf11*$^{+}$ gene with GFP variants, since we had no difficulty producing either the *cbf12*$^{+}$*::EGFP* or *cbf11*$^{+}$*/12*$^{+}$*::TAP* knock-ins (see Chapter 4.6).

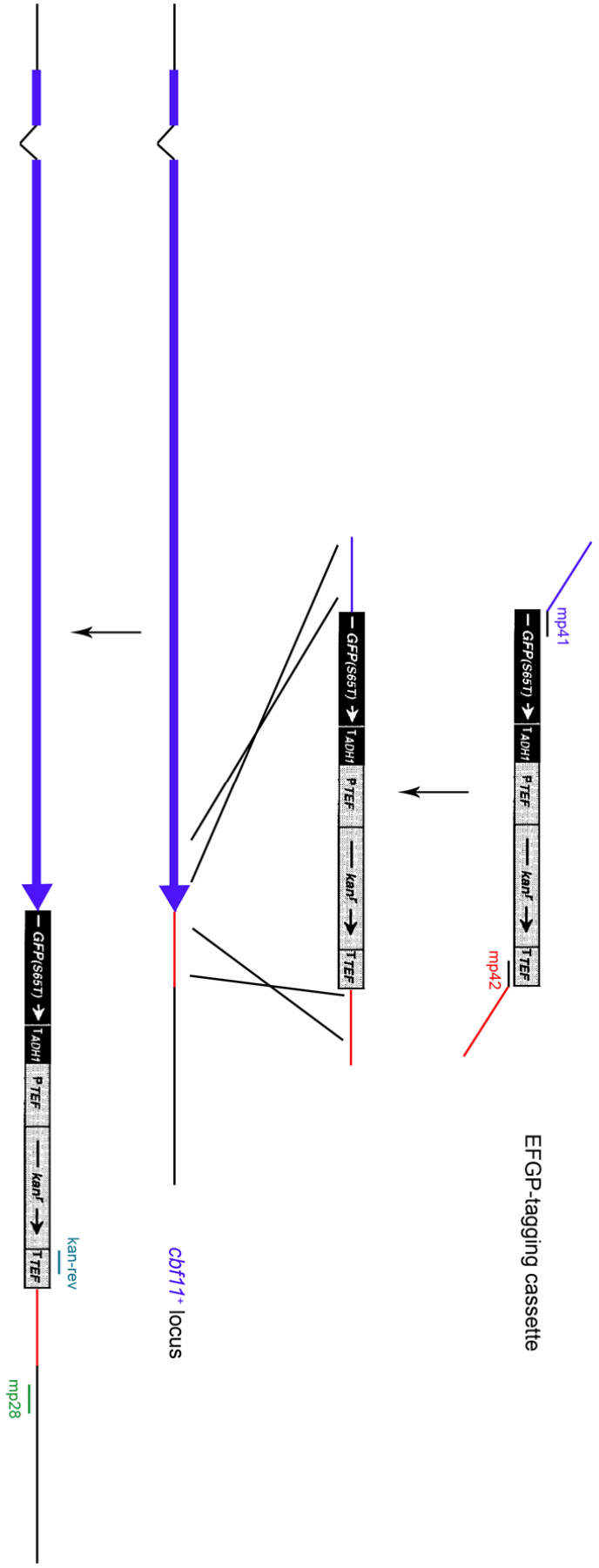

Figure 4.14 – *cbf11*$^{+}$ chromosomal EGFP knock-in construction scheme. The tagging cassette was PCR-amplified using primers with overhangs specific for the target locus, and transformed into fission yeast cells. Recombination events were selected on G418 (geneticin) YES plates and verified by colony PCR. Positions of primers used for the construction and knock-in verification are indicated (adapted from (Bahler *et al.*, 1998)).

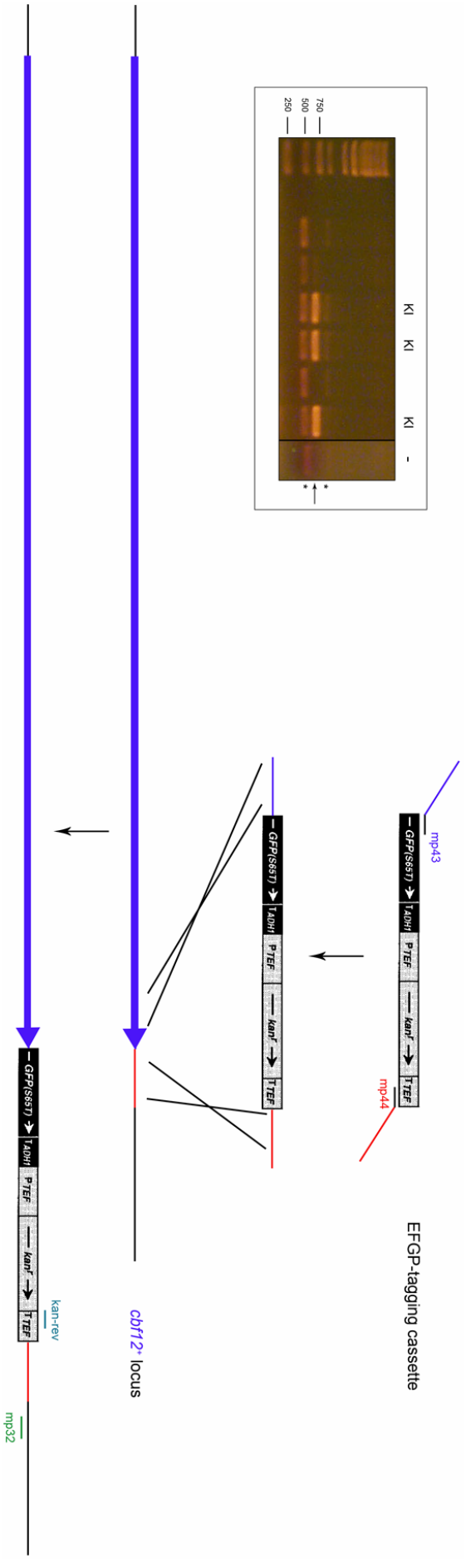

Figure 4.15 – *cbf12*$^{+}$ chromosomal EGFP knock-in construction scheme. The tagging cassette was PCR-amplified using primers with overhangs specific for the target locus, and transformed into fission yeast cells. Recombination events were selected on G418 (geneticin) YES plates. Positions of primers used for the construction and knock-in verification are indicated (adapted from (Bahler *et al.*, 1998)). The inset shows PCR verification of the proper integration – positive clones are denoted as "KI" (strains MP12, MP13, MP14); The PN559 parent strain was used as a negative control; the arrow denotes the specific product, and the asterisks mark non-specific products resulting from the usage of a home-made, impure Taq polymerase.

4.4.2 Confocal microscopy of EGFP-fused Cbf11 and Cbf12

After preparing all the EGFP-fusion constructs described above, we carried out localization analysis using confocal fluorescence microscopy. Both Cbf11 and Cbf12 displayed very similar, rather diffuse nuclear localization (Fig. 4.16A, B), although some fine structuring could be seen on 3D reconstructions from Z-axis optical sections (Fig. 4.16C). Both CSL proteins seemed to be excluded from the nucleolus (dark crescents in the green ball of the nucleus). The results we obtained were consistent for both fixed and living cells. The subcellular distribution of Cbf12 in the EGFP KI strain (close to the physiological levels of the protein) was found to be the same as in the case of overexpression from a plasmid, although, as expected, the signal was considerably weaker. As *cbf12*$^{+}$ is more expressed at the stationary phase than in the log phase (see Chapter 4.3.2), we compared the Cbf12-EGFP localization pattern between these two stages but found no differences (data not shown). The nuclear localization of the fission yeast CSL proteins is in agreement with their proposed role as transcription factors.

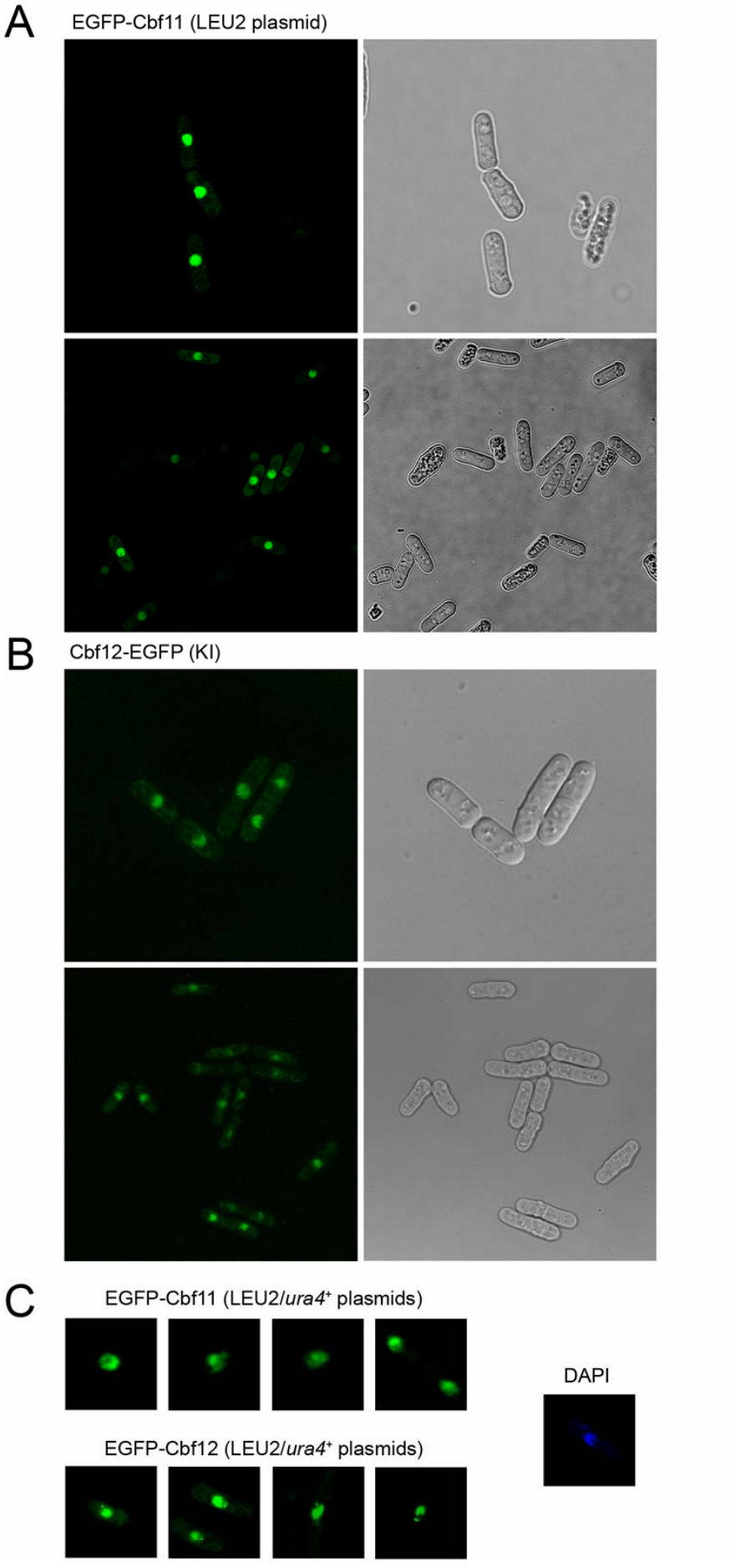
A
EGFP-Cbf11 (LEU2 plasmid)
B
Cbf12-EGFP (KI)
C
EGFP-Cbf11 (LEU2/ura4+ plasmids)
EGFP-Cbf12 (LEU2/ura4+ plasmids)
DAPI

Figure 4.16 – Subcellular localization of Cbf11 and Cbf12. (A) EGFP-Cbf11 expression was induced in FY254 cells carrying the pJR09 plasmid (pREP41EGFPN backbone). Live log-phase cells were washed, placed on an agarose-coated slide and viewed under a confocal microscope. (B) Live log-phase Cbf12-EGFP knock-in cells (strain MP12) were washed, placed on an agarose-coated slide and viewed under a confocal microscope. (C) Details of nuclei from ethanol fixed cells expressing either EGFP-Cbf11 or EGFP-Cbf12 (plasmid-driven). A DAPI-stained nucleus is shown for comparison. The EGFP signal overlaps with that of DAPI but is missing from nucleoli. Tiny green domains are visible on confocal Z sections, but the same is also true for the DAPI signal.

4.5 2H analyses – transcription activation potential of Cbf11 and Cbf12

4.5.1 Gal4 2H system

Next, we wished to search for potential interaction partners of Cbf11 and Cbf12, as their nature would likely be highly informative of the fission yeast CSL function. We utilized the commonly used yeast two-hybrid system based on the Gal4 transcription factor of *S. cerevisiae*. Before conducting any 2H screens, we wanted to test directly one candidate interaction partner – Snw1, the fission yeast member of the SNW/SKIP family of transcriptional and splicing coregulators (Folk *et al.*, 2004), as from the numerous metazoan CSL-interacting proteins, this one seems to be the only (or one of very few) homolog present in *S. pombe* (more details on the 2H experiments concerning Snw1 can be found in the master's thesis of Tomáš Groušl (Groušl, 2007); only general 2H results will be covered in this study). To this end, we have constructed a panel of plasmids containing combinatorial fusions of Cbf11/12 and Snw1 with the Gal4 activation domain (AD) and DNA-binding domain (DBD), respectively (see Table 3.9). Surprisingly, the introduction of both AD- and DBD-Cbf11 fusion proteins into the budding yeast CG-1945 reporter strain negatively affected the viability of the recipient cells. By contrast, the expression of DBD-Cbf12 alone triggered activation of the reporter gene (Fig 4.17B and Table 4.2). Such a situation prevented us from using the Gal4 2H system for any interaction analyses. Nevertheless, we decided to study the killing phenomenon in more detail.

Table 4.2 – CSL behavior in budding yeast 2H reporter cells.

	Gal4 2H (CG-1945 cells)		**LexA 2H (EGY48 cells)**	
	DBD	**AD**	**DBD**	**AD**
Cbf11	† (plasmid pMP27)	†† (plasmid pMP22)	↑ (plasmid pMP36)	N. D. (plasmid pMP37)
Cbf12	↑ (plasmid pMP40)	N. D.	† (plasmid pMP38)	N. D.

† – severe growth impairment; †† – no growth; ↑ – autoactivation; N. D. – not determined (Snw1 alone has been found to trigger activation of the reporter when fused to DBD, data not shown and (Ambrozkova *et al.*, 2001)).

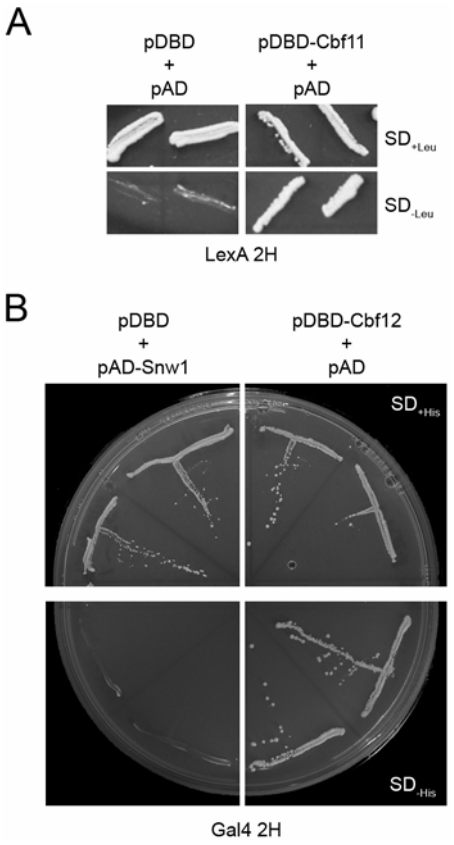

Figure 4.17 – DBD-Cbf11 and DBD-Cbf12 autoactivate reporter genes in *S. cerevisiae*. (A) LexA-Cbf11 can activate the reporter gene and support growth of the EGY48 cells on interaction-selecting medium ($SD_{-leucine}$) without the need for any interaction partner. (B) Gal4 DBD-Cbf12 triggers expression of the reporter gene and supports growth of the CG-1945 cells on interaction-selecting medium ($SD_{-histidine}$) without the need for any interaction partner.

CG-1945 cells expressing the DBD-Cbf11 fusion formed minute colonies; however, the AD-Cbf11 fusion had a more severe impact, as no transformant colonies could be obtained at all. Thus, we focused on the more pronounced effect of

AD-Cbf11. First, we confirmed that the killing was indeed caused by the Cbf11 hybrid protein. While the AD-Cbf11 expressing plasmid (pMP22) could not be transformed, many CG-1945 transformant colonies were obtained for its alternative having a frameshift at the junction of AD and Cbf11 (plasmid pMP23). Furthermore, when Cbf11 was removed from pMP22 and the empty vector was religated (plasmid pMP24), such plasmid regained the ability to be transformed into budding yeast cells (data not shown). We have then subcloned the Cbf11- and the AD-Cbf11-encoding fragments of pMP22 into pYES2, a vector allowing for inducible expression of proteins (plasmids pMP25 and pMP26, respectively) in *S. cerevisiae*. We got transformants for both plasmids in the appropriate EGY48 reporter strain that grew normally on glucose-containing non-inducing plates. Significantly, when transferred to the inducing galactose medium, Cbf11 alone was still tolerated, but the pMP26 plasmid inhibited growth of the EGY48 strain and various budding-related terminal phenotypes were visible upon microscopic examination (Fig. 4.18A, B). Similar phenotypes were seen in cells taken from the (yet again tiny) colonies of another *S. cerevisiae* 2H reporter strain, AH109, transformed with a DBD-Cbf11-producing plasmid (pMP27). In this case, a defective budding pattern and very small buds devoid of DNA were detected (Fig 4.18C). Thus, the decreased *S. cerevisiae* viability associated with the expression of AD- or DBD-Cbf11 is likely a result of the fusion proteins causing cell-cycle/budding misregulation.

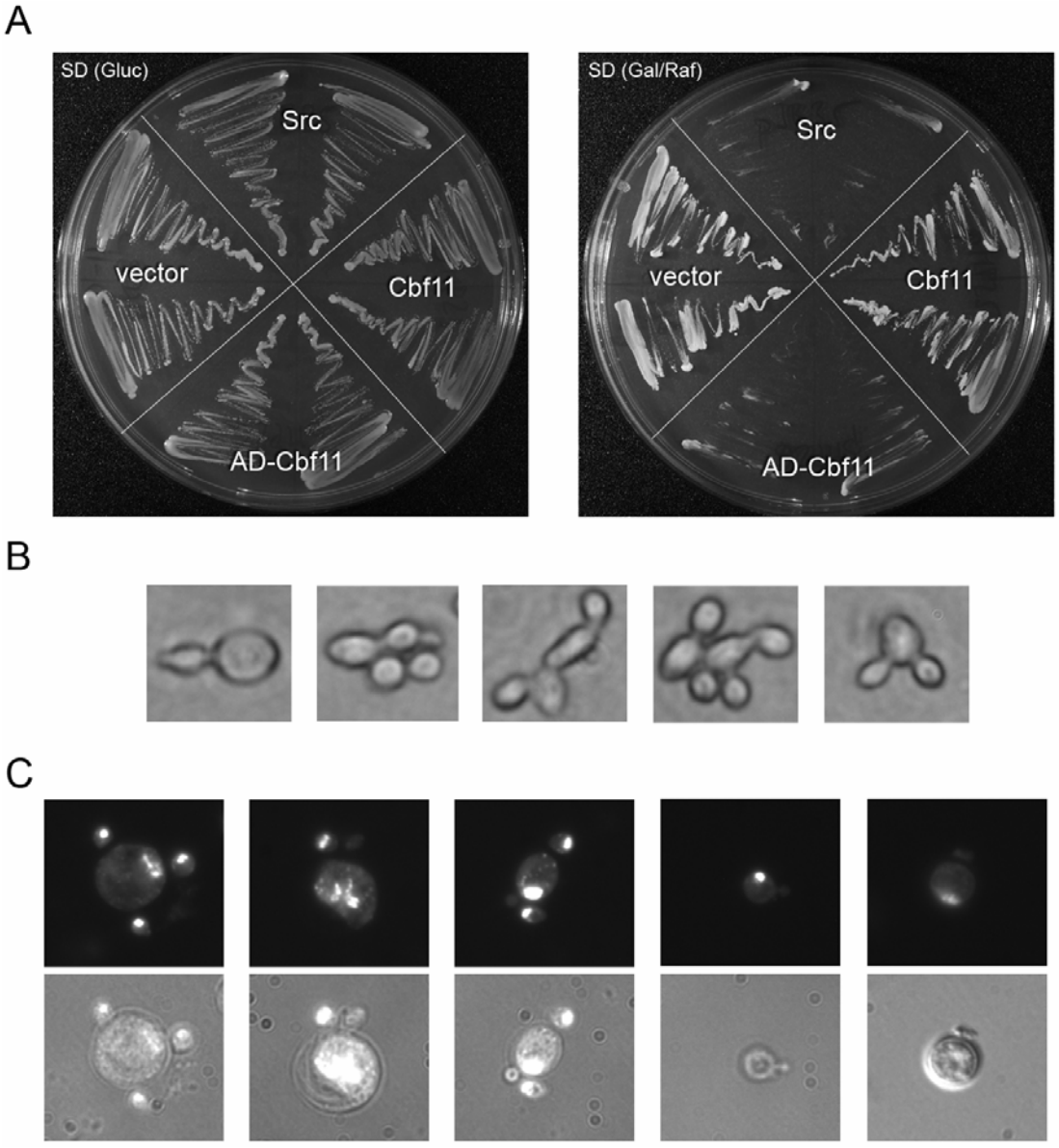

Figure 4.18 – *S. cerevisiae* cells are killed by the expression of Gal4-Cbf11 fusion proteins. (A) EGY48 cells were transformed with either the empty vector (pYES2), an Cbf11- (pMP25) or AD-Cbf11- (pMP26) expressing plasmid, or the Src kinase-producing plasmid which served as a killing control (pJB35; (Brabek *et al.*, 2002)). Growth on non-inducing (Gluc) and inducing (Gal/Raf) plates is shown. While Cbf11 alone is tolerated, AD-Cbf11 kills the cells. (B) The terminal phenotype of the AD-Cbf11-expressing cells from panel A (Gal/Raf plate) was observed under a microscope. (C) AH109 *S. cerevisiae* cells from dwarf colonies expressing DBD-Cbf11 (plasmid pMP27) were fixed and stained with DAPI. Representative examples of aberrant budding pattern are shown; some buds are lacking DNA.

4.5.2 LexA 2H system

Hoping to circumvent the Gal4-related problems described above, we switched to a different 2H system, based on the bacterial LexA DNA-binding protein

and an artificial AD. Another series of fusion plasmid constructs was prepared (see Table 3.9) and assayed. In these settings, the behavior of the individual CSL fusion proteins matched that of their paralog observed in the Gal4 2H system. That is, DBD-Cbf11 alone triggered activation of the reporter gene and DBD-Cbf12 had deleterious impact on the viability of the budding yeast EGY48 reporter cells (Fig. 4.17A and Table 4.2). We judge this capacity as indicative of the presence of an intrinsic activation domain in both Cbf11 and Cbf12. The interaction analysis and screening could still be performed using either truncated CSL proteins lacking the (yet unmapped) activation domains or using, e.g., a cytoplasmic 2H system. As these options are time-consuming and/or not feasible, we used other methods of identifying CSL interaction partners in *S. pombe*.

4.6 Isolation of TAP-tagged Cbf11 and Cbf12

Tandem affinity purification (TAP) is a robust method of isolating highly pure complexes of native target proteins together with their interaction partners (Puig *et al.*, 2001). As this method is a superior alternative to the previously-attempted 2H approach, we have constructed chromosomally tagged knock-in strains expressing either Cbf11-TAP or Cbf12-TAP in an autologous system and at close to physiological levels. The CTAP4-tagging cassette (pFA6a-CTAP4-natMX6; (Van Driessche *et al.*, 2005)), consisting of a calmodulin-binding domain, four protein A modules, followed by a nourseothricin resistance selection marker, was amplified with primers containing gene-specific overhangs, and integrated at the *cbf11*$^+$ and *cbf12*$^+$ loci, respectively, in the PN559 parent strain to produce in-frame C-terminal fusions. Nourseothricin-resistant clones were tested for proper integration by colony PCR. The original and recombinant tagged loci of both CSL paralogs are depicted in Figs. 4.19 and 4.20.

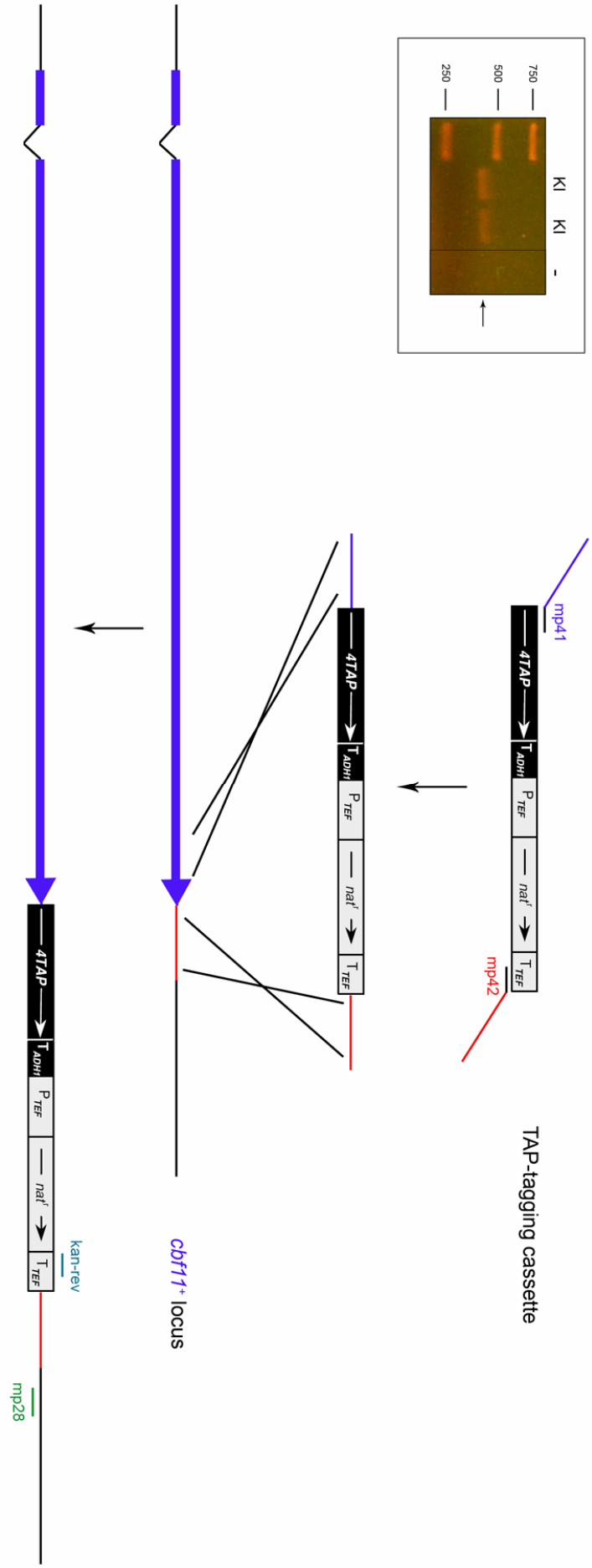

Figure 4.19 – *cbf11*$^{+}$ chromosomal TAP knock-in construction scheme. The tagging cassette was PCR amplified using primers with overhangs specific for the target locus, and transformed into fission yeast cells. Recombination events were selected on ClonNAT (nourseothricin) YES plates. Positions of primers used for the construction and knock-in verification are indicated (adapted from (Van Driessche *et al.*, 2005)). The inset shows PCR verification of the proper integration (strains MP15, MP16); PN559 cells were used as a negative control; the arrow denotes the specific product.

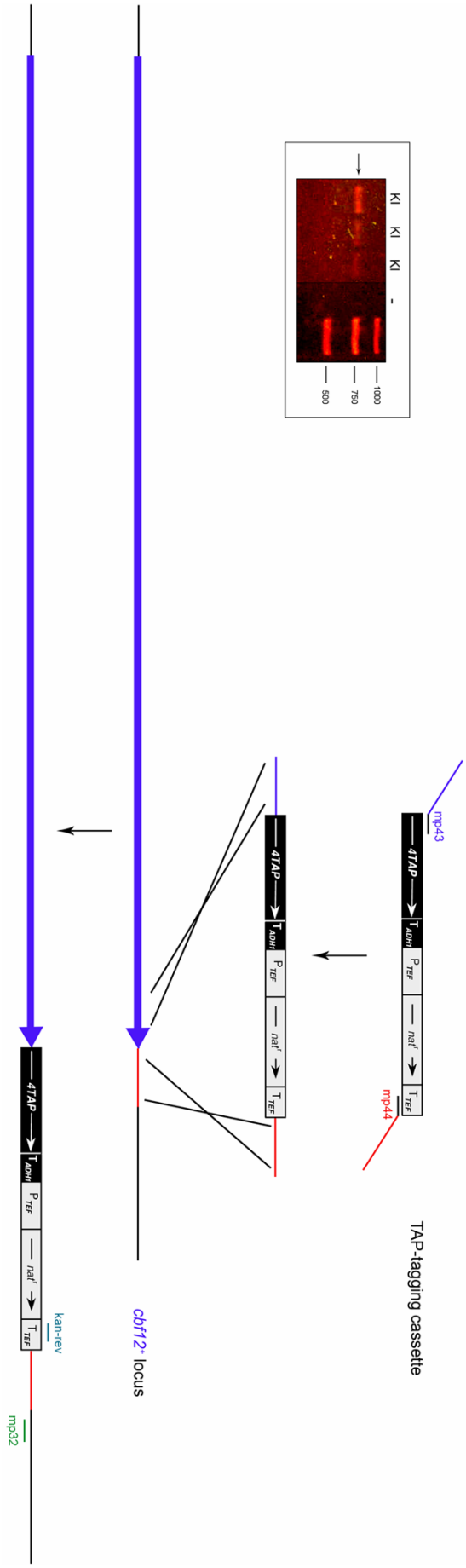

Figure 4.20 – *cbf12*$^{+}$ chromosomal TAP knock-in construction scheme. The tagging cassette was PCR amplified using primers with overhangs specific for the target locus, and transformed into fission yeast cells. Recombination events were selected on ClonNAT (nourseothricin) YES plates. Positions of primers used for the construction and knock-in verification are indicated (adapted from (Van Driessche *et al.*, 2005)). The inset shows PCR verification of the proper integration (strains MP17, MP18, MP19); PN559 cells were used as a negative control; the arrow denotes the specific product.

Once the recombinant TAP-tagged strains were obtained, a pilot purification of Cbf11-TAP was carried out in collaboration with Dr. Michal Skružný, Heidelberg University, Germany. As starting material, 8 liters of culture of the MP15 strain were used. As judged by western analysis (Fig. 4.21A), the tagged protein was captured quantitatively. Nevertheless, the amount of protein obtained was insufficient for mass spectrometry analysis and a band corresponding to Cbf11 could not be identified on a silver stained gel of the purification fractions (Fig. 4.21B and data not shown).

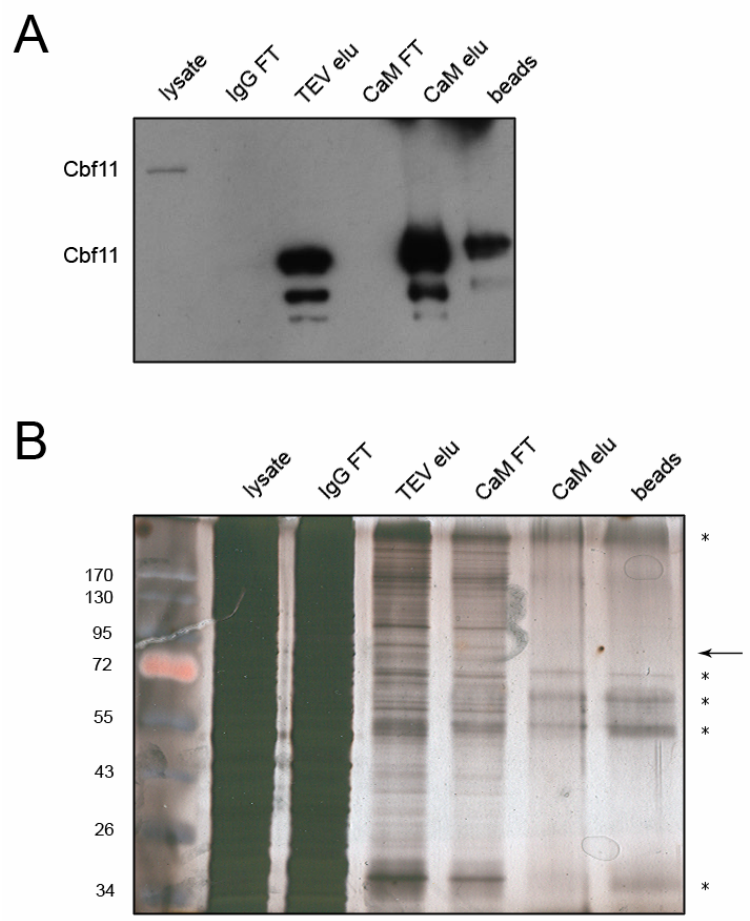

Figure 4.21 – Purification of Cbf11-TAP. (A) Western analysis of the individual purification fractions – lysate of MP15 cells ("lysate"), flow-through from IgG beads ("IgG FT"), eluate released by the TEV protease ("TEV elu"), flow-through from calmodulin beads ("CaM FT"), the final eluate released by calmodulin ("CaM elu"), proteins remaining attached to the calmodulin beads ("beads"). (B) The samples from panel A were run on a polyacrylamide gel and silver-stained. The arrow shows the anticipated position of Cbf11-TAP; the asterisks denote presumed contaminating proteins.

The whole procedure was then repeated with both Cbf11-TAP (strain MP15) and Cbf12-TAP (strain MP17) in collaboration with Tomáš Groušl, Czech Academy

of Science. The parent PN559 strain served as a background control. This time, 4 liters of each stationary culture (OD >4) was used for the purification, and the resulting three eluates were analyzed by mass spectrometry directly from the solution. Unfortunately, only known contaminating proteins were identified (metabolic enzymes, ribosomal proteins; data not shown) and, significantly, we even failed to detect the TAP-tagged proteins themselves. It is possible that much higher amounts of culture would be needed for a successful analysis, which poses serious technical limitations, and we did not pursue this direction further.

4.7 DNA binding properties of Cbf11

The fungal CSL proteins contain all the amino acid motifs and residues necessary for sequence-specific binding of DNA (Fig. 4.3 and (Kovall and Hendrickson, 2004;Prevorovsky *et al.*, 2007)). We have therefore conducted gelshift experiments in order to characterize the DNA binding properties of Cbf11 and Cbf12 *in vitro*. The optimized reaction conditions (such as carrier DNA concentration, incubation temperature) are described in Chapter 3.3.6.

First, we sought for a CSL-type DNA binding activity in the lysates of wild type *S. pombe*. We prepared a panel of double stranded DNA oligonucleotide probes containing CSL consensus binding sites ($GTG^{G}/_{A}GAA$; (Hayward, 2004)) with their respective flanking regions from various mammalian, insect and viral CSL-responsive promoters (see Fig. 4.22A for details). We used two mutated versions of the Kaposi's Sarcoma-Associated Herpesvirus-derived probe as negative controls. The first control probe, termed MUT, contained a single G→C substitution at the G_5 position, that was shown to be critical for metazoan CSL binding (Barolo *et al.*, 2000). The CSL response element was completely scrambled in the second control probe, DEL. As shown in Fig. 4.22B, we were indeed able to see a specific CSL-like DNA binding activity for the RBP and KSHV probes. Weak binding was also observed for the m8 and HES probes (data not shown). This activity was concentration dependent and could be competed with a relatively low excess of unlabeled probe. This is indicative of a very specific binding, given the presence of great excess (10,000×) of carrier DNA in the gelshift reaction. Using protein extracts from deletion strains (see Chapter 4.8) as controls, we have ascribed this DNA binding activity to Cbf11 (Fig. 4.22B, compare the left and the right halves of the

gels). There was clearly no binding to either the MUT (Fig. 4.22B) or DEL control probes in the yeast lysates (data not shown), further confirming that Cbf11 recognizes and binds to the CSL response element in a highly specific manner. So far, we failed to see any DNA binding activity attributable to Cbf12, despite the fact that lysates prepared from cells grown under several different growth conditions and convenient deletion strain controls (Δ*cbf11*, and Δ*cbf11* Δ*cbf12*) were used.

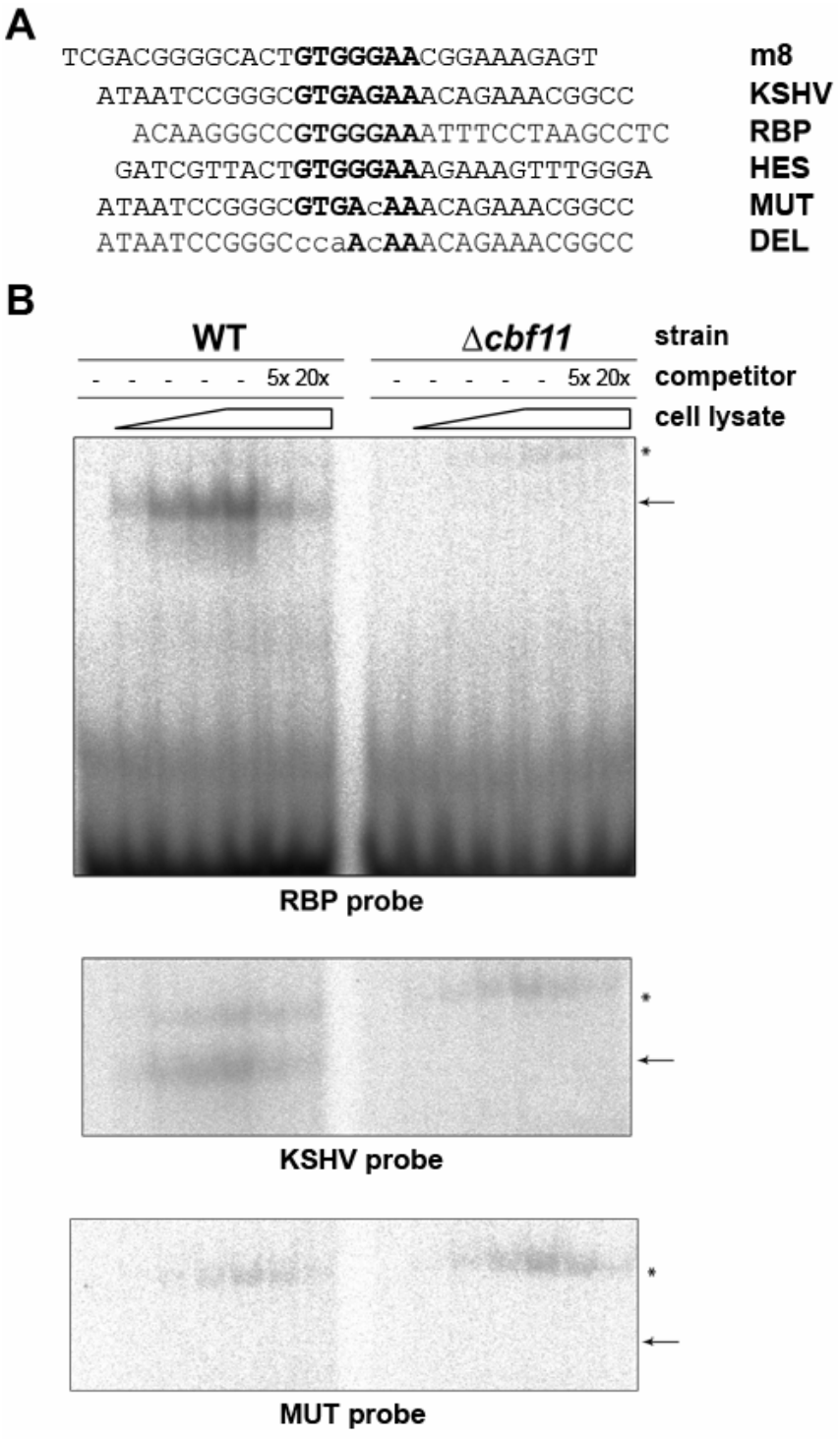

Figure 4.22 – Cbf11 binds to the CSL response element on DNA. (A) The sequences (sense strands only) of the DNA probes used for gelshift experiments. The sequences were derived from the promoters of known CSL-responsive genes from various organisms. "m8" – drosophila m8 gene (Chung *et al.*, 1994), "KSHV" – Kaposi's Sarcoma-Associated Herpesvirus K14/vGPCR gene (Liang and Ganem, 2004), "RBP" and "HES" – mouse RBP-Jκ and HES-1 genes, respectively (Oswald *et al.*, 1998). The control probes were derived from the KSHV sequence by a point mutation of the critical G residue ("MUT") or by a complete disruption of the CSL binding site ("DEL"). The CSL response element is printed in bold. (B) Representative gelshift experiments documenting the existence of a highly specific CSL response element-binding activity in WT *S. pombe* lysates. Significantly, the activity is absent from lysates prepared from Δ*cbf11* cells or when a mutated probe is used. The faint uppermost band (*) corresponds to an unknown non-specific binding activity.

We then repeated the gelshifts with a MycHis-tagged Cbf11 protein affinity-purified from *S. pombe* (see Chapter 3.2.2). The results shown in Fig. 4.23A further support our data from yeast cell lysates and document the varying affinity of Cbf11 for the respective probes. Again, there was no binding to either of the negative control probes. To demonstrate that the binding of Cbf11 to DNA is direct, we expressed the protein in *E. coli* and then carried out gelshifts with Cbf11-containing bacterial lysates in settings similar to these in Fig. 4.22. The optimized protocol for Cbf11 and Cbf12 expression in bacteria is described in Chapter 3.1.1. We were able to recapitulate the results obtained with *S. pombe* proteins/lysates for the RBP and KSHV probes, the ones that were bound most strongly by endogenous Cbf11 (Fig. 4.23B). There was no binding to either the MUT or DEL control probes (data not shown). The binding of the HES and m8 probes was most likely below the detection limit of the assay (data not shown). When *E. coli* cultures expressing Cbf12 were used, no binding could be detected, similar to the fission yeast lysates data (data not shown). Taken together, at least one of the *S. pombe* CSL proteins, Cbf11, is capable of binding DNA in a highly specific way like the classical metazoan family members (class M) – a critical finding that establishes the fungal CSL proteins as genuine family members.

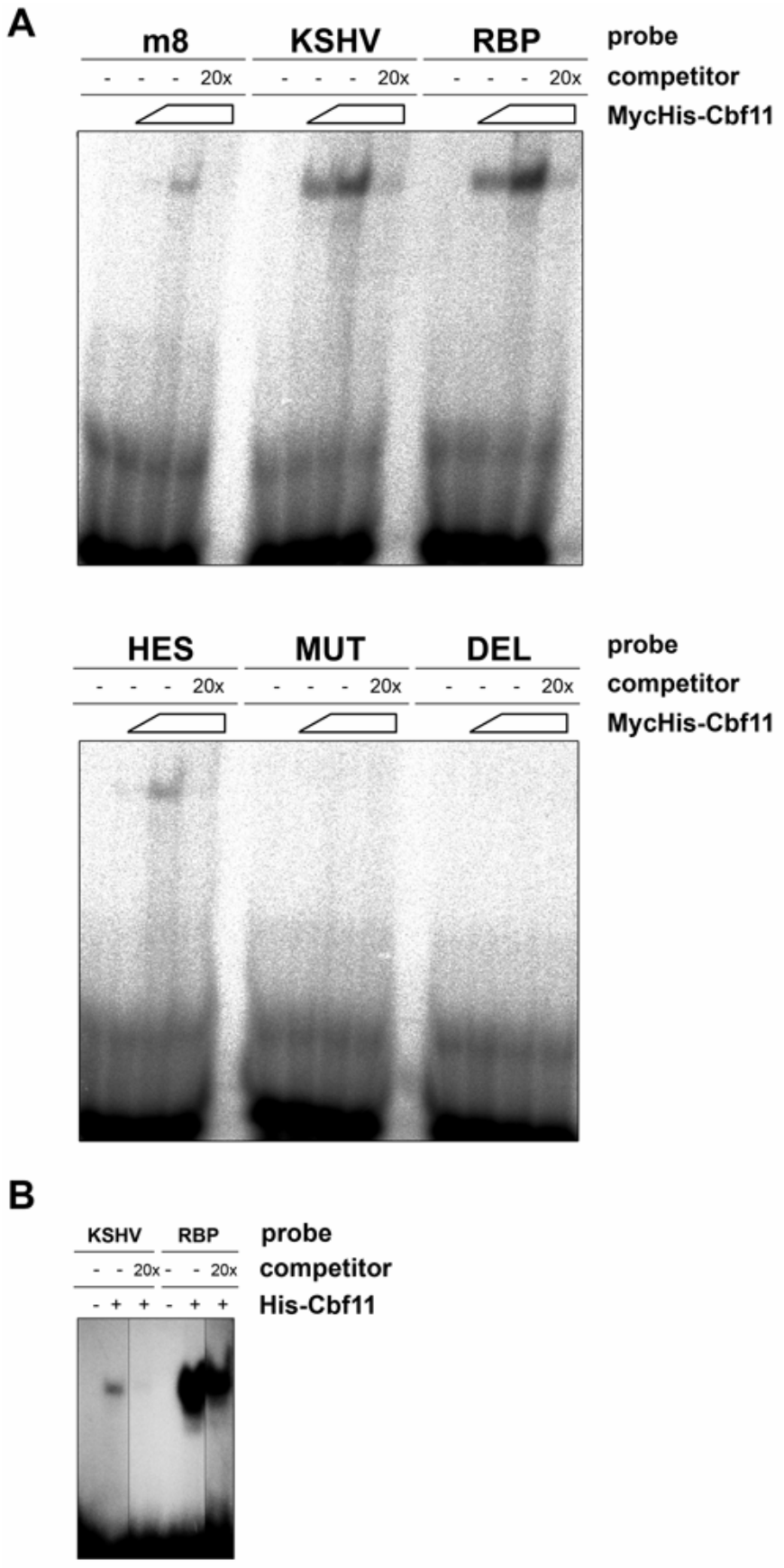

Figure 4.23 – DNA binding activity of recombinant Cbf11. (A) Recombinant MycHis-Cbf11 was affinity-purified from *S. pombe* lysates and subjected to gelshift experiments with the set of probes

introduced in Fig. 4.22A. Cbf11 is capable of binding these probes with very high specificity as there was no binding either to the single point mutation-containing MUT or the scrambled DEL control probes. (B) Recombinant His-Cbf11 was expressed in BL21 *E. coli* and bacterial lysates were subjected to gelshift experiments. Bacterially produced Cbf11 is capable of binding the RBP and KSHV probes. The lysate of cells transformed with the empty vector only was used as a negative control. Only relevant lanes from a single representative gel are shown.

4.8 Phenotypes of the Δ*cbf11* and Δ*cbf12* single and double deletion strains, and overexpression studies

4.8.1 Knock-out construction

To learn more about the function of the fission yeast CSL family members, we next used the classical gene deletion approach. A Δ*cbf11* strain had already been prepared (in a diploid PN558 × PN559 background) as a part of the fission yeast genome-wide gene deletion pilot project (Decottignies *et al.*, 2003). It was found to be viable but was not characterized any further. The strain was constructed using a standard one-step PCR-mediated targeting procedure (pFA6a-kanMX6 template; (Bahler *et al.*, 1998)) and the *cbf11*$^+$ ORF was replaced with a kanamycin resistance cassette by homologous recombination. The construction procedure is schematized in Fig. 4.24. We have obtained an *h*$^-$ haploid Δ*cbf11* strain (CBF11 KO) and the corresponding parental strains (PN558, PN559) from Dr. Anabelle Decottignies, Cancer Research UK, and crossed the deletion into cells of the *h*$^+$ mating type (strains MP05, MP06) to allow for testing of any possible mating type-specific functions. The genotype was verified by PCR (Fig. 4.24, inset; see Chapter 3.1.3.2 for more details).

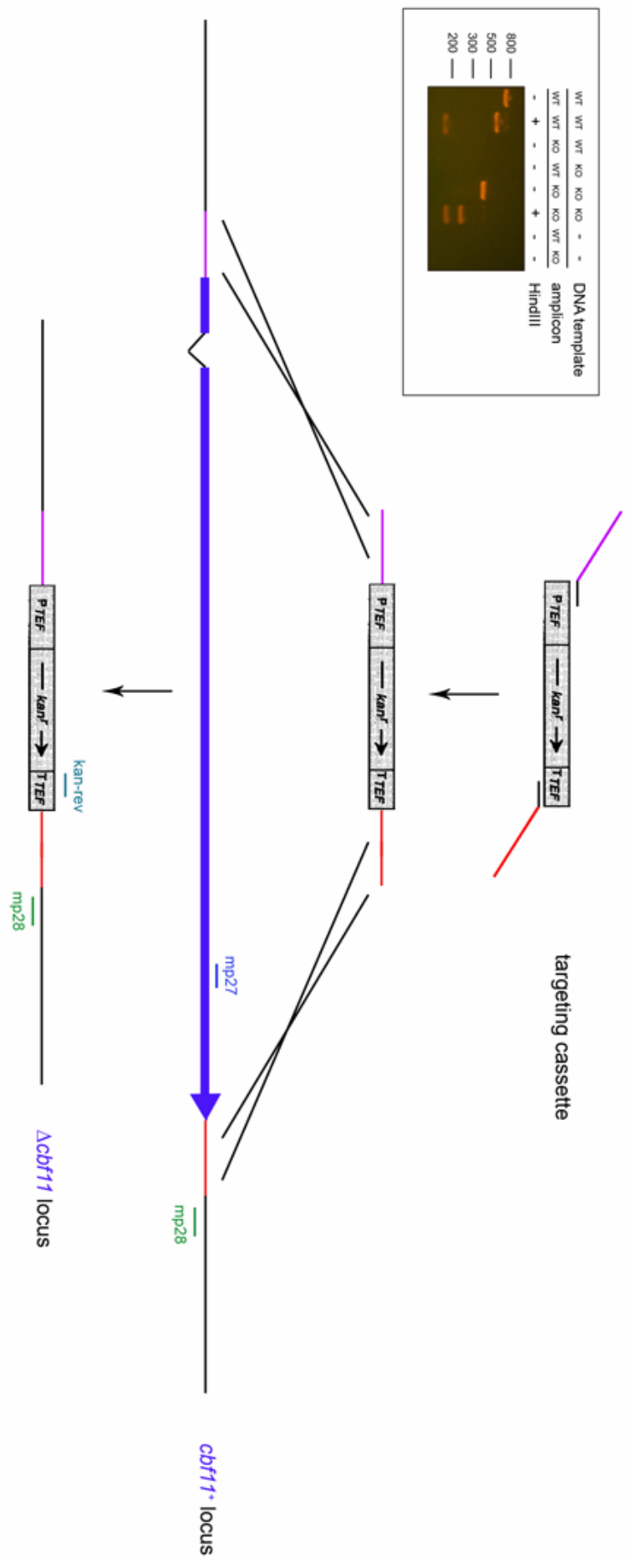
DNA template
WT WT WT KO KO KO - -
amplicon
WT WT KO WT KO KO WT KO
HindIII
- + - - - + - -
800
500
300
200
targeting cassette
kan-rev
mp27
mp28
mp28
cbf11+ locus
Δcbf11 locus

Figure 4.24 – Δ*cbf11* knock-out construction scheme. The targeting cassette was PCR amplified using primers with overhangs specific for the target locus, and transformed into fission yeast cells. Recombination events were selected on G418 (geneticin) YES plates. Positions of primers used for the knock-out verification are indicated (adapted from (Bahler *et al.*, 1998) according to (Decottignies *et al.*, 2003)). The inset shows verification of the KO genotype (strain CBF11 KO) by PCR and restriction analysis. FY254 cells were used as a WT control; the expected band pattern is: WT – uncleaved 718 bp, HindIII-cleaved 548 and 170 bp, KO – uncleaved 381 bp, HindIII-cleaved 211 and 170 bp.

The Δ*cbf12* deletion strain had also been prepared previously during a large-scale study of uncharacterized, meiotically upregulated genes (Gregan *et al.*, 2005). The KO was found to be viable and did not display any meiosis-related phenotypes; other characterization was not performed. Unfortunately, the deletion was constructed in h^{90} homothallic cells (able to switch mating type), which was impractical for our purpose. Thus, we wished to use the available targeting vector (Gregan *et al.*, 2005) to construct the KO in h^- and h^+ heterothallic cells to prevent possible phenotype ambiguities arising from mating-type switching. Surprisingly, the targeting vector (clone 289 in pCloneNAT1; http://mendel.imp.ac.at/Pombe/) failed our initial restriction analysis (Fig. 4.25A, C). A more detailed restriction mapping and sequencing of the recombinogenic arms (performed in collaboration with Dr. Juraj Gregáň, Research Institute of Molecular Pathology, Austria) revealed that one of the arms was inverted (Fig. 4.25D), thus likely prohibiting efficient homologous recombination and KO construction. By excision and religation we switched the orientation of the problematic sequence (Fig. 4.25B), yielding a fully functional targeting vector (plasmid pMP45).

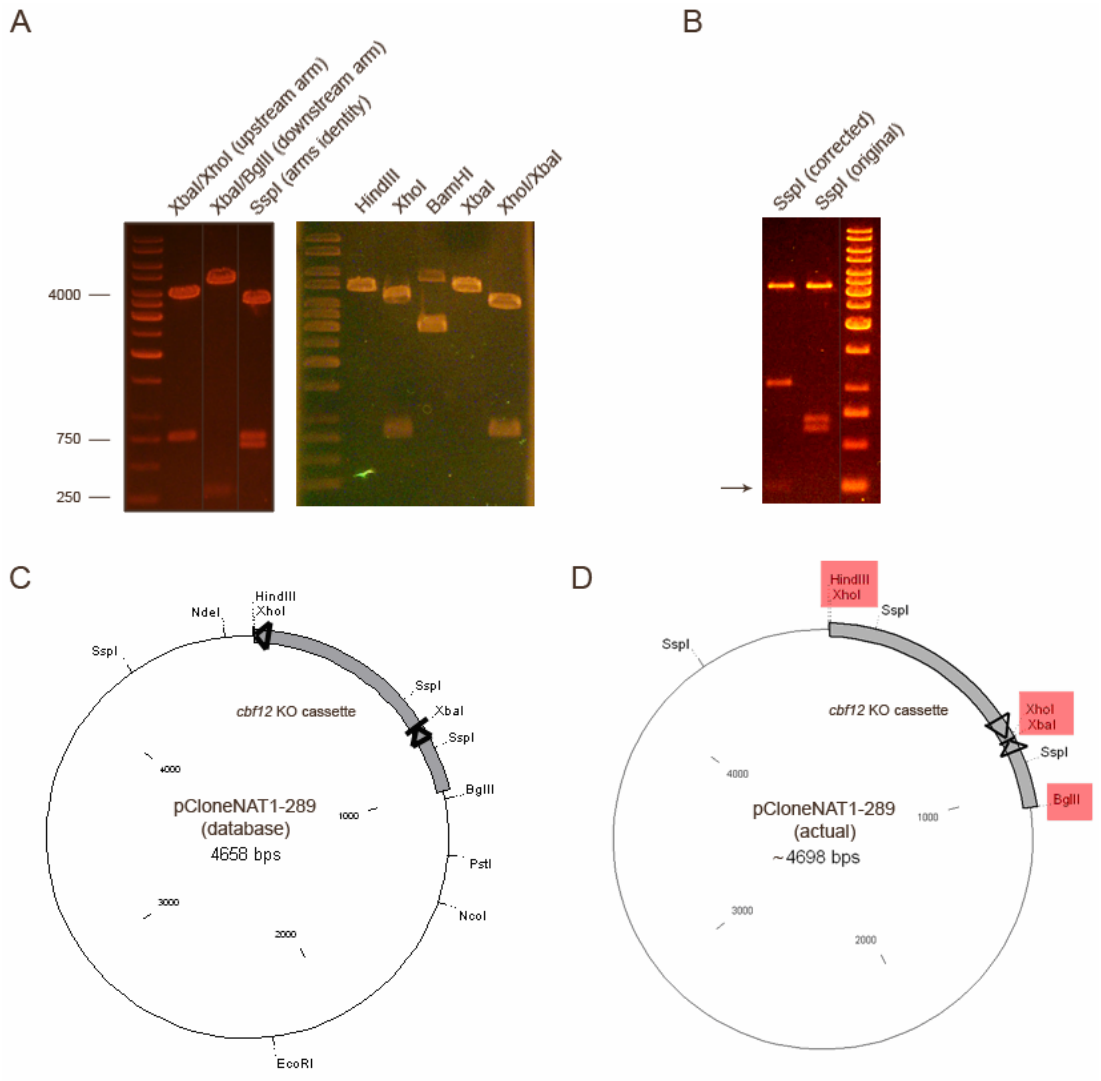

Figure 4.25 – *cbf12*$^{+}$ targeting vector corrections. According to the database record, the recombinogenic arms should have been inserted XhoI/XbaI into XhoI/XbaI (upstream, long) and XbaI/BglII into XbaI/BamHI (downstream, short) as shown in (C). (A) The left panel documents that the long arm seemed to be cleaved out by the digestion with XbaI/XhoI (expected pattern 3946, 712 bp) and the short arm was faithfully released by BglII/XbaI (expected pattern 4374, 284 bp). However, the SspI control cleavage showed discrepancies (expected pattern 3371, 1083, 204 bp). So the arms were sequenced and a more detailed restriction analysis was performed (right panel). Expected band patterns: HindIII – 4698 bp (linearization) – OK; XhoI – 761, 3933 bp – OK; BamHI – 4698 bp (linearization) – no cleavage; XbaI – 4698 bp (linearization) – OK; XhoI/XbaI – 14, 761, 3919 bp – OK. The results indicate that the long arm had been inserted in the wrong orientation and some of the cloning sites are either missing or duplicated (D). The long upstream arm was excised with XhoI, religated, and a clone having the correct orientation was isolated (plasmid pMP45) and verified by SspI digestion (B). The arrow points to the faint 204 bp band.

The corrected targeting vector, containing a nourseothricin (ClonNAT) resistance gene, was linearized with XbaI, and transformed into the PN558 (h^{+}) and

PN559 (h^-) wild type fission yeast strains to delete the *cbf12*$^+$ ORF by homologous recombination. The resulting KO strains were verified by PCR and designated MP01, MP02, and MP03, MP04, respectively. The construction procedure is schematized in Fig. 4.26.

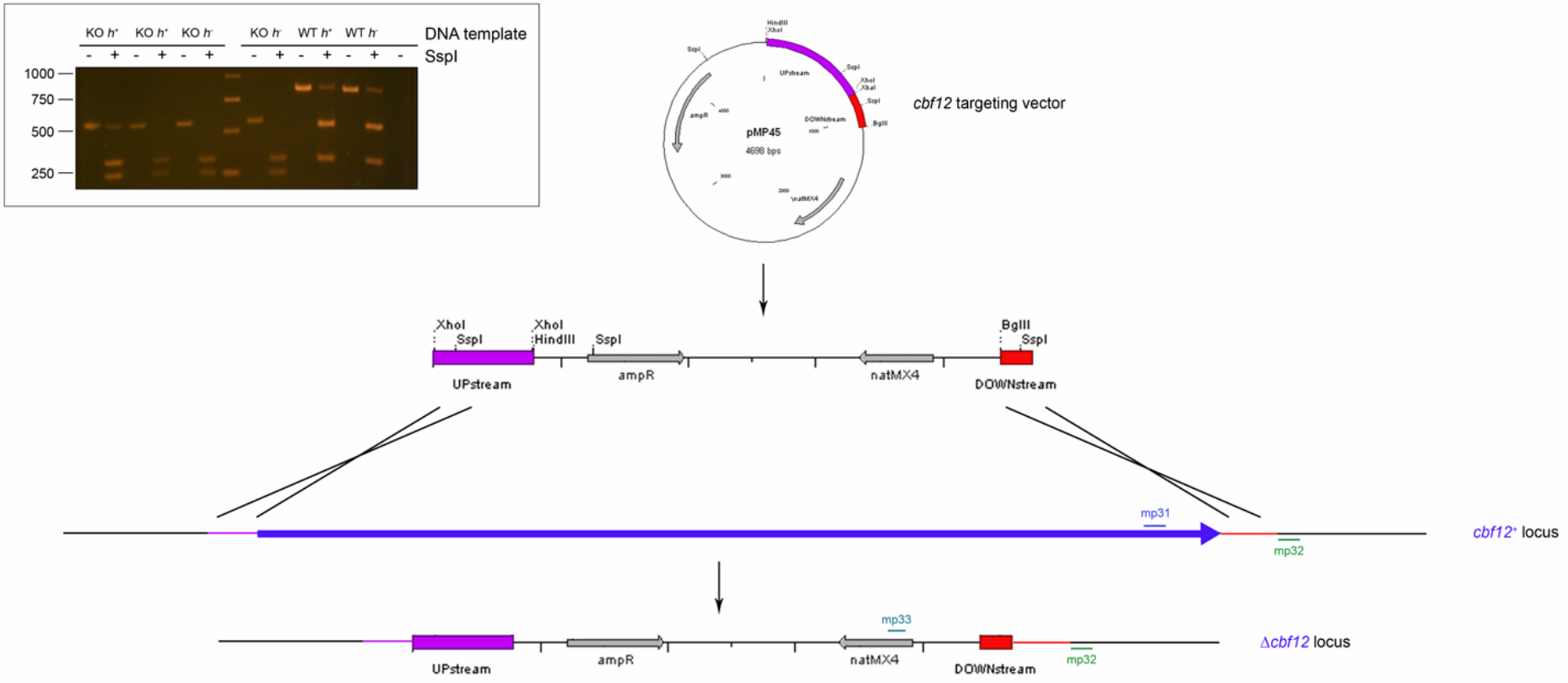
KO h+
KO h+
KO h-
KO h-
WT h+
WT h-
DNA template
SspI
1000
750
500
250
cbf12 targeting vector
pMP45
4698 bps
XhoI
SspI
XhoI
HindIII
SspI
BglII
SspI
UPstream
ampR
natMX4
DOWNstream
mp31
mp32
cbf12+ locus
mp33
mp32
Δcbf12 locus

Figure 4.26 – Δ*cbf12* knock-out construction scheme. The targeting vector (pMP45) was linearized with XbaI and transformed into PN558 and PN559 fission yeast cells. Recombination events were selected on ClonNAT (nourseothricin) YES plates. Positions of primers used for the knock-out verification are indicated. The inset shows verification of the KO genotype (strains MP01, MP02 – h^-; MP03, MP04 – h^+) by colony PCR and restriction analysis. The respective parental strains were used as WT controls; the expected band pattern is: WT – uncleaved 844 bp, SspI-cleaved 527 and 317 bp, KO – uncleaved 590 bp, SspI-cleaved 317 and 273 bp. In some cases the DNA was not digested fully.

Despite their different DNA-binding properties (see Chapter 4.7) the fission yeast CSL paralogs could still have (partially) redundant functions and compensate for each other in the respective mutants. To account for this possibility, we have also constructed haploid Δ*cbf11* Δ*cbf12* double KOs by crossing (MP01 × CBF11 KO) followed by PCR verification of their genotypes (Fig. 4.27). These strains (MP07, MP08 – h^+; MP09, MP10 – h^-) were also viable, thus, neither the *cbf11*$^+$ nor the *cbf12*$^+$ gene is essential under normal growth conditions (already described in the literature), and *S. pombe* cells can sustain even the loss of the entire CSL gene family.

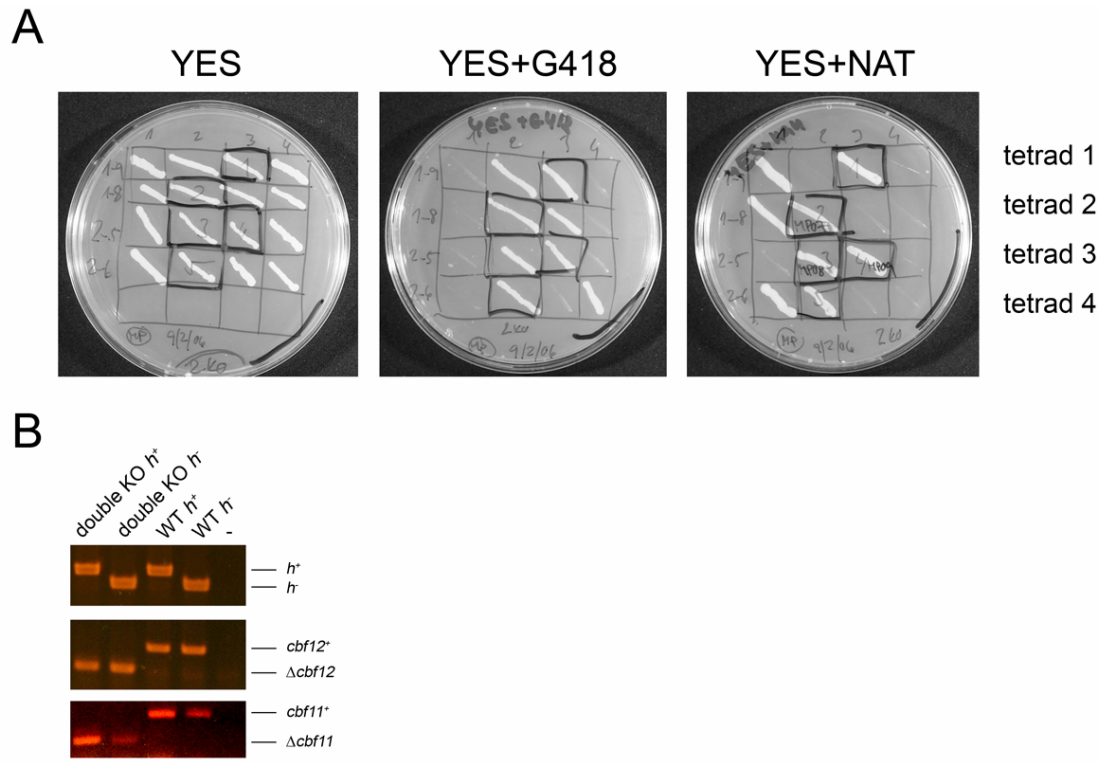

Figure 4.27 – Δ*cbf11* Δ*cbf12* double KO construction. (A) The MP01 and CBF11 KO strains were crossed, sporulated and asci were dissected using a micromanipulator. The resulting haploid segregants were replica plated on YES, YES+G418 and YES+ClonNAT to select for doubly resistant

clones (boxed). (B) The genotype of the double KO strains was verified by colony PCR (representative clones are shown). The PN558 (h^+) and PN559 (h^-) cells were used as WT controls.

4.8.2 Mutant phenotype analyses

4.8.2.1 Growth phenotypes, sensitivity and resistance tests

We then subjected our panel of KO strains (typically strains MP01, MP03, CBF11 KO, MP05, MP07 and MP09, or just the h^- representatives were used; PN558 and PN559 were used as WT controls; see Table 3.3) to a series of standard growth and sensitivity/resistance tests in order to identify the effects of the respective deletions that would help us understand the function of CSL genes in *S. pombe*. Both single deletants and the double KO were found to be capable of conjugation and spore formation by iodine staining (see Chapter 3.1.3.2). The content of asci was also monitored by microscopy of DAPI-stained nuclei of the spores. The majority of asci contained four spores in all strains tested, although no other quantification was performed (data not shown).

All mutants exerted viability comparable to WT controls when serial dilutions were spotted on minimal medium plates, rich medium plates under the conditions of heat, osmotic, salt and oxidative stress, with a non-fermentable carbon source, or in the presence of various substances affecting DNA replication, calcium signaling, translation, or damaging the plasma membrane, cell wall and cytoskeleton (data not shown; see Table 4.3 for the list of treatments used). However, the growth of the strains lacking *cbf11*$^+$ was found to be impaired on solid media at 19°C (Fig. 4.28A).

Table 4.3 – KO sensitivity/resistance tests used.

Treatment/Medium	Dosing	Description
MB	N/A	minimal defined medium
YES	N/A	complete rich medium
glycerol	N/A	a non-fermentable carbon source used instead of glucose
19˚C	N/A	cold stress
36˚C	N/A	heat stress
EGTA	5-40 mM	disruption of calcium signaling
hydroxyurea	7.5-11.25 mM	inhibition of DNA replication
KCl	0.4-1.2 M	osmotic/salt stress
sorbitol	1.2-2 M	osmotic stress

SDS	0.003-0.01%	disruption of membranes
H_2O_2	1-10 mM	oxidative stress
calcofluor	100-800 mg/ml	cell wall damage
cycloheximide	10-40 mg/ml	inhibition of proteosynthesis
latrunculin A	0.25-1 mM	disruption of actin cytoskeleton
carbendazim	10-25 mg/ml	disruption of microtubules

Unless stated otherwise, YES medium was used as a basis.

To investigate the growth defect with a finer resolution, we measured growth curves in shaken cultures at 30°C. We found that while the Δ*cbf12* strain was indistinguishable from the WT control, the growth of the Δ*cbf11* cells was retarded as compared with WT. Intriguingly, there was further growth impairment when the Δ*cbf11* and Δ*cbf12* deletions were combined in one strain, a synthetic effect indicative of some crosstalk between Cbf11 and Cbf12 (Fig. 4.28B). We then performed a rescue experiment of the Δ*cbf11*-associated growth phenotype. WT and double KO strains were transformed with either an empty vector or plasmids encoding *cbf11*$^+$ or *cbf12*$^+$, and monocolonies were grown for 7 days on inducing MB medium containing phloxin B (see Chapter 3.1.3.1). The overexpression of *cbf11*$^+$ in the double KO background resulted in colony size and phloxin B staining (i.e., health status) similar to WT. On the contrary, the high dosage of *cbf12*$^+$ seemed to be toxic for the cells, as the *cbf12*$^+$-overproducing colonies were even darker than the double KO colonies transformed with the empty vector only (Fig. 4.28C). Indeed, when assayed by plating serial dilutions of cells on inducing plates, the overexpression of *cbf12*$^+$ in WT cells resulted in decreased cell viability as well (data not shown).

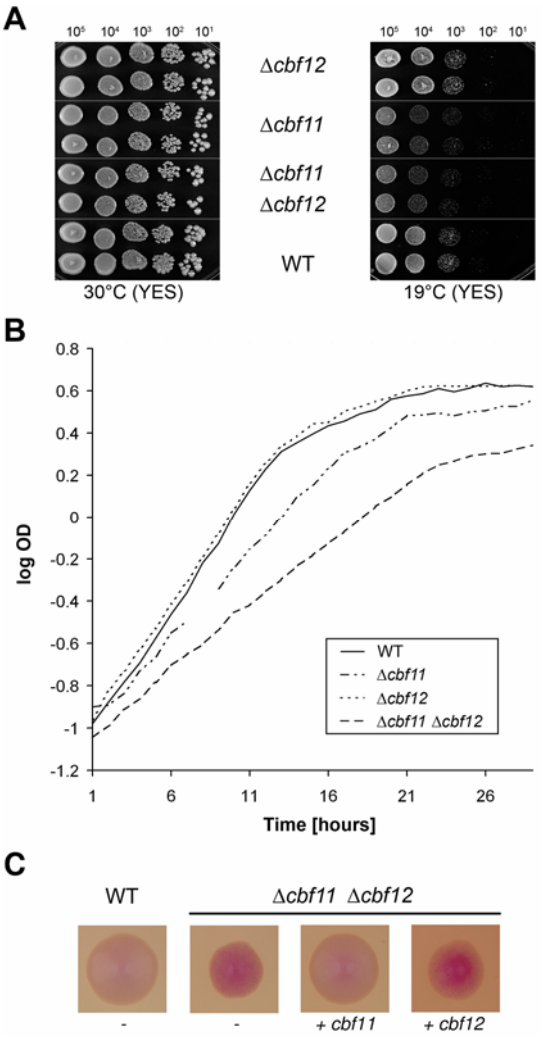

Figure 4.28 – The deletion of *cbf11*$^+$ results in slow growth and cold sensitivity. (A) When cultured on YES plates at 19°C for 5 days, the Δ*cbf11* and Δ*cbf11* Δ*cbf12* strains display marked growth impairment as compared with the Δ*cbf12* and WT cells. (B) The cells were cultured at 30°C in YES and OD was measured every hour. There was no difference between the Δ*cbf12* strain and WT. By contrast, the deletion of *cbf11*$^+$ was found to cause growth retardation, which phenotype is, intriguingly, further potentiated by the simultaneous deletion of *cbf12*$^+$. (C) When overexpressed from a plasmid, *cbf11*$^+$ but not *cbf12*$^+$ rescues the growth defect in the Δ*cbf11* Δ*cbf12* strain. The monocolonies were cultured on inducing $MB_{-ura\text{-}thiamin}$ plates with phloxin B for 7 days. Notably, the overexpression of *cbf12*$^+$ seems to be toxic for the cells as judged by the intense phloxin B staining of the colony.

4.8.2.2 Colony morphology

While carrying out the spot tests described above, we noticed that there were some macroscopically visible differences between the colonies of WT strains and strains carrying the deletion of *cbf11*$^+$ when grown on the rich YES medium. Namely, when illuminated, the surface of the spotted WT and Δ*cbf12* giant colonies

appeared dim, which was in sharp contrast to the Δ*cbf11* and Δ*cbf11* Δ*cbf12* giant colonies, the surface of which reflected much more light, thus displaying a "shiny" phenotype (Fig. 4.29A). When the colonies were submerged gently in water, a thin floating layer of the "shiny" material came off the colony surface (Fig. 4.29B). Thus, it is likely that the Δ*cbf11*-associated "shiny" phenotype is caused by overproduction of some extracellular matrix-like material that contains hydrophobic and reflective compounds. Interestingly, this phenotype was never observed on minimal media.

When observed under higher magnification, the surface of the "shiny" spots appeared as a complicated network of irregular grooves. By contrast, the surface of the dim giant colonies was found to be smooth (Fig. 4.29C). We obtained similar results when we examined the surface morphology of cell patches (data not shown). The "shiny" phenotype in the Δ*cbf11* Δ*cbf12* giant colonies could be rescued by mild overexpression of *cbf11*$^+$ but not *cbf12*$^+$ from a plasmid (Fig. 4.29D). Since the "shiny" phenotype does not appear on MB minimal media, the spots had to be grown on YES plates, which medium neither selects for the retention of the plasmids, nor does it support high expression from the thiamine-repressible *nmt1*-derived promoters due to its natural thiamine content. Nevertheless, the majority of the *cbf11*$^+$-expressing double KO colony surface was not "shiny", and the mutant phenotype only manifested at the spot periphery, where the plasmid had likely been already lost.

We next analyzed the morphology of Δ*cbf11* monocolonies. Since the grooves on giant colonies and patches formed in their older, central parts, containing an increased proportion of starving and old/dying cells, the monocolonies were grown for a prolonged period of time (14 days). To better visualize the physiological state of cells in different regions of the colonies, we added phloxin B into the medium. The phenotypes observed in these settings were in accord with the results obtained with giant colonies and patches (Fig. 4.29E). While the WT and Δ*cbf12* cells formed regularly shaped, evenly stained round colonies, there were significant morphology alterations in the case of the Δ*cbf11* single and Δ*cbf11* Δ*cbf12* double KO strains. These strains formed colonies of irregular shape with (sometimes protruding) sectors of darker-staining cell clones. Furthermore, the rim of these colonies was covered with a network of "shiny" grooves highly similar to those observed on the surface of the giant colonies. Again, the sectoring phenotype could be rescued in the Δ*cbf11* Δ*cbf12* background by introducing functional *cbf11*$^+$ on a

plasmid, and also the overall colony morphology was shifted towards WT (Fig. 4.29F). Any potential cross-complementation of the sectoring by *cbf12*$^{+}$ overexpression could not be determined as whole colonies stained intensely dark, likely due to the toxic effect of excess Cbf12 (data not shown; see also Fig. 4.28C).

Taken together, the absence of *cbf11*$^{+}$ leads to various marked changes in the morphology of multicellular structures formed by fission yeast cells (colonies, patches), suggesting possible involvement of Cbf11 in cell-cell contact formation.

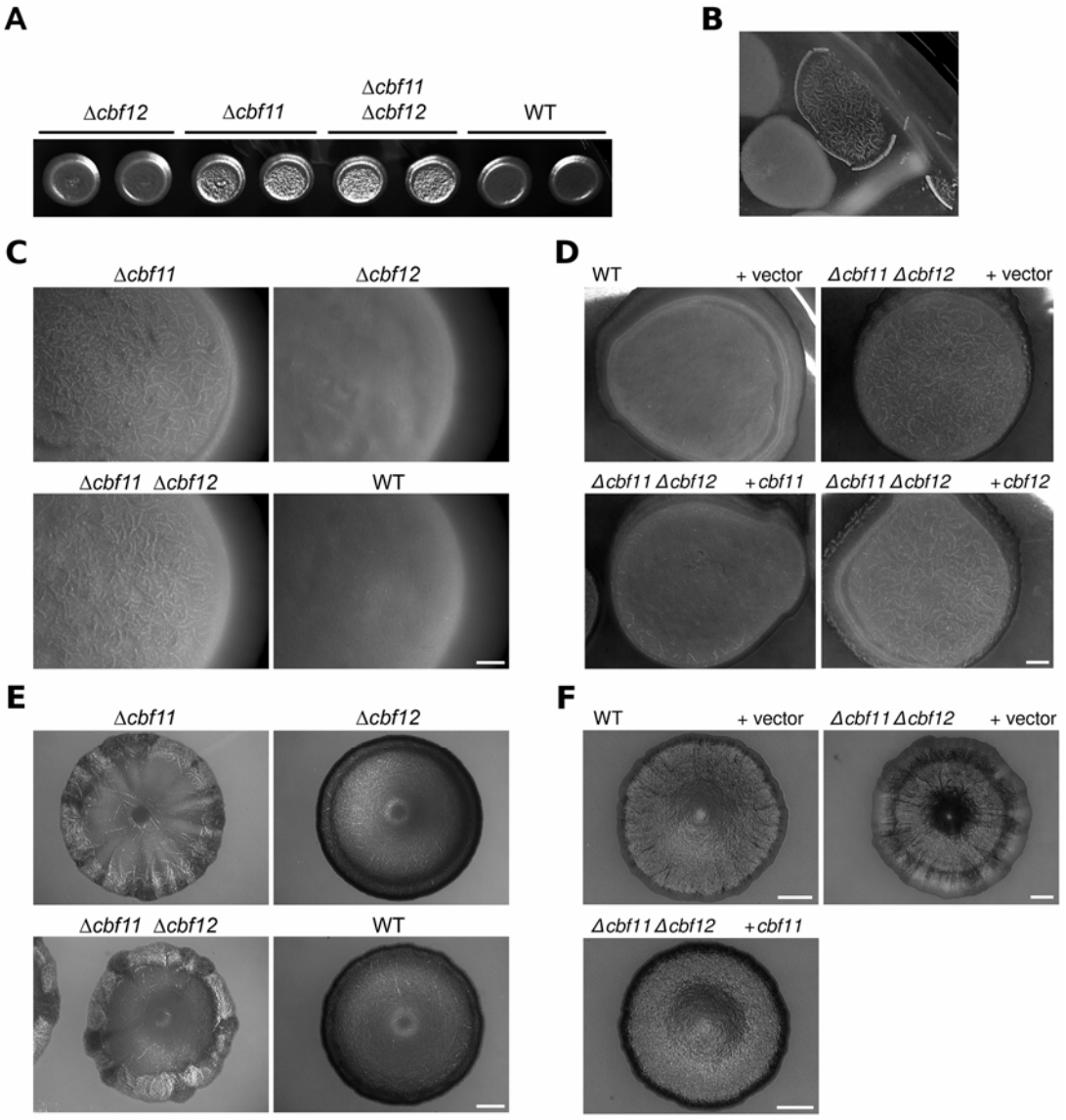

Figure 4.29 – The deletion of *cbf11*$^{+}$ results in altered colony morphology. (A) Cells were spotted on a YES plate and incubated at 30°C for 7 days. The Δ*cbf11* and Δ*cbf11* Δ*cbf12* strains display a "shiny" phenotype, i.e., they appear glossy when illuminated, unlike the dim WT and Δ*cbf12* cells. (B) When submerged in water, a highly reflective floating thin layer detaches from the "shiny" colonies. (C) The surface of the spots from panel A observed under higher magnification. The dim giant colonies are smooth, in contrast to the wrinkled surface of the "shiny" giant colonies, which

appears as a network of shallow grooves. The bars represent 1 mm. (D) Low plasmid-driven expression of *cbf11*$^{+}$ rescues the "shiny" phenotype in the Δ*cbf11* Δ*cbf12* strain. The cells were spotted on a YES plate and cultivated for 26 days. (E) Monocolonies were grown for 14 days on YES plates containing phloxin B. The colonies of the Δ*cbf11* and Δ*cbf11* Δ*cbf12* strains are irregularly shaped, show sectoring of phloxin B staining and their rim is "shiny" and covered with similar grooves as observed for the spotted giant colonies. The Δ*cbf12* monocolonies appear normal. (F) Overexpression of *cbf11*$^{+}$ rescues the sectoring phenotype of the Δ*cbf11* Δ*cbf12* strain, and confers more WT-like colony morphology. The monocolonies were grown on inducing $MB_{\text{-ura-thiamine}}$ plates with phloxin B for 4 weeks.

4.8.2.3 Adhesion and flocculation tests

Our data on Cbf11 affecting colony morphology prompted us to test the effects of fission yeast CSL genes deletion and overexpression on cell adhesive properties. First, we performed washing assays (see Chapter 3.1.3.3) with spotted giant colonies of the respective KO strains grown on YES plates. Significantly, cells lacking *cbf12*$^{+}$ consistently showed decreased adhesion to the agar plate. While some cell mass of the WT and Δ*cbf11* spots remained attached to the agar surface, the Δ*cbf12* and Δ*cbf11* Δ*cbf12* spots were washed off completely. This observation was also documented microscopically (Fig. 4.30A). We performed a rescue experiment of this phenotype in the Δ*cbf11* Δ*cbf12* background. Cells were grown on inducing MB plates and the washing assay was carried out. On this media type, the overall cell adhesion was higher as compared with YES, and not even the double KO spots were washed off completely. As expected, adhesion could be restored by the overexpression of *cbf12*$^{+}$ from a plasmid (Fig. 4.30B). Surprisingly, the residual adhesion displayed by the Δ*cbf11* Δ*cbf12* cells on this type of media was abolished by the overexpression of *cbf11*$^{+}$. Such a result suggested that the two CSL paralogs may have opposing functions in adhesion. Indeed, when we examined the adhesive properties of the *cbf11* single KO strain in more detail, we found that these cells displayed a higher degree of adhesion than the WT control, and the re-introduction of *cbf11*$^{+}$ neutralized this increase (Fig. 4.30C).

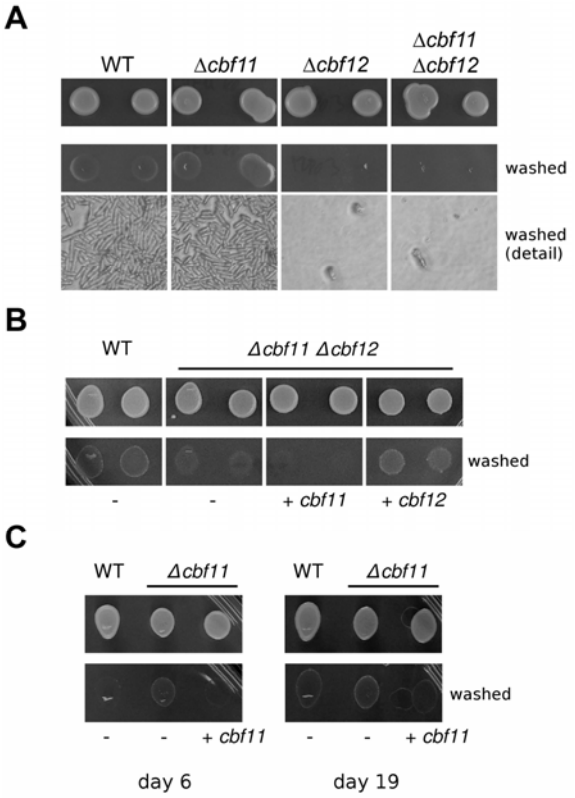

Figure 4.30 – Opposing roles of *cbf11*$^+$ and *cbf12*$^+$ in cell adhesion. (A) Cells were spotted on a YES plate, incubated at 30°C for 2 weeks, and then washed with a stream of water. A layer of cells remained adhering to the agar in the case of the WT and Δ*cbf11* strains. By contrast, strains lacking *cbf12*$^+$ were washed off completely. A microscopic picture of the washed surface is shown in the bottom panel. (B) The defective adhesion of the Δ*cbf11* Δ*cbf12* strain can be rescued by overexpression of *cbf12*$^+$ from a plasmid. Cells were grown on an inducing $MB_{-ura-thiamin}$ plate for 1 week and processed as in A. Note that overexpression of *cbf11*$^+$ further decreased adhesion of the double KO strain. (C) The *cbf11* single KO cells display higher adhesion than WT, which can be lowered again by the overexpression of *cbf11*$^+$ from a plasmid. Spots were grown on inducing $MB_{-ura-thiamin}$ plates for 6 and 19 days, respectively, and processed as in A.

Next, we tested the CSL influence on adhesion in liquid culture (see Chapter 3.1.3.3). When *cbf12*$^+$ was overexpressed in a WT strain, it triggered flocculation (macroscopically visible cell aggregate formation) in a logarithmic-phase culture (Fig. 4.31A). No flocculation was observed for the WT control. As expected, the Cbf12-induced aggregation phenotype was strongly potentiated in the Δ*cbf11* background (earlier onset, larger aggregates), lending further support to our hypothesis that Cbf11 and Cbf12 influence cell adhesion in an antagonistic manner. In accordance to that, when we assayed the Δ*cbf11* strain, we observed a similar flocculation phenotype (Fig. 4.31B). Only this time cultures were grown to the stationary phase, which is generally more supportive of aggregation in yeasts

(Straver *et al.*, 1993). There was also apparent a marked increase of adherence of these cells to the glass cultivation flask walls as compared with WT (data not shown). Once again, plasmid-driven overexpression of *cbf11*$^+$ abolished the flocculation (as well as the adhesion to the cultivation flasks) of the Δ*cbf11* strain. Thus, we conclude that Cbf11 acts as a negative regulator and Cbf12 as a positive regulator of cell adhesion in fission yeast.

While flocculation is mainly mannose-dependent in *S. cerevisiae* (Miki *et al.*, 1982), in *S. pombe* it was found to be mediated rather by cell surface galactosyl residues (Tanaka *et al.*, 1999). In agreement with that, using a sugar competition assay we determined that Cbf12-induced flocculation could be abrogated by the addition of galactose but not mannose to the cells (Fig. 4.31C). Since agar is a galactose polymer, it is likely that both the cell-cell and cell-agar surface adhesion changes caused by CSL manipulation are of the same, galactose-dependent type.

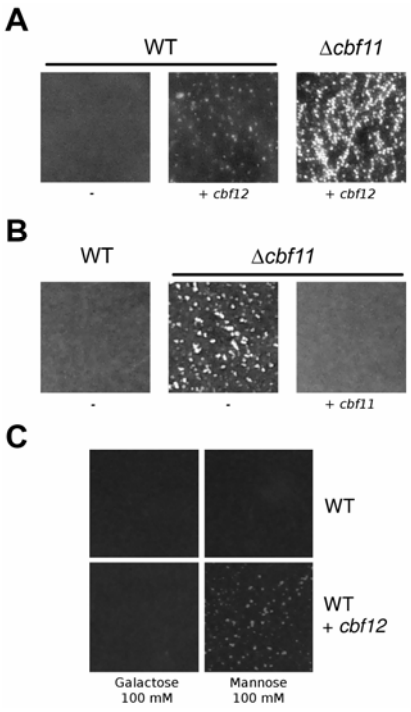

Figure 4.31 – Deletion of *cbf11*$^+$ or overexpression of *cbf12*$^+$ trigger flocculation. (A) Cells transformed with either an empty vector or a plasmid encoding *cbf12*$^+$ were grown in parallel in liquid inducing $MB_{\text{-ura-thiamin}}$ medium at 30°C. The overproduction of Cbf12 triggered flocculation. A synthetic hyper-flocculation phenotype was observed in the Δ*cbf11* background. (B) Cells were grown to stationary phase under the conditions described in A. The Δ*cbf11* strain displayed strong flocculation that was completely abolished by the re-introduction of *cbf11*$^+$ on a plasmid. (C) The Cbf12-induced flocculation is galactose-dependent, as judged by competition assays.

4.8.2.4 FACS analysis

Having investigated the cell-cell contact clue coming from our colony morphology analyses, we turned to the second prominent phenotype displayed by colonies lacking *cbf11*$^{+}$, that is, the dark sectoring of phloxin B staining (see Fig. 4.29E). In *S. pombe*, such dark-red staining is typical of diploid colonies (Forsburg, 2003), suggesting that the dark sectors might represent diploid clones arising in the mutant populations. We employed flow cytometry to determine the ploidy of the respective strains (see Chapter 3.3.7). Normally, most fission yeast cells in an exponentially growing liquid culture are in the G_2 phase, with haploids showing a single 2C peak and diploids showing a single 4C peak on FACS histograms (Sazer and Sherwood, 1990). In contrast to that, the Δ*cbf11* and Δ*cbf11* Δ*cbf12* haploid strains (cultures inoculated from patches) contained a significant fraction of cells with >2C DNA content (Fig. 4.32). When cells were taken separately from the light and dark sectors of the phloxin B-stained monocolonies and cultured further, the former still comprised a mixture giving two peaks on FACS, while the latter sorted as diploids, suggesting the shift to a higher DNA content is stable. As suspected, the overproduction of *cbf12*$^{+}$ in a WT background also resulted in the appearance of a fraction of likely diploid cells. We did not see any significant increase of the >2C cell fraction in a Δ*cbf11* strain after transforming it with a plasmid encoding Cbf12 (data not shown). Nevertheless, the two paralogs again seem to act in opposite directions, this time affecting the maintenance of genome ploidy.

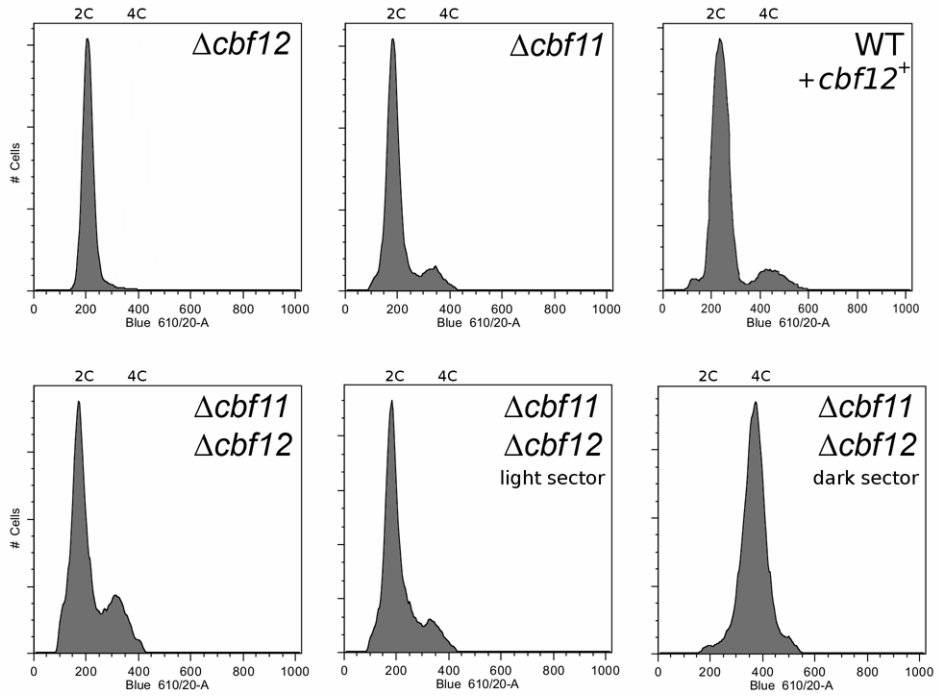

Figure 4.32 – Loss of *cbf11*$^+$ or overexpression of *cbf12*$^+$result in frequent diploidization. Exponentially growing WT cells overexpressing *cbf12*$^+$ from a plasmid, and cells of the single and double CSL mutants were fixed, stained with propidium iodide, and their DNA content was analyzed by flow cytometry. The control haploid and diploid G_2-phase peaks are indicated as 2C and 4C, respectively. While the Δ*cbf12* strain appears wild type, the Δ*cbf11* and Δ*cbf11* Δ*cbf12* mutants, and the *cbf12*$^+$ overexpressor strains contain a significant proportion of cells with a >2C DNA content. When cultures were inoculated from the light/dark sectors shown in Fig. 4.29E, the cells from the dark sectors sorted as diploids.

4.8.2.5 Cell morphology

Importantly, all strains used in our analyses were heterothallic, either h^+ or h^-, unable to switch their mating types, and thus unable to self-conjugate. Nevertheless, stable, non-sporulating homozygous diploids can rarely appear even in WT strains as a result of either low-frequency bypass of M phase, two successive S phases, or an incomplete M phase (http://www-rcf.usc.edu/~forsburg/diploids.html; (Kominami and Toda, 1997)). Therefore, we performed microscopic analysis of the CSL mutant and overexpressor strains in search for hints as to the mechanism of the high-frequency diploid formation observed by FACS.

We analyzed both live and fixed cells from exponentially growing cultures. While there were virtually no aberrations present in the WT controls and very little in the Δ*cbf12* strain, the results revealed a surprising range of defects exerted by either the *cbf11*$^+$-lacking or *cbf12*$^+$-overexpressing cells (Fig. 4.33). The mutant

phenotypes could generally be described as consequences of cell and/or nuclear division misregulation and their respective penetrances varied between particular genotypes, affecting usually only a minor fraction of the cells (see Table 4.4). These phenotypes, generally more severe in the double KO, included a high degree of heterogeneity in both cell size and shape, with frequent large cells with diploid-like nuclei that likely corresponded to the diploid fraction observed by FACS (both Δ*cbf11* and *cbf12*$^+$-overexpression). Extremely large cells with giant, likely polyploid nuclei were seen too, although rarely (Fig. 4.33E, right panel). We also noticed the so-called "sep" phenotype (Grallert *et al.*, 1999) (both Δ*cbf11* and *cbf12*$^+$-overexpression), i.e., various septation defects comprising the formation of multiple septa in a single cell, aberrant septum structure, a failure of daughter cells to separate after septum formation, and pseudohyphal (often multipolar) growth. Short filaments of up to six uninucleate compartments were often seen particularly when *cbf12*$^+$ was overexpressed in a Δ*cbf11* strain (Fig. 4.33H). Finally, the deletion of *cbf11*$^+$ was found to be associated with the "cut" (cell untimely torn) phenotype (Hirano *et al.*, 1986), which is a failure in coordination of the nuclear and cell division. As a consequence, the septum often forms prematurely, either making a lethal cut through the nucleus (if such cells separate, the cut nuclei remain attached to the former septum; see Fig 4.33D), or missing the nucleus and producing one anucleate and one possibly viable "diploid" compartment, respectively. The "cut" phenotype might thus be responsible for the diploidization we observed, although it is rather puzzling that it was almost never detected also for the *cbf12*$^+$ overexpression. In summary, the lack of *cbf11*$^+$ or excess dose of *cbf12*$^+$ both result in pleiotropic defects in cell and nuclear division, highlighting the requirement for proper balance of CSL proteins in these processes.

Table 4.4 – Frequencies of the 'sep' and 'cut' phenotypes in CSL mutant strains.

Strain[*]	**'sep'**	**'cut'**	**Medium**
WT	0.5%	0.0%	YES/MB
Δ*cbf12*	0.7%	0.0%	YES
Δ*cbf11*	4.2%	16.1%	YES
Δ*cbf11* Δ*cbf12*	4.3%	19.7%	YES
WT + *cbf12*$^+$ OE	8.7%	1.2%	MB
Δ*cbf11* + *cbf12*$^+$ OE	9.5%	4.1%	MB

*OE – overexpression; n > 500 cells; note that the 'sep' frequency is underrated due to the fact that multi-compartment filaments were scored as one cell. Both phenotypes may combine in a single cell.

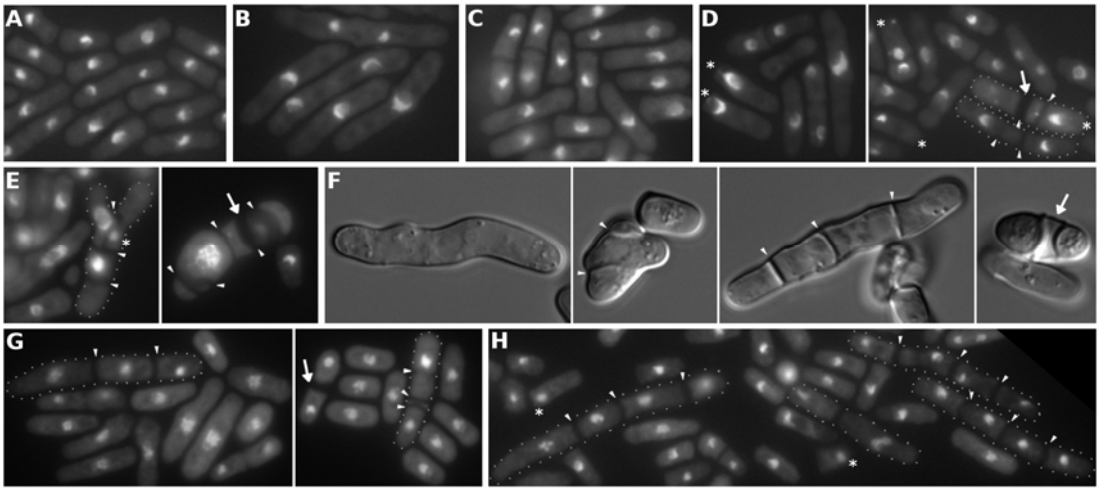

Figure 4.33 – Loss of *cbf11*$^+$ or overexpression of *cbf12*$^+$ lead to multiple defects in cell and nuclear division. Exponentially growing cells, either live (F) or fixed with ethanol and stained with DAPI (A-E, G-H), were observed under an epifluorescence/DIC microscope. WT haploid (A) and dipoid (B) cells are shown for comparison. (C) No significant abnormalities were found for the Δ*cbf12* strain. By contrast, the cultures of the Δ*cbf11* (D, F) and Δ*cbf11* Δ*cbf12* (E) strains are heterogeneous in shape and size of both cells and nuclei. Infrequently, cells display the "cut" phenotype (asterisks), very large nuclei, pseudohyphal growth, multiple septa (arrowheads) or aberrantly thick septa (arrows). (G) When *cbf12*$^+$ is overexpressed in a WT background, similar size/shape heterogeneity and septation defects can be seen (almost no "cut", however). (H) In a Δ*cbf11* background, the increased dosage of *cbf12*$^+$ potentiates the septation defects, and a significant proportion of the cells grow as short unseparated filaments.

4.8.2.6 Microarray experiments

Our initial hypothesis proposed a role for Cbf11 and Cbf12 in the regulation of transcription. So far, our data concerning their subcellular localization, DNA binding, reporter construct activation and mutant phenotypes all support this assumption. However, the pleiotropy of the mutant phenotypes precludes a straightforward and precise determination of the CSL-regulated processes. A possible means to circumvent these obstacles is to perform a global transcriptome analysis of cells in which CSL expression was manipulated. To this end, we performed microarray experiments in collaboration with the laboratory of Dr. Jürg Bähler, Wellcome Trust Sanger Institute, UK (see Chapter 3.3.2). We isolated total RNA from exponentially growing cells of the WT, KO and overexpressor strains listed in Table 4.5 (two biological repetitions; overexpression confirmed by western

analysis). Each experimental sample was co-hybridized with a WT control and relative individual mRNA levels were determined as described (Lyne *et al.*, 2003).

Table 4.5 – Strains used for the microarray experiments.

KO		**Control**
Δ*cbf11* (CBF11 KO)	vs.	WT (PN559)
Δ*cbf12* (MP03)		
Δ*cbf11* Δ*cbf12* (MP09)		
Overexpression		**Control**
WT + *cbf11*$^{+}$ (PN559 + pJR08)	vs.	WT + vector (PN559 + pREP42MHN)
WT + *cbf12*$^{+}$ (PN559 + pMP32)		

Genes were considered as differentially expressed when showing a two-fold increase/decrease in their mRNA levels relative to the WT control in both biological replicates. In some cases, a less stringent threshold of 1.5× change was used for the identification of downregulated genes, and separate candidate gene lists were obtained for both thresholds. The results (two-fold threshold only) are summarized in Table 4.6; full datasets can be found on the accompanying CD. Surprisingly, there were almost no expression changes in response to the deletion of *cbf12*$^{+}$ (adhesion-related changes were expected). However, the two replicates gave very different results (almost no changes vs. hundreds of genes changed) and it is thus possible that the lack of regulated genes is a false negative result caused by some undetermined technical issues. Also, the technical quality of one of the overexpression replicates (both CSL genes) was suboptimal, yielding data for only about 3500 genes (out of 5500). Using a less stringent normalization algorithm we obtained data for another ~1000 genes, leaving still about 1000 that could not be included in our analyses. The transcription of the resistance marker genes was detected in the respective KO strains only; also the levels of the manipulated CSL gene(s) were changed as expected (not included in the analysis). The double KO profile was very similar to that of the Δ*cbf11* strain and is not shown.

Table 4.6 – Genes showing differential expression after CSL manipulation.

Functional category	**Genes**
Δ*cbf11* – upregulated	
stress response	C106.02c, C1105.14, C11C11.06c, C11D3.13, C1223.09, C1281.04, C1281.07c, C12C2.04, C139.05, C1393.12, C15E1.02c, C1677.01c, C16A11.15c, C16A3.02c, C16D10.08c, C16E9.16c, C1739.06c, C1739.08c, C1773.06c, C18B5.02c, C191.01, C191.09c, C1F7.12, C1F8.04c, C215.11c, C21C3.19, C22A12.17c, C22F8.05, C22G7.11c, C22H10.13, C23G7.10c, C24C6.09c, C25H1.01c, C26F1.04c, C26F1.07, C26F1.14c, C27D7.09c, C27D7.10c, C285.01c, C2A9.02, C2E1P3.01, C2F3.05c, C30D10.14, C32A11.02c, C338.12, C338.18, C365.12c, C4F6.17c, C4G3.03, C4H3.03c, C4H3.08, C513.07, C56F2.06, C5H10.02c, C609.04, C660.05, C663.06c, C663.08c, C725.03, C725.10, C757.03c, C8E4.10c, C965.07c, *cta1*, *gpd1*, *gpx1*, *grx1*, *hsp16*, *hsp9*, *isp6*, *ntp1*, *obr1*, PB1A11.03, PB24D3.08c, PJ691.02, *plr*, *pmp20*, *psi*, *rds1*, *tps1*, *vip1*
iron metabolism	C1F8.02c, C947.05c, *fip1*, *frp1*, *str1*, *str3*
other	C1840.12, C26H5.09c, C2H10.01, C3G9.11c, C56F8.12.RC, C736.07c, C794.01c, meu8.RC, misc_RNA_3.3.52.RC, *mug108*, *mug120*, P4H10.12, PB16A4.06c, *prl44*, *prl65*, *wtf5*
Δ*cbf11* – downregulated	
stress response	C1348.06c, C21C3.08c, C977.05c
other	C3A11.07, RRNA.09, *sam1*
Δ*cbf12* – upregulated	
-	-
Δ*cbf12* – downregulated	
stress response	C1348.06c, C977.05c
***cbf11*$^+$ overexpression – upregulated**	
stress response	C1348.13, C15A10.05c, C8E4.10c, PB1A11.03
iron metabolism	*fip1*, *vht1*
other	C1450.09c, C186.05c, C2F3.15, C3H8.01, C6F12.06, C922.02c, C965.12.RC, *prl10*
***cbf11*$^+$ overexpression – downregulated**	
-	-

***cbf12*$^+$ overexpression – upregulated**

stress response	C11D3.01c, C1223.13, C1281.04, C1281.07c, C1348.06c, C1393.12, C13F5.03c, C15E1.02c, C16E9.16c, C22A12.17c, C22G7.11c, C22H10.13, C23C11.06c, C25H1.01c, C27D7.09c, C27D7.11c, C338.18, C359.05, C725.10, C977.05c, *fbp1*, *gpx1*, PB1A11.03, PB2B2.15, *pyp2*, *tms1*
cell surface / adhesion	*agl1*, *bgl2*, C1348.02, C1795.13, C2G2.17c, C359.04c, C750.05c, C977.01, *inv1*, *meu7*, *mok12*, PB2B2.19c
other	C1271.09, C139.03, C1773.12, C1840.12, C186.05c, C24C9.08, C25B2.08, C3G9.11c, C4F10.17, C569.07, C6F12.06, C737.04, C757.02c, C977.04, i21_ade2: min10, *inv1*.rc, *mug168*, *mug2*, PB16A4.06c, PB1A11.02, PB21E7.04c, PB2B2.15, PB8B6.07

***cbf12*$^+$ overexpression – downregulated**

stress response	C36.02c, C1223.09, C869.05c
proteosynthesis	*rpl38-1*, *rpl38-2*, *rpl39*, *rpl41-1*, *rpl41-2*, *rps25-1*, *sen15*
other	C12C2.14c, C17C9.16c, *dad3*, *prl10*, *prl3*, *ura4*

For technical reasons, the first 3 letters of systematic names (SPx) are not shown; the resulting tags are still unique and allow for unambiguous gene identification.

The microarray profiles roughly reflect the observed growth and microscopic phenotypes. The deletion of *cbf12*$^+$ or the overexpression of *cbf11*$^+$ seem to be well tolerated by *S. pombe* and elicit only minor changes of the transcriptome. However, both the deletion of *cbf11*$^+$ and the overexpression of *cbf12*$^+$ are deleterious for the cells and more pronounced gene expression changes occur, the most prominent feature being stress response activation (Chen *et al.*, 2003). In addition, Cbf11 seems to influence the expression of iron uptake genes of both the reductive and non-reductive pathways (Labbe *et al.*, 2007;Rustici *et al.*, 2007). In support of the adhesion-related phenotypes we observed, the overexpression of *cbf12*$^+$ resulted in the upregulation of a number of cell surface glycoproteins and adhesins (Linder and Gustafsson, 2008). There was also extensive downregulation of numerous translation-related genes (particularly evident at the >1.5× threshold), consistent with the poor growth of cells overproducing Cbf12. Surprisingly, we found little (inverse) correlation between the conditions of a CSL gene KO and overexpression. This may be caused by the proposed crosstalk between the two paralogs as one CSL gene might compensate for the manipulation of the other. The only exceptions found are listed in Table 4.7 (stress-response genes were generally not considered).

Table 4.7 – Genes showing expression changes in both KO and overexpression datasets.

Gene	Expression changes[a]	Description
C1840.12	UP in Δ*cbf11* and *cbf12*$^+$ OE	OPT oligopeptide transporter family
PB16A4.06c	UP in Δ*cbf11* and *cbf12*$^+$ OE	sequence orphan
C3G9.11c	UP in Δ*cbf11* and *cbf12*$^+$ OE	pyruvate decarboxylase (predicted)
fip1	UP in Δ*cbf11* and *cbf11*$^+$ OE	iron permease (expression regulated by iron)[c]
C977.05c[b]	DOWN in Δ*cbf11* and Δ*cbf12* × UP in *cbf12*$^+$ OE	conserved fungal protein (cell surface localization; response to cadmium)[d]
C1348.06c[b]	DOWN in Δ*cbf11* and Δ*cbf12* × UP in *cbf12*$^+$ OE	conserved fungal protein (response to cadmium and zinc)[d, e]
vht1	DOWN (>1.5×) in Δ*cbf11* × UP in *cbf11*$^+$ OE	vitamin H transporter (expression regulated by iron)[c]
PB2B2.15[b]	DOWN (>1.5×) in Δ*cbf11* × UP in *cbf12*$^+$ OE	conserved fungal protein
C359.04c	DOWN (>1.5×) in Δ*cbf11* × UP in *cbf12*$^+$ OE	DIPSY family adhesin[f]

[a]UP – upregulated, DOWN – downregulated, OE – overexpression; [b]a family of telomeric, recently-duplicated genes of almost identical DNA sequence; [c](Rustici *et al.*, 2007); [d](Chen *et al.*, 2003); [e](Dainty *et al.*, 2008); [f](Linder and Gustafsson, 2008). Groups of genes with similar expression patterns are indicated by shading; the first 3 letters of systematic names (SPx) are not shown.

We next compared our data with the published fission yeast microarray datasets. Such comparisons would provide us with a more global picture of the CSL-responsive changes in transcription. As stated above, there was a major overlap of the *cbf11* KO (83 genes) and *cbf12*$^+$ overexpression (37 genes) datasets and stress response genes, particularly the so-called core environmental stress response (CESR) genes (Chen *et al.*, 2003). The Δ*cbf11* profile is also similar, both qualitatively (17 genes shared) and quantitatively (similar fold expression changes), to the cellular response to iron starvation or the deletion of the major iron-uptake regulator *fep1* (Rustici *et al.*, 2007). Interestingly, significant overlaps were also found for both *cbf11*- and *cbf12*-related datasets and the microarray profiles of the Mediator subunit mutants Δ*sep10* (Δ*med31*) and *sep15-598* (*med8-598*) (Linder *et al.*, 2008;Miklos *et al.*, 2008). This piece of evidence provides an important link between the CSL family and the regulation of transcription.

Finally, comparisons of the CSL overexpression datasets were also made with data available at the Wellcome Trust Sanger Centre (Dr. Jürg Bähler, personal

communication). An overlap was found between the genes upregulated in response to the increased dose of *cbf11*$^{+}$ and the genes induced in *sep15* mutants. The group of genes upregulated in *cbf12*$^{+}$-overexpressing cells overlapped with late meiotic genes, duplicated orphan genes, genes induced in the *clr6* histone deacetylase mutants, genes induced in *pof3* mutants (a role in telomere maintenance and ubiquitin-dependent protein degradation), and also with genes induced in *sep15* mutants. On the other hand, the genes downregulated under these conditions were classified as highly expressed genes, ribosomal protein genes, short genes, and transcripts occupied with <3 ribosomes (note that these lists are all related with each other).

Taken together, the microarray experiments supported the CSL role in cell adhesion, reflected the growth phenotypes we observed and suggested links between Cbf11/12 and the Mediator complex, a general coregulator of the RNA polymerase II-dependent transcription in yeast (Bjorklund and Gustafsson, 2005). Furthermore, another interesting link was provided as the meotically upregulated *cbf12*$^{+}$ (see Chapter 4.3.2) induces meiotic genes when overexpressed in vegetative haploid cells.

5 *DISCUSSION*

5.1 CSL family in fungi

In contrast to the general belief that the CSL family is a hallmark of metazoans (Pursglove and Mackay, 2005), we found putative CSL family members in several fungal species of the ascomycetes (the basal subphylum Taphrinomycotina), zygomycetes and basidiomycetes groups (Prevorovsky *et al.*, 2007). These organisms range in complexity from the simple unicellular fission yeast to the macroscopic multicellular and highly differentiated *C. cinereus*. The novel family members share the unique CLS-type domain organization and show a high degree of sequence conservation in functionally important regions. Yet indeed, the CSL phylogenetic distribution is not universal. We found no CSL homologs in either plants or protozoa, and, notably, there were no representatives found in either of the later branching ascomycetal groups, Saccharomycotina (including the important model organism *S. cerevisiae*) and Pezizomycotina (see (James *et al.*, 2006) for explanation of the nomenclature used). Our data support the idea that the ancestral CSL gene originated in the last common ancestor of animals and fungi, thus much earlier than previously assumed, and that a duplication event took place in the fungal lineage, creating the two CSL classes (F1, F2) we see there today. There have been independent losses of CSL family genes in the fungal branch later on in evolution as well (Prevorovsky *et al.*, 2007). As more and more (fungal) genomes get sequenced, our knowledge of the CSL family phylogeny and its "logic" will certainly increase.

The current understanding of the CSL family function derives exclusively from metazoan model organisms and is based mostly on studies concerning development and the Notch pathway (Artavanis-Tsakonas *et al.*, 1999;Bray and Furriols, 2001;Lai, 2002;Pursglove and Mackay, 2005). It is now clear that this is not the whole picture as we have presented evidence of CSL proteins in several organisms that are evolutionarily distant to animals and lack the critical Notch pathway components (and most other known interacting partners). Moreover, recent reports on metazoan models indicate, that there are yet unrecognized CSL activities in animals as well, and this family participates also in Notch-independent regulation of transcription (Barolo *et al.*, 2000;Beres *et al.*, 2006;Kaspar and Klein, 2006;Koelzer and Klein, 2003). Given the bioinformatical and experimental data we

gathered, it is likely that all three CSL classes share an ancestral function of gene expression regulation, however, different signals and contexts are presumably interpreted, and processes regulated.

5.2 CSL function in *S. pombe*

To address the question of CSL genes (and proteins) function in fungi, we investigated the properties of this family members present in the fission yeast *S. pombe* – *cbf11*$^+$ (class F1) and *cbf12*$^+$ (class F2). We analyzed their expression profiles, studied the biochemical properties of their protein products, and collected a relatively large body of evidence concerning the phenotypes associated with the manipulations (deletion, overexpression) of these two CSL genes. Both classical and relatively novel approaches were used to detect any potential CSL-responsive phenotype alterations.

One of the advanced techniques used was a genome-wide transcriptome analysis using spotted oligonucleotide microarrays (Lyne *et al.*, 2003). A few facts should be noted regarding the data produced and their interpretation. Due to the inherent properties of the technology (a large-scale parallel analysis), technical issues (a suboptimal batch of arrays), and normalization and filtering procedures (genes lacking data from one repetition not included in the analysis) the resulting data have a considerable false negative rate. Another important point is that steady-state transcriptomes were analyzed, with any transient CSL-responsive changes in gene expression likely escaping our notice. Finally, only a limited number of conditions could be tested, thus, especially in the case of *cbf12*$^+$, additional relevant and insightful data would likely be generated were, e.g., meiotic or stationary-phase cells assayed too. Nevertheless, the experiments performed proved extremely helpful and yielded many valuable answers (and further questions). The datasets now await an independent confirmation using qRT-PCR, which will be carried out as part of the master's thesis of Jana Staňurová. As the relatively sparse fission yeast genome annotation is improving constantly (Aslett and Wood, 2006), a re-evaluation of the microarray data might be considered in (near) future. The array results have also been compared with datasets coming from genome-wide *in silico* CSL binding site predictions prepared by Martina Ptáčková for her master's thesis. The overlaps found

have been used to direct a next round of *in vitro* and *in vivo* DNA binding studies of Cbf11/12 (will be presented elsewhere).

In principle, the pleiotropy of the CSL-associated phenotypes we observed at the molecular, cellular and multicellular levels (see below) is suggestive of a more general regulatory role, likely in transcription. Similar range of phenotypes was reported for mutants of other established or presumed general transcription regulators, such as several constituents of the Mediator complex (Szilagyi *et al.*, 2002;Zilahi *et al.*, 2000). Interestingly, a few uncharacterized zinc-finger transcription factor genes were affected by the deletion of *cbf11*$^+$ (SPAC2H10.01) or the overexpression of *cbf12*$^+$ (SPAC139.03, SPBC1773.12), suggesting a possibility for the fission yeast CSL proteins to act as "master" regulators controlling the expression of downstream factors. A similar scheme is employed by their metazoan counterparts that serve as upstream regulators of numerous subordinate repressors and activators of the bHlH type (Iso *et al.*, 2003).

5.2.1 Adhesion and colony morphology

We found that both Cbf11 and Cbf12 affect cell-cell and cell-surface adhesion of *S. pombe*. While Cbf11 behaves as a negative regulator of adhesion, Cbf12 acts to increase it. In support of these findings, our microarray data showed markedly increased expression of several known or predicted adhesins and cell-surface glycoproteins (Hertz-Fowler *et al.*, 2004;Linder and Gustafsson, 2008). For example the absence of Cbf11 resulted in 17-fold upregulation of the SPAC1F8.02c predicted GPI-anchored glycoprotein (top-regulated gene in Δ*cbf11*); the overproduced Cbf12 triggered 25-fold and 6-fold upregulation of the SPBC359.04c and SPCC1795.13 adhesins, respectively. Interestingly, the last two were shown to be negatively regulated by the Cdk8 (Srb10/Prk1) kinase (Linder *et al.*, 2008), another subunit of the Mediator complex (Bjorklund and Gustafsson, 2005), the mutants of which are also hyperflocculent (Watson and Davey, 1998). Under physiological conditions, one of the reasons cells aggregate (flocculate) is the exhaustion of nutrients coinciding with the stationary phase of growth. It is a stress response with the aim of escaping the unfavorable environment either by sedimentation or by floating (Verstrepen and Klis, 2006). Notably, one of the *cbf12*$^+$ expression peaks occurs in the stationary phase, and we hypothesize that one of the

Cbf12 functions may be to trigger the increase of adhesion at this stage, possibly by counteracting or replacing Cbf11 at the respective promoters.

It was described that changes in adhesive properties of cells have profound impact on yeast colony morphology (Nguyen *et al.*, 2004;Reynolds and Fink, 2001;Vopalenska *et al.*, 2005). Also, extracellular matrix-like material was found to be produced by some *S. cerevisiae* strains, which forms a capsule around the colony and seems to serve as a scaffold for the cells within the colony (Kuthan *et al.*, 2003). It is thus possible that the Δ*cbf11*-associated alterations of colony morphology we observed result from the increased adhesion and/or massive "shiny" material secretion of these strains. Alternatively, the aberrant colony morphology could be a consequence of the cell separation defects and pseudohyphal growth noticed for a fraction of cells in the Δ*cbf11* colonies, as reported for other fungal species (Vopalenska *et al.*, 2005;Voth *et al.*, 2005;Weinzierl *et al.*, 2002). These two explanations, however, are not mutually exclusive, and the effects may combine.

5.2.2 Cell separation defects

When the expression of the fission yeast CSL genes was experimentally thrown off balance (*cbf11* KO or *cbf12*$^{+}$ overexpression), various cell separation defects appeared, although their penetrance was usually rather low. Taking into account our microarray data, this may be explained as a result of an overall decrease in fidelity of a number of cellular processes that may lead to stochastic manifestations in only a minor fraction of cells. These phenotypes, which were virtually never found in the WT control cells, included multiple septation events not followed by daughter cell separation, resulting in pseudohyphal growth, and formation of aberrantly thick septa (taking up to $^{1}/_{3}$ of the cell length). Infrequently, large (or even giant) uninucleate cells with several septa scattered at various positions were also seen. This is highly reminiscent of the fission yeast "sep" mutants which display very similar cell separation-related phenotypes, although often accompanied by sterility and impaired stress response to various substances (Grallert *et al.*, 1999;Sipiczki *et al.*, 1993). Some of the "sep" mutations have already been cloned and found to reside in genes encoding (general) regulators of transcription, rather than factors involved directly in cell separation (Ribar *et al.*, 1997;Szilagyi *et al.*, 2002;Zilahi *et al.*, 2000). This had been expected given the

range of mutant phenotypes elicited by these mutations (Grallert *et al.*, 1999). Two outstanding examples are the *sep10*$^+$ and *sep15*$^+$ genes encoding the Med30 and Med8 subunits of the RNA polymerase II Mediator, respectively. The Mediator is a multiprotein complex, conserved from yeasts to humans, serving to bridge both stimulatory and inhibitory signals from gene-specific transcription factors to the RNA polymerase II machinery (Bjorklund and Gustafsson, 2005). Microarray analyses of the Δ*sep10* and *sep15-598* mutants revealed overlapping but distinct groups comprising hundreds of diverse target genes (Linder *et al.*, 2008;Miklos *et al.*, 2008). Notably, we found a significant overlap of these datasets with our own microarray data (*cbf11* KO, *cbf11*$^+$ and *cbf12*$^+$ overexpression), extending the similarity of CSL and "sep" mutant phenotypes to the molecular level. This includes a large set of stress-response genes that might potentially represent direct regulatory targets of the Mediator, rather than their expression being changed due to a genuine stress response to the respective mutations (Linder *et al.*, 2008). As mentioned in Chapter 5.2.1, there are also physiological and molecular resemblances between the CSL mutants and strains lacking functional Cdk8, another Mediator component (Linder *et al.*, 2008). Moreover, there are indications that the transcription of the *cbf12*$^+$ gene is Med30-dependent (Lee *et al.*, 2005;Miklos *et al.*, 2008). We conclude that there is evident interplay between the CSL proteins and the Mediator complex, however, its exact nature remains elusive. We will address this question in a future study focused on genetic interactions between the CSL family and *sep10*$^+$, *sep15*$^+$ and *cdk8*$^+$.

5.2.3 Diploidization

The probably most intriguing effect of the dysregulated CSL expression (again, Δ*cbf11*, or *cbf12*$^+$ overexpression) was the emergence of stable diploid-like subpopulations. These manifested as dark-staining clonal sectors in monocolonies grown in the presence of phloxin B, as a >2C peak on FACS histograms of the mutant cultures, and as large cells with 2n-like nuclei observed under a microscope. As already mentioned in Chapter 4.8.2.5, spontaneous diploidization occurs even in WT heterothallic strains, however, at a very low frequency (estimated as less than 1 in 10^3 by Prof. Susan Forsburg, University of Southern California, USA; http://www-rcf.usc.edu/~forsburg/diploids.html). Indeed, we have occasionally

found dark sectors on WT monocolonies as well, although their occurrence was about 1 sector in 100 colonies (data not shown). In contrast to that, for the Δ*cbf11* and double KO strains there were typically ~10 or more dark sectors in each colony. A number of mutations, mostly in genes involved in the cell cycle regulation and progression, were shown to increase the so-called endoreduplication or re-replication frequency, and the respective mutant populations contain varying fractions of diploid (or even polyploid) cells. These mutations have been classified into three types according to the mechanism whereby the increase in ploidy occurs. The first type represents a bypass of M phase resulting, e.g., from the inactivation of the major cyclin dependent kinase Cdc2 or the B-type cyclin Cdc13 (Hayles *et al.*, 1994). The second type comprises multiple successive S phases without the G_1, G_2 and M phases taking place. This happens, for example, when Cdc18, the critical regulator of S-phase entry, is overproduced or its degradation is blocked (Jallepalli *et al.*, 1998;Jallepalli and Kelly, 1996;Kominami and Toda, 1997). We consider unlikely the possibility that these two sources of re-replication can be accounted for in the case of the manipulated CSL-induced diploids we found. First, there are no indications in our microarray data of altered expression of cell cycle-regulating genes (although there might well be changes at the posttranscriptional level). Second, we do have indications of expression changes (with the accompanying phenotypes) of genes belonging to the third type of diploidization inducers. An incomplete M phase occurs in the type three mutants, caused by the lack of coordination between the nuclear and cell division, resulting in the "cut" phenotype (Hirano *et al.*, 1986;Saitoh *et al.*, 1996). In this case, the septum develops prematurely and cuts through the nucleus before the latter completes its division. Although lethal in most cases, the septum occasionally forms without hitting the nucleus, and, as a result, a diploid and an anucleate compartment are formed. If the cell division proceeds further, a viable and stable (because homozygous, thus non-sporulating) diploid daughter cell is born and may start its clonal diploid subpopulation.

Remarkably, we have observed the "cut" phenotype in association with the deletion of *cbf11*$^+$, and cut cells (both before and after daughter cell separation) were often seen in DAPI-stained Δ*cbf11* and especially double KO cultures. Accordingly, the expression of *cut6*$^+$, an essential gene encoding an acetyl coenzyme A carboxylase, the conditional mutant of which is "cut", was decreased significantly (>1.5× threshold) in both the Δ*cbf11* and double KO strains. However, other factors

are likely involved as this explanation does not account for the diploidization observed when *cbf12*$^{+}$ was overexpressed. First, we did not see almost any "cut" cells under these conditions and second, *cut6*$^{+}$ expression was not significantly altered (22% decrease) either. A speculative *cbf12*$^{+}$-specific scenario of diploid formation may be envisioned as a result of *dad3*$^{+}$ downregulation (>2× threshold) that was detected in *cbf12*$^{+}$-overexpressing cells. Dad3 is a part of the DASH complex, a transient kinetochore component required for precise chromosome segregation during nuclear division (Liu *et al.*, 2005). It was found that about 10% of cells lacking the functional DASH complex become septated with the undivided nucleus displaced to one cell end, thus recapitulating the situation of the non-lethal "cut" events described above. As already stated, there is a considerable false-negative rate in our microarray data, and also a lot of fission yeast genes still await being characterized and annotated in more detail. It is therefore possible that other mechanisms (even shared by Δ*cbf11* and *cbf12*$^{+}$ overexpressor) are solely responsible for or participate in the formation of CSL-induced diploids. In any case, our experiments have established an important requirement for the CSL family in the maintenance of the fission yeast genome ploidy.

5.2.4 Meiosis

The *cbf12*$^{+}$ gene was repeatedly found to be upregulated about 5-8 hrs after induction of meiosis (this study and (Mata *et al.*, 2002;Wilhelm *et al.*, 2008)). Its deletion mutant was prepared in *h*^{90} cells, but no meiosis-associated phenotypes were found ((Gregan *et al.*, 2005) and http://mendel.imp.ac.at/Pombe/targets/162.html). Neither in this study have we found any conjugation or sporulation-related defects in the Δ*cbf12* and Δ*cbf11* Δ*cbf12* strains. Nevertheless, the transcriptomic analysis of *cbf12*$^{+}$ overexpressing cultures revealed a group of late meiotic genes that were upregulated under these conditions, likely in response to the increased levels of Cbf12 (Dr. Jürg Bähler, personal communication). It is possible that this ectopic meiotic transcription was deleterious to the cells, and responsible for the poor growth (and intense phloxin B staining) we observed. Notably, a number of genes normally induced in (late) meiosis (Mata *et al.*, 2002;Wilhelm *et al.*, 2008) were also present among the set of genes upregulated in the Δ*cbf11* strain (SPCC1840.12, SPAC2H10.01, SPAC3G9.11c, SPCC794.01c, *mug108*, *mug120*, SPBP4H10.12,

prl65, *wtf5*). It is tempting to speculate that Cbf11 actually functions as a "default" repressor of these genes, and Cbf12 activates their expression at the appropriate time during meiosis. This putative CSL function, however, is obviously not essential for the completion of the sexual differentiation program in fission yeast.

5.2.5 Uptake of iron and biotin

There are two uptake routes for iron in *S. pombe*. In the reductive pathway, Fe^{3+} ions from the environment are first reduced to Fe^{2+} by the cell-surface reductase Frp1, then re-oxidized by the Fio1 oxidase, and imported into the cell lumen by the Fip1 permease. The non-reductive pathway relies on the Str1, Str2 and Str3 transporters in the plasma membrane that recognize iron complexed with the siderophore chelators. The genes encoding these uptake proteins are transcriptionally regulated by iron via the Fep1 transcription factor that represses them when iron is abundant (Labbe *et al.*, 2007). The list of Fep1/iron-regulated genes was recently determined (Rustici *et al.*, 2007) and overlaps significantly with the group of genes differentially regulated in Δ*cbf11* cells. One of these genes, the vitamin H (biotin) transporter *vht1*$^{+}$, is actually the only gene showing reciprocal correlation of its mRNA level with *cbf11*$^{+}$ deletion/overexpression we could find. Such observations would suggest a role for CSL proteins in the regulation of iron homeostasis. This question was addressed by Jana Staňurová in her master's thesis. However, no physiological response was found of either CSL mutant to low/excess iron or biotin. A search for genetic interactions with the Δ*vht1* and Δ*fep1* deletion strains (Pelletier *et al.*, 2002;Stolz, 2003) will be carried out to shed more light on the CSL-iron/biotin relationship. Since the iron-regulated genes in question show altered expression levels also in the mediator mutants described above (Linder *et al.*, 2008;Miklos *et al.*, 2008) and under several other conditions (Gatti *et al.*, 2004;Harrison *et al.*, 2005;Sharma *et al.*, 2006), we consider a specific role of CSL proteins in the iron/biotin metabolism unlikely.

5.3 Cbf11 and Cbf12 as novel fission yeast transcription factors

The two fission yeast CSL proteins display a number of features typical of genuine transcription factors. They share domain composition and important

sequence motifs with the class M CSL family members (Prevorovsky *et al.*, 2007) and, similar to their metazoan counterparts, Cbf11 and Cbf12 localize to the cell nucleus (Chen *et al.*, 1997;de la Pompa *et al.*, 1997). Both proteins have an ability to activate transcription in a heterologous reporter system (an autologous reporter assay is currently in development), and one of them, Cbf11, was found to specifically recognize and bind directly to the canonical CSL response element on DNA (Tun *et al.*, 1994). We favor a hypothesis that the lack of binding observed for Cbf12 is due to, e.g., an inhibitory posttranslational modification, rather to its actual inability to bind DNA. We suspect that the large, low-complexity N-terminal domain of Cbf12, containing many potential phosphorylation sites (data not shown), may be involved in this regulation, and a truncation mutant have already been prepared by Martina Ptáčková to test this hypothesis (will be presented elsewhere). Seemingly in contrast to the metazoan CSL family members (Artavanis-Tsakonas *et al.*, 1999), neither *cbf11*$^+$ nor *cbf12*$^+$ is an essential gene in *S. pombe*. However, even though the murine CBF1 is essential for embryonic development, it is dispensable at the cellular level and knock-out cell lines can be established (Oka *et al.*, 1995). All clues taken together, we propose a role for Cbf11 and Cbf12 as novel transcription factors in *S. pombe* that regulate or fine-tune a number of important processes (Fig. 5.1). Their regulatory engagements differ from those of the metazoan CSL family members, following a distinct logic of the unicellular organism stemming from the vast evolutionary distance between these species (Hedges, 2002). Instead of embryonic development and cell fate decisions, the CSL paralogs in fission yeast seem to regulate cell adhesion, extracellular material production, colony morphology, septation and daughter cell separation, coordination of the nuclear and cell division, and the resulting proper maintenance of genome ploidy. In addition to that, they likely participate in the regulation of meoitic transcription as well.

For all the phenotypes detected, *cbf11*$^+$ behaves consistently as a negative and *cbf12*$^+$ as a positive regulator affecting the same processes. Thus, a general conclusion may be drawn that Cbf11-mediated repression might be the default state of many (if not all) CSL-responsive genes in *S. pombe*, and Cbf12 would activate their expression when required, in a specific context (stationary phase, meiosis). A similar scenario might be envisioned for the two fungal CSL classes in general. This would be highly reminiscent of the class M functioning in animals, where CSL proteins are capable of both repression (a default state) and context-dependent

activation of transcription of a target gene, brought about by changes in the spectrum of interaction partners bound (Hsieh *et al.*, 1996;Zhou *et al.*, 2000). Fungi might have tackled the same problem by using two "loyal specialists" instead of just one "double agent".

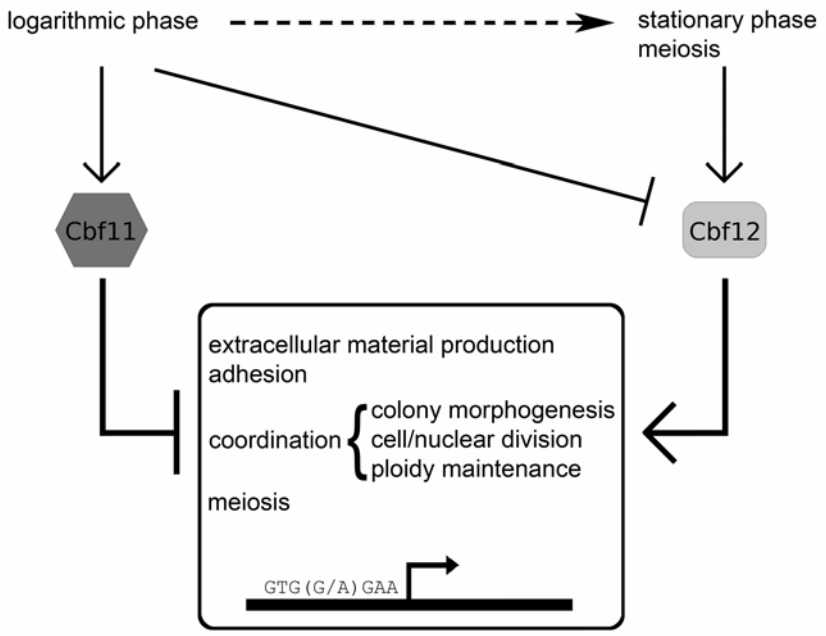

Figure 5.1 – A proposed model of CSL functioning in *S. pombe*. In log-phase vegetative cells Cbf11, the class F1 CSL representative, is bound to CSL-responsive promoters containing the GTG(G/A)GAA recognition sequence, and mediates their repression. Cbf12, the class F2 paralog, is expressed at low levels under these conditions and cannot overcome the effect of Cbf11. Upon entry into the stationary phase of growth (high cell density, depleted nutrients) or during meiosis, the Cbf12 protein levels rise and trigger the activation of (a subset of) the CSL target genes, e.g., by canceling the effect of Cbf11 or by replacing Cbf11 at the respective promoters. The target genes are likely organized into several subsets (e.g., meiotic, stationary-phase) differing in their responsiveness to Cbf11/12, and are involved in processes such as extracellular material production, cell adhesion, colony morphology establishment, cell and nuclear division and their mutual coordination, maintenance of genome ploidy, and meiosis. These genes seem to include several transcription factors, thus some apparently CSL-responsive genes may actually be regulated indirectly, by proteins downstream of Cbf11/12. At all times, a proper balance between the Cbf11 and Cbf12 activities seems to be important for the above-mentioned processes not to be perturbed

6 *CONCLUSIONS*

- We have identified and characterized *in silico* two novel fungi-specific classes (F1 and F2) of the CSL family of transcription factors, previously know from metazoan organisms only (class M). We have chosen the fission yeast *cbf11*$^{+}$ (SPCC736.08, class F1) and *cbf12*$^{+}$ (SPCC1223.13, class F2) genes for experimental characterization as representatives of the CSL family in an important model organism.

- We have cloned the cDNAs of both fission yeast CSL genes and prepared a series of plasmids allowing for recombinant tagged or fusion protein expression in *S. pombe*, *S. cerevisiae* and *E. coli*.

- We have prepared chromosomally tagged *cbf11*$^{+}$*::CTAP4* and *cbf12*$^{+}$*::CTAP4* fission yeast strains for the purpose of native protein complex purification by the TAP method.

- We have determined the expression profiles of *cbf11*$^{+}$ and *cbf12*$^{+}$ by qRT-PCR and found that while the former seems to be expressed constitutively, the latter is upregulated during stationary phase and meiosis.

- We have prepared a C-terminal chromosomal *cbf11*$^{+}$*::EGFP* fusion strain for *in vivo* localization studies. Using this knock-in strain and/or plasmid-driven overexpression, we found both Cbf11 and Cbf12 to be nuclear proteins excluded from the nucleolus.

- We have documented the ability of both Cbf11 and Cbf12 to activate reporter gene transcription when fused to a heterologous DNA-binding domain of the LexA or Gal4-derived 2H systems, respectively.

- We have presented evidence that Cbf11 is able to recognize with high specificity and bind directly to the GTG$^{G}/_{A}$GAA canonical CSL response element on DNA.

- We have constructed single and double deletion strains for both fission yeast CSL genes, together with respective overexpressor strains, and assayed their mutant phenotypes using a number of approaches.

- We have shown that strains harboring the deletion of *cbf11*$^{+}$ have impaired growth, are cold-sensitive, overproduce "shiny" extracellular matrix-like material, and have altered colony morphology. In addition, the overexpression of *cbf12*$^{+}$ seems to be toxic for the cells.

- We have demonstrated that either the deletion of *cbf11*$^{+}$ or overexpression of *cbf12*$^{+}$ result in increased cell adhesion, various cell separation defects (multiple septa, aberrantly thick septa, pseudohyphal growth, "cut"), and high-frequency stable diploid formation in cells of heterothallic strains. These phenotypes are supported at the molecular level by microarray data.

- We have proposed a role for Cbf11 and Cbf12 as novel transcription factors of *S. pombe* with contradicting, repressive and activating effects on target gene expression, respectively.

7 REFERENCES

1. Ambrozková, M., Půta, F., Fuková, I., Skružný, M., Brábek, J., and Folk, P. (2001) The fission yeast ortholog of the coregulator SKIP interacts with the small subunit of U2AF. *Biochem Biophys Res Commun* **284:** 1148-1154.

2. Ansieau, S., Strobl, L. J., and Leutz, A. (2001) Activation of the Notch-regulated transcription factor CBF1/RBP-Jkappa through the 13SE1A oncoprotein. *Genes Dev* **15:** 380-385.

3. Artavanis-Tsakonas, S., Rand, M. D., and Lake, R. J. (1999) Notch signaling: cell fate control and signal integration in development. *Science* **284:** 770-776.

4. Aslett, M. and Wood, V. (2006) Gene Ontology annotation status of the fission yeast genome: preliminary coverage approaches 100%. *Yeast* **23:** 913-919.

5. Bahler, J., Wu, J. Q., Longtine, M. S., Shah, N. G., McKenzie, A., III, Steever, A. B., Wach, A., Philippsen, P., and Pringle, J. R. (1998) Heterologous modules for efficient and versatile PCR-based gene targeting in *Schizosaccharomyces pombe*. *Yeast* **14:** 943-951.

6. Barolo, S., Walker, R. G., Polyanovsky, A. D., Freschi, G., Keil, T., and Posakony, J. W. (2000) A notch-independent activity of suppressor of hairless is required for normal mechanoreceptor physiology. *Cell* **103:** 957-969.

7. Basi, G., Schmid, E., and Maundrell, K. (1993) TATA box mutations in the *Schizosaccharomyces pombe* nmt1 promoter affect transcription efficiency but not the transcription start point or thiamine repressibility. *Gene* **123:** 131-136.

8. Beres, T. M., Masui, T., Swift, G. H., Shi, L., Henke, R. M., and MacDonald, R. J. (2006) PTF1 is an organ-specific and Notch-independent basic helix-loop-helix complex containing the mammalian Suppressor of Hairless (RBP-J) or its paralogue, RBP-L. *Mol Cell Biol* **26:** 117-130.

9. Birnboim, H. C. and Doly, J. (1979) A rapid alkaline extraction procedure for screening recombinant plasmid DNA. *Nucleic Acids Res* **7:** 1513-1523.

10. Bjorklund, S. and Gustafsson, C. M. (2005) The yeast Mediator complex and its regulation. *Trends Biochem Sci* **30:** 240-244.

11. Brábek, J., Mojžita, D., Hamplová, L., and Folk, P. (2002) The regulatory region of Prague C v-Src inhibits the activity of the Schmidt-Ruppin A v-Src kinase domain. *Folia Biol (Praha)* **48:** 28-33.

12. Bray, S. and Furriols, M. (2001) Notch pathway: making sense of suppressor of hairless. *Curr Biol* **11:** R217-R221.

13. Bray, S. J. (2006) Notch signalling: a simple pathway becomes complex. *Nat Rev Mol Cell Biol* **7:** 678-689.

14. Brou, C., Logeat, F., Lecourtois, M., Vandekerckhove, J., Kourilsky, P., Schweisguth, F., and Israel, A. (1994) Inhibition of the DNA-binding activity of *Drosophila* suppressor of hairless and of its human homolog, KBF2/RBP-J kappa, by direct protein-protein interaction with *Drosophila* hairless. *Genes Dev* **8:** 2491-2503.

15. Burge, C. and Karlin, S. (1997) Prediction of complete gene structures in human genomic DNA. *J Mol Biol* **268:** 78-94.

16. Chen, D., Toone, W. M., Mata, J., Lyne, R., Burns, G., Kivinen, K., Brazma, A., Jones, N., and Bahler, J. (2003) Global transcriptional responses of fission yeast to environmental stress. *Mol Biol Cell* **14:** 214-229.

17. Chen, Y., Fischer, W. H., and Gill, G. N. (1997) Regulation of the ERBB-2 promoter by RBPJkappa and NOTCH. *J Biol Chem* **272:** 14110-14114.

18. Chenna, R., Sugawara, H., Koike, T., Lopez, R., Gibson, T. J., Higgins, D. G., and Thompson, J. D. (2003) Multiple sequence alignment with the Clustal series of programs. *Nucleic Acids Res* **31:** 3497-3500.

19. Chung, C. N., Hamaguchi, Y., Honjo, T., and Kawaichi, M. (1994) Site-directed mutagenesis study on DNA binding regions of the mouse homologue of Suppressor of Hairless, RBP-J kappa. *Nucleic Acids Res* **22:** 2938-2944.

20. Craven, R. A., Griffiths, D. J., Sheldrick, K. S., Randall, R. E., Hagan, I. M., and Carr, A. M. (1998) Vectors for the expression of tagged proteins in *Schizosaccharomyces pombe*. *Gene* **221:** 59-68.

21. D'Alessio, C., Trombetta, E. S., and Parodi, A. J. (2003) Nucleoside diphosphatase and glycosyltransferase activities can localize to different subcellular compartments in *Schizosaccharomyces pombe*. *J Biol Chem* **278:** 22379-22387.

22. Dainty, S. J., Kennedy, C. A., Watt, S., Bahler, J., and Whitehall, S. K. (2008) Response of *Schizosaccharomyces pombe* to zinc deficiency. *Eukaryot Cell* **7:** 454-464.

23. de la Pompa, J. L., Wakeham, A., Correia, K. M., Samper, E., Brown, S., Aguilera, R. J., Nakano, T., Honjo, T., Mak, T. W., Rossant, J., and Conlon, R. A. (1997) Conservation of the Notch signalling pathway in mammalian neurogenesis. *Development* **124:** 1139-1148.

24. Decottignies, A., Sanchez-Perez, I., and Nurse, P. (2003) *Schizosaccharomyces pombe* essential genes: a pilot study. *Genome Res* **13:** 399-406.

25. Dou, S., Zeng, X., Cortes, P., Erdjument-Bromage, H., Tempst, P., Honjo, T., and Vales, L. D. (1994) The recombination signal sequence-binding protein

RBP-2N functions as a transcriptional repressor. *Mol Cell Biol* **14:** 3310-3319.

26. Egel, R. (Ed.) (2004) The Molecular Biology of *Schizosaccharomyces pombe* - Genetics, Genomics and Beyond. Springer-Verlag Berlin Heidelberg New York.

27. Finn, R. D., Mistry, J., Schuster-Bockler, B., Griffiths-Jones, S., Hollich, V., Lassmann, T., Moxon, S., Marshall, M., Khanna, A., Durbin, R., Eddy, S. R., Sonnhammer, E. L., and Bateman, A. (2006) Pfam: clans, web tools and services. *Nucleic Acids Res* **34:** D247-D251.

28. Folk, P., Půta, F., and Skružný, M. (2004) Transcriptional coregulator SNW/SKIP: the concealed tie of dissimilar pathways. *Cell Mol Life Sci* **61:** 629-640.

29. Forsburg, S. L. (2003) *S. pombe* strain maintenance and media. *Curr Protoc Mol Biol* **Chapter 13:** Unit 13.15.

30. Fryer, C. J., White, J. B., and Jones, K. A. (2004) Mastermind recruits CycC:CDK8 to phosphorylate the Notch ICD and coordinate activation with turnover. *Mol Cell* **16:** 509-520.

31. Fuchs, K. P., Bommer, G., Dumont, E., Christoph, B., Vidal, M., Kremmer, E., and Kempkes, B. (2001) Mutational analysis of the J recombination signal sequence binding protein (RBP-J)/Epstein-Barr virus nuclear antigen 2 (EBNA2) and RBP-J/Notch interaction. *Eur J Biochem* **268:** 4639-4646.

32. Gatti, L., Chen, D., Beretta, G. L., Rustici, G., Carenini, N., Corna, E., Colangelo, D., Zunino, F., Bahler, J., and Perego, P. (2004) Global gene expression of fission yeast in response to cisplatin. *Cell Mol Life Sci* **61:** 2253-2263.

33. Gho, M., Lecourtois, M., Geraud, G., Posakony, J. W., and Schweisguth, F. (1996) Subcellular localization of Suppressor of Hairless in *Drosophila* sense organ cells during Notch signalling. *Development* **122:** 1673-1682.

34. Gouet, P., Courcelle, E., Stuart, D. I., and Metoz, F. (1999) ESPript: analysis of multiple sequence alignments in PostScript. *Bioinformatics* **15:** 305-308.

35. Grallert, A., Grallert, B., Zilahi, E., Szilagyi, Z., and Sipiczki, M. (1999) Eleven novel sep genes of *Schizosaccharomyces pombe* required for efficient cell separation and sexual differentiation. *Yeast* **15:** 669-686.

36. Gregan, J., Rabitsch, P. K., Rumpf, C., Novatchkova, M., Schleiffer, A., and Nasmyth, K. (2006) High-throughput knockout screen in fission yeast. *Nat Protoc* **1:** 2457-2464.

37. Gregan, J., Rabitsch, P. K., Sakem, B., Csutak, O., Latypov, V., Lehmann, E., Kohli, J., and Nasmyth, K. (2005) Novel genes required for meiotic chromosome segregation are identified by a high-throughput knockout screen in fission yeast. *Curr Biol* **15:** 1663-1669.

38. Groušl, T. (2007) Analýzy proteinů rodiny CSL kvasinky *Schizosaccharomyces pombe*. Master's Thesis, Faculty of Science, Charles University in Prague.

39. Guex, N. and Peitsch, M. C. (1997) SWISS-MODEL and the Swiss-PdbViewer: an environment for comparative protein modeling. *Electrophoresis* **18:** 2714-2723.

40. Guldal, C. G. and Broach, J. (2006) Assay for adhesion and agar invasion in *S. cerevisiae*. *J Vis Exp* **1**: 64.

41. Hamaguchi, Y., Matsunami, N., Yamamoto, Y., and Honjo, T. (1989) Purification and characterization of a protein that binds to the recombination signal sequence of the immunoglobulin J kappa segment. *Nucleic Acids Res* **17:** 9015-9026.

42. Hamaguchi, Y., Yamamoto, Y., Iwanari, H., Maruyama, S., Furukawa, T., Matsunami, N., and Honjo, T. (1992) Biochemical and immunological characterization of the DNA binding protein (RBP-J kappa) to mouse J kappa recombination signal sequence. *J Biochem (Tokyo)* **112:** 314-320.

43. Harrison, C., Katayama, S., Dhut, S., Chen, D., Jones, N., Bahler, J., and Toda, T. (2005) SCF(Pof1)-ubiquitin and its target Zip1 transcription factor mediate cadmium response in fission yeast. *EMBO J* **24:** 599-610.

44. Hayles, J., Fisher, D., Woollard, A., and Nurse, P. (1994) Temporal order of S phase and mitosis in fission yeast is determined by the state of the p34cdc2-mitotic B cyclin complex. *Cell* **78:** 813-822.

45. Hayward, S. D. (2004) Viral interactions with the Notch pathway. *Semin Cancer Biol* **14:** 387-396.

46. Hedges, S. B. (2002) The origin and evolution of model organisms. *Nat Rev Genet* **3:** 838-849.

47. Henkel, T., Ling, P. D., Hayward, S. D., and Peterson, M. G. (1994) Mediation of Epstein-Barr virus EBNA2 transactivation by recombination signal-binding protein J kappa. *Science* **265:** 92-95.

48. Hertz-Fowler, C., Peacock, C. S., Wood, V., Aslett, M., Kerhornou, A., Mooney, P., Tivey, A., Berriman, M., Hall, N., Rutherford, K., Parkhill, J., Ivens, A. C., Rajandream, M. A., and Barrell, B. (2004) GeneDB: a resource for prokaryotic and eukaryotic organisms. *Nucleic Acids Res* **32:** D339-D343.

49. Higuchi, R., Krummel, B., and Saiki, R. K. (1988) A general method of in vitro preparation and specific mutagenesis of DNA fragments: study of protein and DNA interactions. *Nucleic Acids Res* **16:** 7351-7367.

50. Hirano, T., Funahashi, S. I., Uemura, T., and Yanagida, M. (1986) Isolation and characterization of *Schizosaccharomyces pombe* cut mutants that block nuclear division but not cytokinesis. *EMBO J* **5:** 2973-2979.

51. Honjo, T. (1996) The shortest path from the surface to the nucleus: RBP-J kappa/Su(H) transcription factor. *Genes Cells* **1:** 1-9.

52. Hsieh, J. J., Henkel, T., Salmon, P., Robey, E., Peterson, M. G., and Hayward, S. D. (1996) Truncated mammalian Notch1 activates CBF1/RBPJk-repressed genes by a mechanism resembling that of Epstein-Barr virus EBNA2. *Mol Cell Biol* **16:** 952-959.

53. Hsieh, J. J., Zhou, S., Chen, L., Young, D. B., and Hayward, S. D. (1999) CIR, a corepressor linking the DNA binding factor CBF1 to the histone deacetylase complex. *Proc Natl Acad Sci U S A* **96:** 23-28.

54. Hua, S. and Sun, Z. (2001) Support vector machine approach for protein subcellular localization prediction. *Bioinformatics* **17:** 721-728.

55. Iso, T., Kedes, L., and Hamamori, Y. (2003) HES and HERP families: multiple effectors of the Notch signaling pathway. *J Cell Physiol* **194:** 237-255.

56. Ito, H., Fukuda, Y., Murata, K., and Kimura, A. (1983) Transformation of intact yeast cells treated with alkali cations. *J Bacteriol* **153:** 163-168.

57. Jallepalli, P. V. and Kelly, T. J. (1996) Rum1 and Cdc18 link inhibition of cyclin-dependent kinase to the initiation of DNA replication in *Schizosaccharomyces pombe*. *Genes Dev* **10:** 541-552.

58. Jallepalli, P. V., Tien, D., and Kelly, T. J. (1998) sud1(+) targets cyclin-dependent kinase-phosphorylated Cdc18 and Rum1 proteins for degradation and stops unwanted diploidization in fission yeast. *Proc Natl Acad Sci U S A* **95:** 8159-8164.

59. James, T. Y., Kauff, F., Schoch, C. L., Matheny, P. B., Hofstetter, V., Cox, C. J., Celio, G., Gueidan, C., Fraker, E., Miadlikowska, J., Lumbsch, H. T., Rauhut, A., Reeb, V., Arnold, A. E., Amtoft, A., Stajich, J. E., Hosaka, K., Sung, G. H., Johnson, D., O'Rourke, B., Crockett, M., Binder, M., Curtis, J. M., Slot, J. C., Wang, Z., Wilson, A. W., Schussler, A., Longcore, J. E., O'Donnell, K., Mozley-Standridge, S., Porter, D., Letcher, P. M., Powell, M. J., Taylor, J. W., White, M. M., Griffith, G. W., Davies, D. R., Humber, R. A., Morton, J. B., Sugiyama, J., Rossman, A. Y., Rogers, J. D., Pfister, D. H., Hewitt, D., Hansen, K., Hambleton, S., Shoemaker, R. A., Kohlmeyer, J., Volkmann-Kohlmeyer, B., Spotts, R. A., Serdani, M., Crous, P. W., Hughes, K. W., Matsuura, K., Langer, E., Langer, G., Untereiner, W. A., Lucking, R., Budel, B., Geiser, D. M., Aptroot, A., Diederich, P., Schmitt, I., Schultz, M., Yahr, R., Hibbett, D. S., Lutzoni, F., McLaughlin, D. J., Spatafora, J. W., and Vilgalys, R. (2006) Reconstructing the early evolution of Fungi using a six-gene phylogeny. *Nature* **443:** 818-822.

60. Janke, C., Magiera, M. M., Rathfelder, N., Taxis, C., Reber, S., Maekawa, H., Moreno-Borchart, A., Doenges, G., Schwob, E., Schiebel, E., and Knop, M. (2004) A versatile toolbox for PCR-based tagging of yeast genes: new

fluorescent proteins, more markers and promoter substitution cassettes. *Yeast* **21:** 947-962.

61. Kannabiran, C., Zeng, X., and Vales, L. D. (1997) The mammalian transcriptional repressor RBP (CBF1) regulates interleukin-6 gene expression. *Mol Cell Biol* **17:** 1-9.

62. Kao, H. Y., Ordentlich, P., Koyano-Nakagawa, N., Tang, Z., Downes, M., Kintner, C. R., Evans, R. M., and Kadesch, T. (1998) A histone deacetylase corepressor complex regulates the Notch signal transduction pathway. *Genes Dev* **12:** 2269-2277.

63. Kaspar, M. and Klein, T. (2006) Functional analysis of murine CBF1 during *Drosophila* development. *Dev Dyn* **235:** 918-927.

64. Kawaichi, M., Oka, C., Shibayama, S., Koromilas, A. E., Matsunami, N., Hamaguchi, Y., and Honjo, T. (1992) Genomic organization of mouse J kappa recombination signal binding protein (RBP-J kappa) gene. *J Biol Chem* **267:** 4016-4022.

65. Koelzer, S. and Klein, T. (2003) A Notch-independent function of Suppressor of Hairless during the development of the bristle sensory organ precursor cell of *Drosophila*. *Development* **130:** 1973-1988.

66. Kominami, K. and Toda, T. (1997) Fission yeast WD-repeat protein pop1 regulates genome ploidy through ubiquitin-proteasome-mediated degradation of the CDK inhibitor Rum1 and the S-phase initiator Cdc18. *Genes Dev* **11:** 1548-1560.

67. Kovall, R. A. (2007) Structures of CSL, Notch and Mastermind proteins: piecing together an active transcription complex. *Curr Opin Struct Biol* **17:** 117-127.

68. Kovall, R. A. and Hendrickson, W. A. (2004) Crystal structure of the nuclear effector of Notch signaling, CSL, bound to DNA. *EMBO J* **23:** 3441-3451.

69. Kumar, S., Tamura, K., and Nei, M. (1994) MEGA: Molecular Evolutionary Genetics Analysis software for microcomputers. *Comput Appl Biosci* **10:** 189-191.

70. Kuramae, E. E., Robert, V., Snel, B., Weiss, M., and Boekhout, T. (2006) Phylogenomics reveal a robust fungal tree of life. *FEMS Yeast Res* **6:** 1213-1220.

71. Kuroda, K., Han, H., Tani, S., Tanigaki, K., Tun, T., Furukawa, T., Taniguchi, Y., Kurooka, H., Hamada, Y., Toyokuni, S., and Honjo, T. (2003) Regulation of marginal zone B cell development by MINT, a suppressor of Notch/RBP-J signaling pathway. *Immunity* **18:** 301-312.

72. Kuthan, M., Devaux, F., Janderová, B., Slaninová, I., Jacq, C., and Palková, Z. (2003) Domestication of wild *Saccharomyces cerevisiae* is accompanied

by changes in gene expression and colony morphology. *Mol Microbiol* **47:** 745-754.

73. Labbe, S., Pelletier, B., and Mercier, A. (2007) Iron homeostasis in the fission yeast *Schizosaccharomyces pombe*. *Biometals* **20:** 523-537.

74. Lai, E. C. (2002) Keeping a good pathway down: transcriptional repression of Notch pathway target genes by CSL proteins. *EMBO Rep* **3:** 840-845.

75. Lai, E. C. (2004) Notch signaling: control of cell communication and cell fate. *Development* **131:** 965-973.

76. Laky, K. and Fowlkes, B. J. (2008) Notch signaling in CD4 and CD8 T cell development. *Curr Opin Immunol* **20:** 197-202.

77. Lam, L. T. and Bresnick, E. H. (1998) Identity of the beta-globin locus control region binding protein HS2NF5 as the mammalian homolog of the notch-regulated transcription factor suppressor of hairless. *J Biol Chem* **273:** 24223-24231.

78. Lamar, E., Deblandre, G., Wettstein, D., Gawantka, V., Pollet, N., Niehrs, C., and Kintner, C. (2001) Nrarp is a novel intracellular component of the Notch signaling pathway. *Genes Dev* **15:** 1885-1899.

79. Lee, K. M., Miklos, I., Du, H., Watt, S., Szilagyi, Z., Saiz, J. E., Madabhushi, R., Penkett, C. J., Sipiczki, M., Bahler, J., and Fisher, R. P. (2005) Impairment of the TFIIH-associated CDK-activating kinase selectively affects cell cycle-regulated gene expression in fission yeast. *Mol Biol Cell* **16:** 2734-2745.

80. Lee, S. H., Wang, X., and DeJong, J. (2000) Functional interactions between an atypical NF-kappaB site from the rat CYP2B1 promoter and the transcriptional repressor RBP-Jkappa/CBF1. *Nucleic Acids Res* **28:** 2091-2098.

81. Liang, Y., Chang, J., Lynch, S. J., Lukac, D. M., and Ganem, D. (2002) The lytic switch protein of KSHV activates gene expression via functional interaction with RBP-Jkappa (CSL), the target of the Notch signaling pathway. *Genes Dev* **16:** 1977-1989.

82. Liang, Y. and Ganem, D. (2004) RBP-J (CSL) is essential for activation of the K14/vGPCR promoter of Kaposi's sarcoma-associated herpesvirus by the lytic switch protein RTA. *J Virol* **78:** 6818-6826.

83. Linder, T. and Gustafsson, C. M. (2008) Molecular phylogenetics of ascomycotal adhesins – a novel family of putative cell-surface adhesive proteins in fission yeasts. *Fungal Genet Biol* **45:** 485-497.

84. Linder, T., Rasmussen, N. N., Samuelsen, C. O., Chatzidaki, E., Baraznenok, V., Beve, J., Henriksen, P., Gustafsson, C. M., and Holmberg, S. (2008) Two conserved modules of *Schizosaccharomyces pombe* Mediator regulate distinct cellular pathways. *Nucleic Acids Res* **36:** 2489-2504.

85. Liu, X., McLeod, I., Anderson, S., Yates, J. R., III, and He, X. (2005) Molecular analysis of kinetochore architecture in fission yeast. *EMBO J* **24:** 2919-2930.

86. Livak, K. J. and Schmittgen, T. D. (2001) Analysis of relative gene expression data using real-time quantitative PCR and the 2(-Delta Delta C(T)) Method. *Methods* **25:** 402-408.

87. Lubman, O. Y., Korolev, S. V., and Kopan, R. (2004) Anchoring notch genetics and biochemistry; structural analysis of the ankyrin domain sheds light on existing data. *Mol Cell* **13:** 619-626.

88. Lyne, R., Burns, G., Mata, J., Penkett, C. J., Rustici, G., Chen, D., Langford, C., Vetrie, D., and Bahler, J. (2003) Whole-genome microarrays of fission yeast: characteristics, accuracy, reproducibility, and processing of array data. *BMC Genomics* **4:** 27.

89. Maillard, I., Adler, S. H., and Pear, W. S. (2003) Notch and the immune system. *Immunity* **19:** 781-791.

90. Martinez, Arias A., Zecchini, V., and Brennan, K. (2002) CSL-independent Notch signalling: a checkpoint in cell fate decisions during development? *Curr Opin Genet Dev* **12:** 524-533.

91. Mata, J., Lyne, R., Burns, G., and Bahler, J. (2002) The transcriptional program of meiosis and sporulation in fission yeast. *Nat Genet* **32:** 143-147.

92. Matsunami, N., Hamaguchi, Y., Yamamoto, Y., Kuze, K., Kangawa, K., Matsuo, H., Kawaichi, M., and Honjo, T. (1989) A protein binding to the J kappa recombination sequence of immunoglobulin genes contains a sequence related to the integrase motif. *Nature* **342:** 934-937.

93. Matsuyama, A., Arai, R., Yashiroda, Y., Shirai, A., Kamata, A., Sekido, S., Kobayashi, Y., Hashimoto, A., Hamamoto, M., Hiraoka, Y., Horinouchi, S., and Yoshida, M. (2006) ORFeome cloning and global analysis of protein localization in the fission yeast *Schizosaccharomyces pombe*. *Nat Biotechnol* **24:** 841-847.

94. Miki, B. L., Poon, N. H., James, A. P., and Seligy, V. L. (1982) Possible mechanism for flocculation interactions governed by gene FLO1 in *Saccharomyces cerevisiae*. *J Bacteriol* **150:** 878-889.

95. Miklos, I., Szilagyi, Z., Watt, S., Zilahi, E., Batta, G., Antunovics, Z., Enczi, K., Bahler, J., and Sipiczki, M. (2008) Genomic expression patterns in cell separation mutants of *Schizosaccharomyces pombe* defective in the genes sep10(+) and sep15(+) coding for the Mediator subunits Med31 and Med8. *Mol Genet Genomics* **279:** 225-238.

96. Milanesi, L., D'Angelo, D., and Rogozin, I. B. (1999) GeneBuilder: interactive in silico prediction of gene structure. *Bioinformatics* **15:** 612-621.

97. Minoguchi, S., Ikeda, T., Itohara, S., Kaneko, T., Okaichi, H., and Honjo, T. (1999) Studies on the cell-type specific expression of RBP-L, a RBP-J family member, by replacement insertion of beta-galactosidase. *J Biochem (Tokyo)* **126:** 738-747.

98. Minoguchi, S., Taniguchi, Y., Kato, H., Okazaki, T., Strobl, L. J., Zimber-Strobl, U., Bornkamm, G. W., and Honjo, T. (1997) RBP-L, a transcription factor related to RBP-Jkappa. *Mol Cell Biol* **17:** 2679-2687.

99. Miyatsuka, T., Matsuoka, T. A., Shiraiwa, T., Yamamoto, T., Kojima, I., and Kaneto, H. (2007) Ptf1a and RBP-J cooperate in activating Pdx1 gene expression through binding to Area III. *Biochem Biophys Res Commun* **362:** 905-909.

100. Morel, V. and Schweisguth, F. (2000) Repression by suppressor of hairless and activation by Notch are required to define a single row of single-minded expressing cells in the *Drosophila* embryo. *Genes Dev* **14:** 377-388.

101. Morita, T. and Takegawa, K. (2004) A simple and efficient procedure for transformation of *Schizosaccharomyces pombe*. *Yeast* **21:** 613-617.

102. Muller, P. Y., Janovjak, H., Miserez, A. R., and Dobbie, Z. (2002) Processing of gene expression data generated by quantitative real-time RT-PCR. *Biotechniques* **32:** 1372-1379.

103. Nakai, K. and Horton, P. (1999) PSORT: a program for detecting sorting signals in proteins and predicting their subcellular localization. *Trends Biochem Sci* **24:** 34-36.

104. Nam, Y., Sliz, P., Song, L., Aster, J. C., and Blacklow, S. C. (2006) Structural basis for cooperativity in recruitment of MAML coactivators to Notch transcription complexes. *Cell* **124:** 973-983.

105. Nguyen, B., Upadhyaya, A., van Oudenaarden, A., and Brenner, M. P. (2004) Elastic instability in growing yeast colonies. *Biophys J* **86:** 2740-2747.

106. Obata, J., Yano, M., Mimura, H., Goto, T., Nakayama, R., Mibu, Y., Oka, C., and Kawaichi, M. (2001) p48 subunit of mouse PTF1 binds to RBP-Jkappa/CBF-1, the intracellular mediator of Notch signalling, and is expressed in the neural tube of early stage embryos. *Genes Cells* **6:** 345-360.

107. Oka, C., Nakano, T., Wakeham, A., de la Pompa, J. L., Mori, C., Sakai, T., Okazaki, S., Kawaichi, M., Shiota, K., Mak, T. W., and Honjo, T. (1995) Disruption of the mouse RBP-J kappa gene results in early embryonic death. *Development* **121:** 3291-3301.

108. Olave, I., Reinberg, D., and Vales, L. D. (1998) The mammalian transcriptional repressor RBP (CBF1) targets TFIID and TFIIA to prevent activated transcription. *Genes Dev* **12:** 1621-1637.

109. Oswald, F., Kostezka, U., Astrahantseff, K., Bourteele, S., Dillinger, K., Zechner, U., Ludwig, L., Wilda, M., Hameister, H., Knochel, W., Liptay, S.,

and Schmid, R. M. (2002) SHARP is a novel component of the Notch/RBP-Jkappa signalling pathway. *EMBO J* **21:** 5417-5426.

110. Oswald, F., Liptay, S., Adler, G., and Schmid, R. M. (1998) NF-kappaB2 is a putative target gene of activated Notch-1 via RBP-Jkappa. *Mol Cell Biol* **18:** 2077-2088.

111. Pelletier, B., Beaudoin, J., Mukai, Y., and Labbe, S. (2002) Fep1, an iron sensor regulating iron transporter gene expression in *Schizosaccharomyces pombe*. *J Biol Chem* **277:** 22950-22958.

112. Petcherski, A. G. and Kimble, J. (2000) LAG-3 is a putative transcriptional activator in the *C. elegans* Notch pathway. *Nature* **405:** 364-368.

113. Plaisance, S., Vanden Berghe, W., Boone, E., Fiers, W., and Haegeman, G. (1997) Recombination signal sequence binding protein Jkappa is constitutively bound to the NF-kappaB site of the interleukin-6 promoter and acts as a negative regulatory factor. *Mol Cell Biol* **17:** 3733-3743.

114. Převorovský, M., Půta, F., and Folk, P. (2007) Fungal CSL transcription factors. *BMC Genomics* **8:** 233.

115. Puig, O., Caspary, F., Rigaut, G., Rutz, B., Bouveret, E., Bragado-Nilsson, E., Wilm, M., and Seraphin, B. (2001) The tandem affinity purification (TAP) method: a general procedure of protein complex purification. *Methods* **24:** 218-229.

116. Pursglove, S. E. and Mackay, J. P. (2005) CSL: a notch above the rest. *Int J Biochem Cell Biol* **37:** 2472-2477.

117. Rep, M., Duyvesteijn, R. G., Gale, L., Usgaard, T., Cornelissen, B. J., Ma, L. J., and Ward, T. J. (2006) The presence of GC-AG introns in *Neurospora crassa* and other euascomycetes determined from analyses of complete genomes: implications for automated gene prediction. *Genomics* **87:** 338-347.

118. Reynolds, T. B. and Fink, G. R. (2001) Bakers' yeast, a model for fungal biofilm formation. *Science* **291:** 878-881.

119. Ribar, B., Banrevi, A., and Sipiczki, M. (1997) sep1+ encodes a transcription-factor homologue of the HNF-3/forkhead DNA-binding-domain family in *Schizosaccharomyces pombe*. *Gene* **202:** 1-5.

120. Ronchini, C. and Capobianco, A. J. (2001) Induction of cyclin D1 transcription and CDK2 activity by Notch(ic): implication for cell cycle disruption in transformation by Notch(ic). *Mol Cell Biol* **21:** 5925-5934.

121. Rustici, G., van Bakel, H., Lackner, D. H., Holstege, F. C., Wijmenga, C., Bahler, J., and Brazma, A. (2007) Global transcriptional responses of fission and budding yeast to changes in copper and iron levels: a comparative study. *Genome Biol* **8:** R73.

122. Ryneš, J. (2005) Homolog transkripčního faktoru CBF1 identifikován ve *Schizosaccharomyces pombe*. Master's Thesis, Faculty of Science, Charles University in Prague.

123. Saitoh, S., Takahashi, K., Nabeshima, K., Yamashita, Y., Nakaseko, Y., Hirata, A., and Yanagida, M. (1996) Aberrant mitosis in fission yeast mutants defective in fatty acid synthetase and acetyl CoA carboxylase. *J Cell Biol* **134:** 949-961.

124. Sakai, T., Taniguchi, Y., Tamura, K., Minoguchi, S., Fukuhara, T., Strobl, L. J., Zimber-Strobl, U., Bornkamm, G. W., and Honjo, T. (1998) Functional replacement of the intracellular region of the Notch1 receptor by Epstein-Barr virus nuclear antigen 2. *J Virol* **72:** 6034-6039.

125. Sazer, S. and Sherwood, S. W. (1990) Mitochondrial growth and DNA synthesis occur in the absence of nuclear DNA replication in fission yeast. *J Cell Sci* **97 (Pt 3):** 509-516.

126. Schwede, T., Kopp, J., Guex, N., and Peitsch, M. C. (2003) SWISS-MODEL: An automated protein homology-modeling server. *Nucleic Acids Res* **31:** 3381-3385.

127. Schweisguth, F., Nero, P., and Posakony, J. W. (1994) The sequence similarity of the *Drosophila* suppressor of hairless protein to the integrase domain has no functional significance in vivo. *Dev Biol* **166:** 812-814.

128. Sharma, N., Marguerat, S., Mehta, S., Watt, S., and Bahler, J. (2006) The fission yeast Rpb4 subunit of RNA polymerase II plays a specialized role in cell separation. *Mol Genet Genomics* **276:** 545-554.

129. Shirakata, Y., Shuman, J. D., and Coligan, J. E. (1996) Purification of a novel MHC class I element binding activity from thymus nuclear extracts reveals that thymic RBP-Jkappa/CBF1 binds to NF-kappaB-like elements. *J Immunol* **156:** 4672-4679.

130. Sipiczki, M., Grallert, B., and Miklos, I. (1993) Mycelial and syncytial growth in *Schizosaccharomyces pombe* induced by novel septation mutations. *J Cell Sci* **104 (Pt 2):** 485-493.

131. Stolz, J. (2003) Isolation and characterization of the plasma membrane biotin transporter from *Schizosaccharomyces pombe*. *Yeast* **20:** 221-231.

132. Straver, M. H., Kijne, J. W., and Smit, G. (1993) Cause and control of flocculation in yeast. *Trends Biotechnol* **11:** 228-232.

133. Szilagyi, Z., Grallert, A., Nemeth, N., and Sipiczki, M. (2002) The *Schizosaccharomyces pombe* genes sep10 and sep11 encode putative general transcriptional regulators involved in multiple cellular processes. *Mol Genet Genomics* **268:** 553-562.

134. Tanaka, N., Awai, A., Bhuiyan, M. S., Fujita, K., Fukui, H., and Takegawa, K. (1999) Cell surface galactosylation is essential for nonsexual flocculation in *Schizosaccharomyces pombe*. *J Bacteriol* **181:** 1356-1359.

135. Tang, Z. and Kadesch, T. (2001) Identification of a novel activation domain in the Notch-responsive transcription factor CSL. *Nucleic Acids Res* **29:** 2284-2291.

136. Taniguchi, Y., Furukawa, T., Tun, T., Han, H., and Honjo, T. (1998) LIM protein KyoT2 negatively regulates transcription by association with the RBP-J DNA-binding protein. *Mol Cell Biol* **18:** 644-654.

137. Thompson, J. D., Gibson, T. J., Plewniak, F., Jeanmougin, F., and Higgins, D. G. (1997) The CLUSTAL_X windows interface: flexible strategies for multiple sequence alignment aided by quality analysis tools. *Nucleic Acids Res* **25:** 4876-4882.

138. Tun, T., Hamaguchi, Y., Matsunami, N., Furukawa, T., Honjo, T., and Kawaichi, M. (1994) Recognition sequence of a highly conserved DNA binding protein RBP-J kappa. *Nucleic Acids Res* **22:** 965-971.

139. UniProt Consortium (2007) The Universal Protein Resource (UniProt). *Nucleic Acids Res* **35:** D193-D197.

140. Van Driessche, B., Tafforeau, L., Hentges, P., Carr, A. M., and Vandenhaute, J. (2005) Additional vectors for PCR-based gene tagging in *Saccharomyces cerevisiae* and *Schizosaccharomyces pombe* using nourseothricin resistance. *Yeast* **22:** 1061-1068.

141. Verstrepen, K. J. and Klis, F. M. (2006) Flocculation, adhesion and biofilm formation in yeasts. *Mol Microbiol* **60:** 5-15.

142. Vopálenská, I., Hůlková, M., Janderová, B., and Palková, Z. (2005) The morphology of *Saccharomyces cerevisiae* colonies is affected by cell adhesion and the budding pattern. *Res Microbiol* **156:** 921-931.

143. Voth, W. P., Olsen, A. E., Sbia, M., Freedman, K. H., and Stillman, D. J. (2005) ACE2, CBK1, and BUD4 in budding and cell separation. *Eukaryot Cell* **4:** 1018-1028.

144. Watson, P. and Davey, J. (1998) Characterization of the Prk1 protein kinase from *Schizosaccharomyces pombe*. *Yeast* **14:** 485-492.

145. Watt, T. J. and Doyle, D. F. (2005) ESPSearch: a program for finding exact sequences and patterns in DNA, RNA, or protein. *Biotechniques* **38:** 109-115.

146. Weinmaster, G. and Kintner, C. (2003) Modulation of Notch signaling during somitogenesis. *Annu Rev Cell Dev Biol* **19:** 367-395.

147. Weinzierl, G., Leveleki, L., Hassel, A., Kost, G., Wanner, G., and Bolker, M. (2002) Regulation of cell separation in the dimorphic fungus *Ustilago maydis*. *Mol Microbiol* **45:** 219-231.

148. Weng, A. P. and Aster, J. C. (2004) Multiple niches for Notch in cancer: context is everything. *Curr Opin Genet Dev* **14:** 48-54.

149. Wilhelm, B. T., Marguerat, S., Watt, S., Schubert, F., Wood, V., Goodhead, I., Penkett, C. J., Rogers, J., and Bahler, J. (2008) Dynamic repertoire of a eukaryotic transcriptome surveyed at single-nucleotide resolution. *Nature* **453:** 1239-1243.

150. Wilson, J. J. and Kovall, R. A. (2006) Crystal structure of the CSL-Notch-Mastermind ternary complex bound to DNA. *Cell* **124:** 985-996.

151. Wood, V., Gwilliam, R., Rajandream, M. A., Lyne, M., Lyne, R., Stewart, A., Sgouros, J., Peat, N., Hayles, J., Baker, S., Basham, D., Bowman, S., Brooks, K., Brown, D., Brown, S., Chillingworth, T., Churcher, C., Collins, M., Connor, R., Cronin, A., Davis, P., Feltwell, T., Fraser, A., Gentles, S., Goble, A., Hamlin, N., Harris, D., Hidalgo, J., Hodgson, G., Holroyd, S., Hornsby, T., Howarth, S., Huckle, E. J., Hunt, S., Jagels, K., James, K., Jones, L., Jones, M., Leather, S., McDonald, S., McLean, J., Mooney, P., Moule, S., Mungall, K., Murphy, L., Niblett, D., Odell, C., Oliver, K., O'Neil, S., Pearson, D., Quail, M. A., Rabbinowitsch, E., Rutherford, K., Rutter, S., Saunders, D., Seeger, K., Sharp, S., Skelton, J., Simmonds, M., Squares, R., Squares, S., Stevens, K., Taylor, K., Taylor, R. G., Tivey, A., Walsh, S., Warren, T., Whitehead, S., Woodward, J., Volckaert, G., Aert, R., Robben, J., Grymonprez, B., Weltjens, I., Vanstreels, E., Rieger, M., Schafer, M., Muller-Auer, S., Gabel, C., Fuchs, M., Dusterhoft, A., Fritzc, C., Holzer, E., Moestl, D., Hilbert, H., Borzym, K., Langer, I., Beck, A., Lehrach, H., Reinhardt, R., Pohl, T. M., Eger, P., Zimmermann, W., Wedler, H., Wambutt, R., Purnelle, B., Goffeau, A., Cadieu, E., Dreano, S., Gloux, S., Lelaure, V., Mottier, S., Galibert, F., Aves, S. J., Xiang, Z., Hunt, C., Moore, K., Hurst, S. M., Lucas, M., Rochet, M., Gaillardin, C., Tallada, V. A., Garzon, A., Thode, G., Daga, R. R., Cruzado, L., Jimenez, J., Sanchez, M., del Rey, F., Benito, J., Dominguez, A., Revuelta, J. L., Moreno, S., Armstrong, J., Forsburg, S. L., Cerutti, L., Lowe, T., McCombie, W. R., Paulsen, I., Potashkin, J., Shpakovski, G. V., Ussery, D., Barrell, B. G., Nurse, P., and Cerrutti, L. (2002) The genome sequence of *Schizosaccharomyces pombe*. *Nature* **415:** 871-880.

152. Yoo, A. S. and Greenwald, I. (2005) LIN-12/Notch activation leads to microRNA-mediated down-regulation of Vav in *C. elegans*. *Science* **310:** 1330-1333.

153. Yu, C. S., Chen, Y. C., Lu, C. H., and Hwang, J. K. (2006) Prediction of protein subcellular localization. *Proteins* **64:** 643-651.

154. Zhang, J., Chen, H., Weinmaster, G., and Hayward, S. D. (2001) Epstein-Barr virus BamHI-a rightward transcript-encoded RPMS protein interacts with the CBF1-associated corepressor CIR to negatively regulate the activity of EBNA2 and NotchIC. *J Virol* **75:** 2946-2956.

155. Zhao, B., Marshall, D. R., and Sample, C. E. (1996) A conserved domain of the Epstein-Barr virus nuclear antigens 3A and 3C binds to a discrete domain of Jkappa. *J Virol* **70:** 4228-4236.

156. Zhou, S., Fujimuro, M., Hsieh, J. J., Chen, L., Miyamoto, A., Weinmaster, G., and Hayward, S. D. (2000) SKIP, a CBF1-associated protein, interacts with the ankyrin repeat domain of NotchIC To facilitate NotchIC function. *Mol Cell Biol* **20:** 2400-2410.

157. Zhou, S. and Hayward, S. D. (2001) Nuclear localization of CBF1 is regulated by interactions with the SMRT corepressor complex. *Mol Cell Biol* **21:** 6222-6232.

158. Zilahi, E., Miklos, I., and Sipiczki, M. (2000) The *Schizosaccharomyces pombe* sep15+ gene encodes a protein homologous to the Med8 subunit of the *Saccharomyces cerevisiae* transcriptional mediator complex. *Curr Genet* **38:** 227-232.

8 *APPENDICES*

This PhD thesis is accompanied by a CD containing the following supplementary materials:

8.1 Publications

A copy of this thesis in the PDF format.

Electronic versions of all articles (+ supplementary data files) of this author published, accepted or submitted for publication during the course of this PhD study.

A/T-rich inverted DNA repeats are destabilized by chaotrope-containing buffer during purification using silica gel membrane technology
Martin Převorovský and František Půta
BioTechniques 2003, 35:698-702

Fungal CSL transcription factors
Martin Převorovský, František Půta and Petr Folk
BMC Genomics 2007, 8:233

Cbf11 and Cbf12, the fission yeast CSL proteins, play opposing roles in cell adhesion and coordination of cell and nuclear division
Martin Převorovský, Tomáš Groušl, Jana Staňurová, Jan Ryneš, Wolfgang Nellen, František Půta, Petr Folk
Experimental Cell Research, 2008 (accepted for publication)

High environmental iron concentrations stimulate adhesion and invasive growth of *Schizosaccharomyces pombe*
Martin Převorovský, Jana Staňurová, František Půta, Petr Folk
FEMS Microbiology Letters, 2008 (manuscript in revision)

8.2 Microarray data

Complete datasets from the microarray analyses described in Chapter 4.8.2.6 in the XLS format.

8.3 Plasmid sequences

Nucleotide sequences and maps of the plasmids used and constructed in this study (where available).